ROYAUME DU MAROC
Université Mohammed V - RABAT -
جامعة محمد الخامس – الرباط –
Faculté des sciences
كلية العلوم
CENTRE D'ÉTUDES DOCTORALES - SCIENCES ET TECHNOLOGIES

N° d'ordre : 4022

THÈSE

en vue de l'obtention du : **DOCTORAT**

Centre de Recherche : Centre Eau, Ressources Naturelles, Environnement et Développement Durable (CERNE2D)
Structure de Recherche : Laboratoire de Spectroscopie, Modélisation Moléculaire, Matériaux, Nanomatériaux, Eau et Environnement (LS3MN2E)
Discipline : Chimie
Spécialité : Sciences des Matériaux et Environnement

Présentée et Soutenue le : *07 / 12 / 2024*

par :

Asmae EL-YAHYAOUI

Synthesis and characterization of halide perovskite $MAPbX_3$: physicochemical properties and stability improvement for photovoltaic application

Devant le JURY :

Mohammed EL MAHI	PES, Ecole Nationale supérieure d'Arts et Métiers, Université Mohammed V Rabat	Président
Mounir FAHOUME	PES, Faculté des Sciences, Université Ibn Tofail Kenitra	Examinateur/Rapporteur
Jamil TOYIR	PES, Faculté Polydisciplinaire, Université Sidi Mohamed Ben Abdellah Taza	Examinateur/Rapporteur
Noureddine TOUACH	PH, Ecole Nationale supérieure d'Arts et Métiers, Université Mohammed V Rabat	Examinateur/Rapporteur
Larbi LAANAB	PES, Faculté des Sciences, Université Mohammed V Rabat	Examinateur
Abdellah BENZAOUAK	PH, Ecole Nationale supérieure d'Arts et Métiers, Université Mohammed V Rabat	Examinateur
Boujemaâ JABER	PES, Chef division des UATRS, Centre National pour la Recherche Scientifique et Technique Rabat	Co-Directeur de thèse
El Mostapha LOTFI	PES, Ecole Nationale supérieure d'Arts et Métiers, Université Mohammed V Rabat	Directeur de thèse

Année Universitaire : 2023 - 24

Dedication

I dedicate this work to:

My dear parents

With all my feelings of respect, love, gratitude and appreciation for all the sacrifices made to raise me worthily and ensure my education in the best conditions. May God preserve their health and long life.

My sisters

I hope it has reached the threshold of your expectations. May this work be an expression of my deep affection I thank you for the moral support and encouragement that you have given me. I wish you all the happiness you deserve.

My uncles, aunts, cousins

Which I could not name for fear of forgetting, my attachment and my most sincere affections.

My best friends

To all those who have been able to give me help and support at the right times, I dedicate this work, thanking and thanking warmly.

Acknowledgements

This thesis work was carried out within the framework of a collaboration between the Laboratory of Spectroscopy, Molecular Modeling, Materials, Nanomaterials, Water and Environment (LS3MN2E) of the National School of Arts and Crafts of Rabat and the Technical Support Unit for Scientific Research division of the National Center for Scientific and Technical Research (UATRS-CNRST), Rabat, Morocco.

First of all, I would like to express my most sincere thanks and deep gratitude to my thesis director **Mr. El Mostapha LOTFI**, Professor and Deputy Director in charge of Scientific Research and Cooperation at the National School of Arts and Crafts of Rabat, not only for having supervised this thesis, but especially for his valuable advice, his scientific rigor, his availability and the trust he has shown me throughout these years of work.

I am particularly grateful to **Mr. Boujemaâ JABER**, Co-director of my thesis, head of the UATRS division within CNRST-Rabat, for welcoming me to the materials characterization platform, for believing in me, and for helping me to carry out this work well by giving me all the means to achieve it. Thank you for his kindness and good humor. Thank you also for his advice and support during the period of doubt that I went through.

I would also like to thank **Mr. Mohammed EL MAHI**, Professor at the National School of Arts and Crafts in Rabat, for agreeing to chair the jury of this thesis, and for his availability, his help at all times and for many in-depth discussions.

My gratitude goes also to **Mr. Mounir FAHOUME**, Professor at the Faculty of Sciences of the Ibn Tofail University of Kenitra, for his interest in this work by agreeing to participate in the jury as rapporteur.

I couldn’t miss the chance to thank **Mr. Jamil TOYIR**, Professor at the poly-disciplinary Faculty of Taza of the Sidi Mohamed Ben Abdellah University, for his presence as rapporteur, and for his interest in this work.

I would also like to extend my sincere thanks to **Mr. Noureddine TOUACH**, Professor at the National School of Arts and Crafts of Rabat, who kindly reported this work and participated in the jury.

Special gratitude goes to **Mr. Larbi LAANAB** Professor at the Faculty of Sciences of the Mohammed V University of Rabat, for his precious advices, for his wisdom and guidance. And also, for having agreed to participate in this jury as an examiner, beside the many fruitful and in-depth exchanges which were truly the source of all learning and his willingness to share his knowledge.

My sincere appreciation also goes to **Mr. Abdellah BENZAOUAK**, Professor at the National School of Arts and Crafts of Rabat, who kindly agreed to examine this work and participate in the jury.

Let me also address My gratitude to all the staff of CNRST and in particular to the UATRS team with whom I shared very good moments for their welcome, their daily good humor and for the use of their equipment and their technical assistance.

I cannot forget to thank my family and friends for their love and support, without their company it would not have been easy for me to reach this position where I could attempt a doctorate. Finally, I would like to thank my colleagues at the Laboratory for the exchange we had and the good times we shared.

Finally, I would like to thank all those who contributed directly or indirectly to the completion of this work.

Thank you all

Asmae EL-YAHYAOUI

Résumé

L'énergie joue un rôle majeur dans le monde moderne et contribue de manière significative au développement de l'humanité. Pour répondre à la croissante demande d'énergie et surmonter le problème du réchauffement climatique, de nombreux chercheurs se sont concentrés sur le développement des sources d'énergie renouvelables telles que l'énergie solaire. Dans cette optique plusieurs matériaux ont été étudiés pour être insérés dans les cellules photovoltaïques. Actuellement, les pérovskites hybrides d'halogénures de plomb utilisés comme absorbeurs de lumière dans les cellules photovoltaïques ont suscité un grand intérêt en raison de leurs propriétés optoélectroniques impressionnantes et de leur rendement élevé. Cependant, ils ont également montré certains inconvénients, tels que leur forte dégradation vis-à-vis des conditions climatiques (température, humidité, UV, …) qui influence leur performance.

L'objectif principal de ce travail de thèse est de synthétiser et d'étudier les propriétés physiques, la stabilité aux UV et la compacité des films minces à base de pérovskites hybrides $MAPbX_3$. Nous avons ensuite étudié l'intérêt d'associer un flux d'air chaud au procédé de spin-coating durant de la croissance du film $MAPbCl_3$. Les résultats obtenus dans ce contexte montrent que l'optimisation de la température et de la distance du flux permet de produire des structures cristallines de pérovskite $MAPbCl_3$ ayant un taux de couverture très élevée avec une nucléation homogène et significative. 100 °C et 5 cm sont donc la température et la distance optimales du flux d'air chaud pour une meilleure cristallinité et absorbance associée à une faible concentration de défauts non radiatifs. Dans la deuxième partie, nous avons aussi montré expérimentalement qu'il est possible d'améliorer significativement la stabilité contre les radiations UV de la pérovskite $MAPbI_3$ en modifiant sa composition chimique. Dans ce contexte, l'étude de l'effet de l'incorporation des atomes de chlorure dans la matrice pérovskite $MAPb(I_{1-x}Cl_x)_3$ sur les propriétés structurales, morphologiques et optiques a clairement montré qu'il est possible de rendre cette pérovskite plus stable par rapport à l'irradiation UV lorsqu'au moins 20% du chlorure sont incorporés dans la matrice. A partir de ce taux de chlorure, la structure pérovskite transite de la structure quadratique vers la structure cubique plus stable. Cette transition est à l'origine de la nette amélioration de la stabilité UV de la pérovskite $MAPbI_3$.

Mots-clefs (5): Perovskite; films minces $MAPbCl_3$; flux d'air chaud; revêtement par centrifugation; films minces $MAPb(I_{1-x}Cl_x)_3$.

Abstract

Nowadays it becomes more and more clear to the eye this Major role that Energy plays in the modern world. It contributes significantly to the development of humanity. Hence, to meet the increasing demand for energy and overcome the problem of global warming, the Majority of researchers have set their focus on the development of renewable energy sources such as solar energy. In this regard, several candidate materials have been studied to be implemented into photovoltaic cells. Currently, lead halide hybrid perovskites used as light absorbers in photovoltaic cells have attracted great interest due to their impressive optoelectronic properties and high efficiency. However, they have also shown some drawbacks, such as their strong degradation with respect to climatic conditions (temperature, humidity, UV, …) which influences their performance.

This leads to the main objective of the current thesis, which is to synthesize and study the physical properties, UV stability and its improvement beside the compactness of thin films based on $MAPbX_3$ hybrid perovskites. We then studied the interesting effect of associating a hot air flow with the spin-coating process during the growth of the $MAPbCl_3$ film. In this context, the obtained results show that the optimization of the temperature and the distance of the flow makes it possible to produce crystalline structures of $MAPbCl_3$ perovskite having a very high coverage rate with a homogeneous and significant nucleation. Also, it was shown that 100 °C and 5 cm are therefore the optimal temperature and distance of the hot air flow for a better crystallinity and absorbance associated with a low concentration of non-radiative defects. In the second part, we also experimentally proved that it is possible to significantly improve the stability against UV radiation of the $MAPbI_3$ perovskite by modifying its chemical composition. In this regard, the study of the effect of the incorporation of chloride atoms in the $MAPb(I_{1-x}Cl_x)_3$ perovskite matrix on the structural, morphological and optical properties has clearly shown that it is possible to make this perovskite more stable with respect to UV irradiation when at least 20% of the chloride is incorporated into the matrix. Starting from this Chloride content, the perovskite structure transitions from the tetragonal structure to the more stable cubic structure. This transition is at the origin of the clear improvement in the UV stability of the $MAPbI_3$ perovskite.

Keywords (5): Perovskite; $MAPbCl_3$ thin films; Hot airflow; Spin-coating; $MAPb(I_{1-x}Cl_x)_3$ thin films.

List of abbreviations

Abbreviation	Designation
CNRST	Centre National pour la Recherche Scientifique et Technique
NASA	National Aeronautics and Space Administration
GISS	Goddard Institute for Space Studies
NREL	National Renewable Energy Laboratory
STC	Standard Test Conditions
ETL	Electron Transporter Layer
HTL	Hole Transporter Layer
MA	Methylammonium
FA	Formamidinium
EA	Ethylammonium
DRX	Diffraction de Rayon X
MEB	Microscope électronique à balayage
UV-Vis	Spectroscopie Ultraviolet-Visible
FTIR	Fourier Transform Infrared Spectroscopy
DMSO	dimethylsulfoxide
DMF	N,N-Diméthylformamide
EDS	Energy-dispersive X-ray spectroscopy
JCPDS	Joint Committee on Powder Diffraction Standards)
ASTM	American Society for Testing and Materials
cfm	Cubic foot per minute
wt	weight percent
PV	Photovoltaic
UV	Ultrat Violet
PSCs	Perovskite solar cells
ALD	Atomic Layer Deposition
FC	Front Contact

List of Figures

List of Tables

Contents

General introduction

General introduction

Energy plays a major role in the modern world and contributes significantly in humanity's development. The world's energy demand increased during the recent years due to the increase of both the population and the living standard which are estimated to grow up by 25% in 2050 [1] leading to a rise of the energy cost [2]. Most of this energy comes from conventional fossil resources such as oil, coal and natural gas, which account for 86% of all energy needs and are constantly increasing [3]. These resources are limited and are gradually collapsing, and their cost has a major impact on the socio-economic and political situations of countries [4]. What's more, the massive use of these resources is leading to a flagrant increase in global warming as a result of carbon dioxide emissions. Over the last century, according to NASA space studies (GISS), the Earth's average temperature has risen by around 0.8°C [5]. This has led to a number of drastic changes, such as a rise in sea level (~ 3 mm/year) [6] following the melting of glaciers and the polar ice caps.

In these dangerous circumstances, renewable energies like biomass, wind, and solar power, have emerged as alternative solutions that provide green energy without releasing greenhouse gases. Photovoltaic solar energy is one of the best alternatives, characterized by its high availability and low environmental impact [7]. Since the first solar cell was developed by the American Charles Fritz in 1883, the efficiency of light-to-electricity conversion has increased steadily [5,7]. More recently, thin-film photovoltaic technology based on perovskites has seen an unprecedented emergence, outstripping all other technologies, namely those based on crystalline silicon, GaAs, multi-junction cells and thin films based on CIGS, CdTe, etc. [8].

Perovskite was discovered by Gustav Rose in 1839 as the mineral structure of calcium titanium oxide ($CaTiO_3$). This structure was then studied by the Russian mineralogist Lev A. Perovskite [9], from whom it takes its name. The family of perovskite materials adopts an ABX_3 stoichiometry, where A and B are cations and X is an anion, typically oxygen, halogens or alkali metals [10]. Notably, Morocco exemplifies a shift towards renewables, investing $9 billion to bolster wind, hydroelectric, and solar photovoltaic development [11]. Solar technology has evolved from traditional crystalline Silicon to innovative hybrid perovskite materials, boasting impressive power conversion efficiencies [12]. Since 2009, hybrid perovskites have been used for the first time by the Miyasaka group as an absorber layer in a solar cell with a conversion efficiency of 3.8%. The efficiency of these cells increased very

rapidly, reaching 24.2% in April 2019 [11,12]. Perovskites have excellent optoelectronic properties, such as: high charge mobility, long diffusion length and carrier lifetime [10], low non-radiative carrier recombination rate [8] and wide absorption range [13].

As a result, high-efficiency devices have been developed with a scalable, low-cost technology that can be implemented on an industrial scale. However, certain problems limit the exploitation of the perovskite-based solar cell. These are essentially its poor stability in the face of humidity, UV radiation and high temperature. Added to this is its environmental incompatibility due to the toxicity and contamination associated with water-soluble lead compounds [12-13]. Current research is focused on these concerns, with the aim of achieving a stable, highly efficient, low-cost perovskite-based photovoltaic cell via a simpler synthesis process that can be manufactured on a large scale [14-17]. It is therefore in this context that we have chosen the present subject. On one hand, the aim is to study and demonstrate the benefit of the applied hot air flow parameters, namely, the temperature and distance, on the quality of the elaborated $MAPbCl_3$ thin films and the improvement of structural, morphological, and optical properties of the prepared films. On the other hand, our purpose is to show that the stability of the MAPI perovskite can be improved by the incorporation of Chloride in the structure of $CH_3NH_3Pb(I_{1-x}Cl_x)_3$.

This thesis can be divided into three chapters, in addition to the introduction and general conclusion. An overview of the basic concepts regarding solar energy, photovoltaic effect and the latest developments in hybrid perovskite devices for photovoltaic applications are presented in the first chapter.

In the second chapter, we present the procedures for the synthesis and characterization of thin films based $CH_3NH_3PbX_3$ perovskites. In the first part, we describe all the synthesis processes we have used the spin-coating technique associated to the hot airflow. The second part highlights the characterization methods applied to study the physical, structural and optical properties of the synthesis thin films.

Chapter III is split in two parts which covers the main experimental results for thin films based on $MAPbCl_3$ and $MAPb(I_{1-x}Cl_x)_3$ hybrid perovskites. The first part of this chapter presents the results of the structural, morphological and optical characterizations of the $MAPbCl_3$ hybrid perovskites that we have synthesized, both in powder form and as thin films, as we investigate the advantages of the hot airflow performed during synthesis of $MAPbCl_3$ by spin-coating process and the effect on the different properties of the material. We show that

an airflow heated up to 100°C and placed on a specific distance, significantly improves the structural, optical and morphological properties of the films produced.

On the other hand, the second part presents the obtained results regarding the effect of incorporating chloride atoms into the $MAPb(I_{1-x}Cl_x)_3$ perovskite on its structural, morphological and optical properties when exposed to UV irradiation. In fact, many $CH_3NH_3Pb(I_{1-x}Cl_x)_3$ samples with various Cl ratios have been synthesized and analyzed via XRD, SEM, UV–Vis Spectroscopy and FTIR technics. we demonstrated that it is possible to improve the stability of $MAPbI_3$ under UV light by the integration of adequate chloride concentration into the perovskite structure.

The conclusion underscores the significance of this research in addressing hybrid perovskite deficiencies and outlines future experimental projects, including prototype development for photovoltaic cells.

Chapter I:

State of the art on Photovoltaic Solar cells, Hybrid perovskites and their industrial challenges

I.1. Introduction

The purpose of this chapter is to present the state of the art on hybrid perovskites and Perovskite based solar and their potential applications. Hybrid perovskite (PH) crystals with the chemical formula $(R\text{-}NH_3)_2MX_4$ (2D perovskites), with R an organic group, M a divalent metal such as Pb^{2+} and X a halide ion such as Cl, Br, or I, have attracted the attention of researchers since the 1990s, because of the particular optical properties of these semiconductors, which make them good candidates for incorporation into optoelectronic devices such as OLEDs, and OFETs (Organic Field Effect Transistors) [18,19]. More recently, the perovskite $CH_3NH_3PbI_3$ (3D perovskite) has made a remarkable entry into photovoltaic devices [20,21]. Indeed, over the past two years, work on PHs has led to an explosion in the performance of low-cost solar cells containing them, to the point of competing in the laboratory with silicon cells, due to its rapid evolution of efficiency from 3.1 to 23.7% in April 2019 [22,23]. Currently, scientific research on ABX_3 organo/inorgano metal halide hybrid perovskites is focused on the realization of a highly efficient solar cell, a simpler and less expensive synthesis procedure, as well as the elimination of obstacles related to: stability, commercialization and environmental compatibility. In this regard, the objective of this chapter is to present in a comprehensive manner some general notions on solar energy and the state of the art of hybrid perovskite components used for photovoltaic applications.

Hence, photovoltaic effect description as well as the working principle of a solar cell are introduced. Furthermore, the different photovoltaic technology and generation are discussed in this chapter in order to present a detailed description of hybrid perovskites. For this purpose, we begin by giving a description of hybrid perovskite based-solar cells as well as the synthesis, and deposition method used for their fabrication. Their material properties, structure variations and the important effect of the organic molecule on the material performance will be discussed also in this chapter.

Even with all the above qualities, Hybrid perovskites suffer from a degradation in different environmental conditions. In addition to their infamous toxicity, which are the underlying drawbacks that limit the commercialization of these materials. Here below, we give a deep understanding of the degradation mechanism of hybrid perovskites as well as the potential technologies used to improve the perovskite solar cells stability. Research progress summary on the performance of lead-free PSCs will be also provided in this chapter.

I.2. Solar Cell Main Principle

Photovoltaic (PV) systems are a dependable option for meeting the world's energy demand since they convert solar radiation into electricity. Solar cells, often known as photovoltaic cells, collect solar light and use the photoelectric effect to produce direct current. Through a semiconductor substance that carries electric charges (holes and electrons), the photovoltaic effect enables cells to directly transform light energy from photons into electricity. Electric current will flow through a circuit attached to the electrodes and a potential difference will arise at the electrode terminals as a result of the production of charges. A photovoltaic

electricity generator's working principle is depicted in Figure I.1. Three main mechanisms form the foundation of the photovoltaic effect:

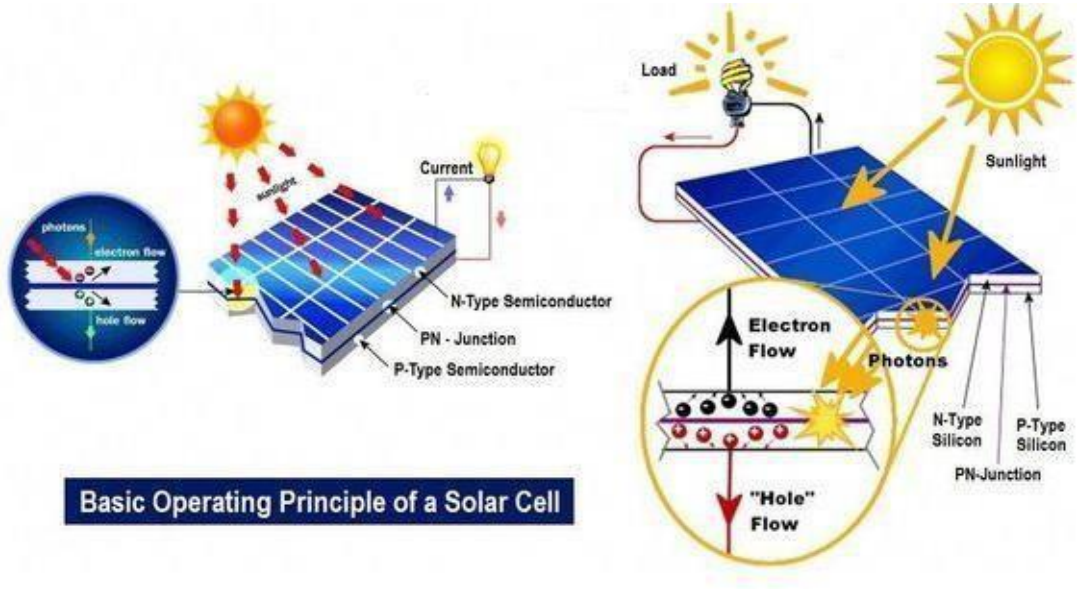

Figure I.1: Schematic representation of a simple photovoltaic cell

I.3. Sun Light absorption and electricity production

The energy of the absorbed photon is represented by the difference between two levels, which is equal to $E_{Ph}= hv= E_f - E_i$. When a photon is absorbed, the electron is excited, moving from a low energy level E_i to a high energy level E_f. The gap energy is referred to as direct if the conduction band maximum and valence band minimum coincide at the same k-vector. Meanwhile, the gap energy is referred to as indirect in the other case. Note that, the energy required for an electron to move from the valence band to the conduction band is known as the energy gap. The electron can pass through this band and enter the conduction band by absorption of a photon with energy greater than the band gap. There is a vacancy in the valence band caused by the electron moving to the conduction band. This void is known as a hole and it functions similarly to an elementary charge particle. Consequently, an electron-hole pair is created.

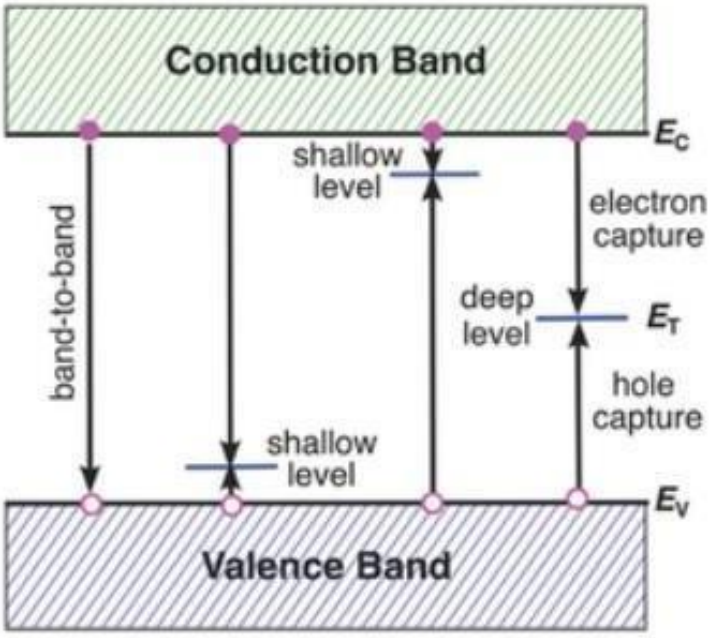

Figure I. 2: Electron-Hole recombination between the Conduction and Valence bands

I.4. Solar energy

The sun is a major source of inexhaustible clean energy for our planet [24]. The distance between the earth and the sun is about 150 million kilometers and the speed of sunlight is 3.108 m/s, so the sun's rays take about 8 minutes to reach the Earth.

The power flux of sunlight reaching the outer edge of the Earth's atmosphere is about 1367 Watts for each square meter; this is called the solar constant. Indeed, the sun is characterized by three types of solar radiation: direct radiation that arrives directly at the Earth's surface, diffuse radiation that is diffused by solid or liquid particles suspended in the atmosphere and global radiation that is the sum of direct and diffuse radiation, this is what is used to operate thermal and photovoltaic solar panels.

Extra-atmospheric solar radiation is also described as an electromagnetic wave whose wavelength extends from ultraviolet 0.2 μm to far infrared 3 μm. As illustrated in figure I.3, this radiation is roughly decomposed into [25]:

• 9% in the ultraviolet band (<0.4 μm).

• 47% in the visible band (0.4 to 0.8 μm).

• 44% in the infrared band (>0.8 μm).

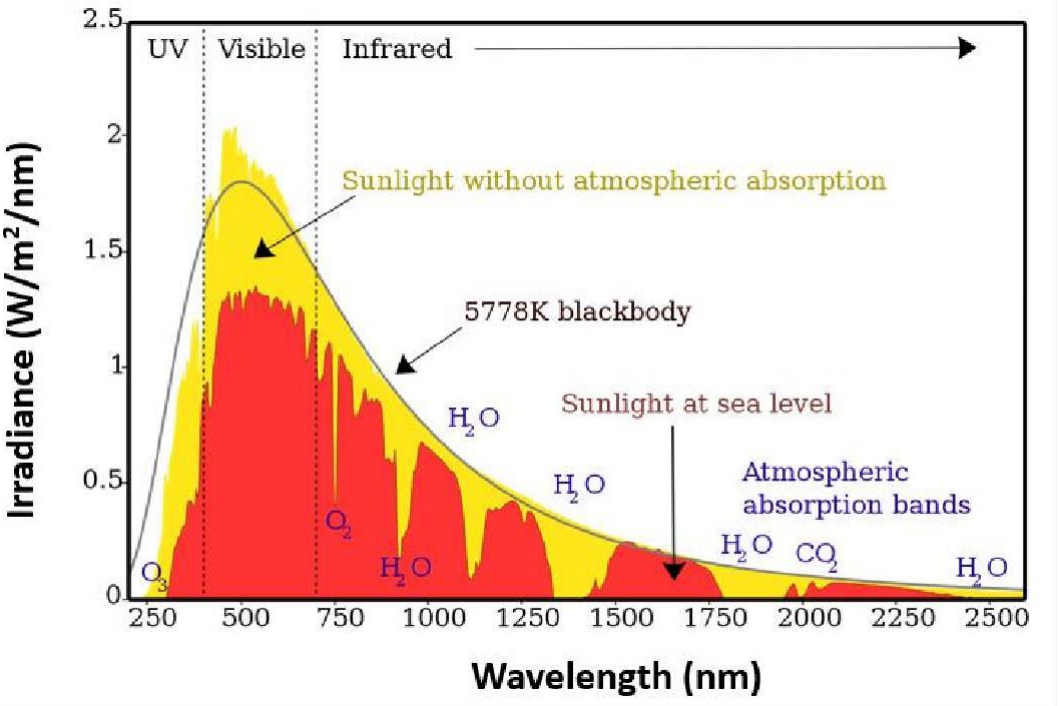

Figure I. 3: Representation of solar radiation irradiation

According to the quantum theory initiated by Max Planck in 1900, then developed essentially by Albert Einstein, solar radiation had only a wave character, but also had the properties of multiple particles called photons (elementary particles). Photons are the carriers of discrete quantities of energy called quanta (quantum of energy). The energy of a photon as a function of its wavelength is given by the following Planck-Einstein equation [26]:

$$E(ev) = \frac{h.c}{\lambda} \qquad \text{(I-1)}$$

Where h is Planck's constant; c is the speed of light and λ is the wavelength.

I.5. Photovoltaic energy

I.5.1. Definition

The word "Photovoltaic" is the combination of two words: "photo", a word of Greek origin meaning light and "voltaic", which comes from "volt" and represents the unit used to measure electrical potential. Also, it is named in honor of the Italian physicist Alessandro Volta, who invented the first electric battery in the 18th century [27]. The photovoltaic effect is the process of transforming light energy from the sun into electrical energy through a solar cell that is made of semiconductor materials. The effect depends on the interaction of photons, with an energy equal to or greater than the band gap of semiconductors.

I.5.2. History of the photovoltaic effect

The photovoltaic effect was demonstrated by the French physicist Antoine Becquerel in 1839, at the age of nineteen [28]. He discovered it by the appearance of a potential between two metal electrodes placed in a conductive solution when they are exposed to light [29,30]. In 1875, the physicist Werner Von Siemens presented, before the Academy of Sciences of Berlin, an article on the photovoltaic effect in semiconductors. Unfortunately, the phenomenon was still considered anecdotal until the Second World War [31]. However, the first functional solar cell was not built until 1883 by the American inventor Charles Fritts. The solar cell is based on selenium platelets which have an extremely low efficiency of the order of 1% [32].

At the beginning of the 20th century, Albert Einstein published the first paper on the photovoltaic effect in 1905 [33]. Later, Ohl realized the first silicon-based p-n junction photovoltaic effect in 1941. He found that the efficiency can reach 6% [34] which was increased to 11% by Bell Laboratories in 1955 [32,33]. Since then, intense research activity has been focused on different materials in order to achieve high-efficiency solar cells, thus the photovoltaic industry has experienced phenomenal growth since the 1960s [35].

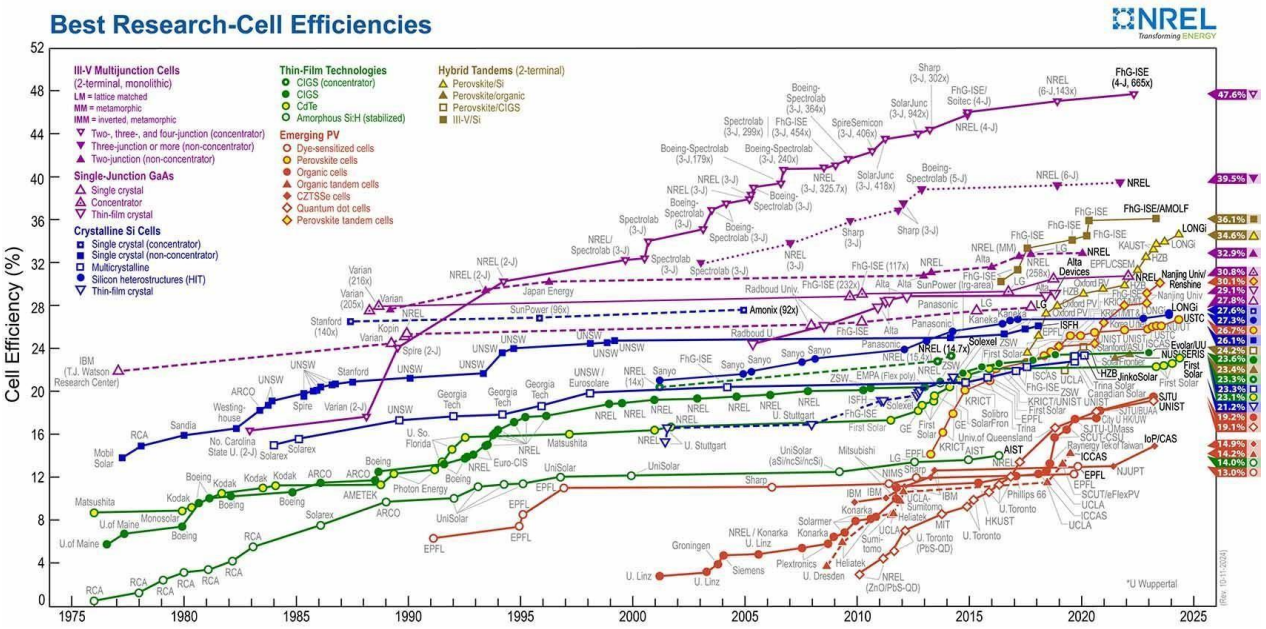

Figure I. 4: Evolution of the efficiency records of different photovoltaic cell sectors (Source: National Renewable Energy Laboratory [36]).

Figure I.4 illustrates the evolution of the world record efficiency of solar cells of different sectors from 1975 to 2024. According to this figure, first-generation solar cells (based on crystalline silicon), which represent 90% of the market, can reach efficiencies of 27.6% (in blue in the figure) [37]. Thin-film sectors that can be classified into three major categories of solar cells based on: amorphous silicon, cadmium telluride (CdTe), and an alloy of copper, indium, gallium and selenium (CIGS) are in full development, whose efficiencies can range from 14 to 22.7%. It should be noted that multi-junction solar cells have higher efficiencies (46% in 2014) among all other solar cell materials. In recent years, part of the research on the efficiency of highly efficient solar cells has been focused on photovoltaic technology based on

thin films of hybrid halide perovskites. In terms of efficiency, the efficiency has been significantly increased from 24 to 26.7% in a very short period of 5 years [38,39].

For comparison, the first-generation solar cells (crystalline silicon), took about 18 years compared to perovskite cells to achieve similar progress. Despite this rapid efficiency development, the poor stability of these perovskite materials against: humidity, high temperature, UV, etc. remains a major problem to achieve excellent efficiency of hybrid perovskite solar cells.

I.6. Parameters affecting the solar cells Performance

The electrodes' gathered charge carriers are capable of operating in an external circuit. Current flowing through a free electron in the conduction band is referred to as electron current. The motion of the hole can also produce current in the valence band. Though they cannot travel as freely as they may in the conduction band, valence band electrons can recombine with neighboring holes to create new holes in their original energy levels with only a slight energy level change. As a result, a hole current is created in the valence band due to the displacement of holes from one location to another. Thus, the photovoltaic effect is ultimately responsible for converting solar energy into electrical energy.

I.7. Hybrid perovskites

I.7.1. Definition

The first perovskite was discovered by A. Kemmerer, during an expedition to the Russian mountains of the Urals in 1839, more precisely at the Achmatovsh mine. Then, the German mineralogist Gustave Rose worked there and dedicated the discovery of this mineral to the Russian politician and mineralogist Lev Alexeievich Perovski (1792-1856), from which the name "perovskite" finally came [40].

Perovskite is a mineral composed of calcium and titanium oxide with the formula $CaTiO_3$, with a cubic morphology, it is a black or red-brown mineral, with a metallic appearance, it is very rare and linked to contact metamorphism.

In 2012, scientists found that some perovskites had good charge separation and migration capabilities, as well as good absorption of sunlight, which could increase the efficiency of photovoltaic cells.

I.7.2. Structural properties

a- Crystal structure

In our study, the nature of the perovskites studied is of the organic/inorganic metal halide (ABX_3) type. The ideal crystal structure of these perovskites generally consists of a five-atom unit cell in a cubic structure as illustrated in figure I.5.a. Indeed, component A is a large organic or inorganic cation that occupies the cuboctahedral sites formed (coordinated) by the

12 nearest X halide ions, while component B is a small divalent metal cation coordinated to six X halide anions forming a regular octahedron (figure I.5.b) [41-43].

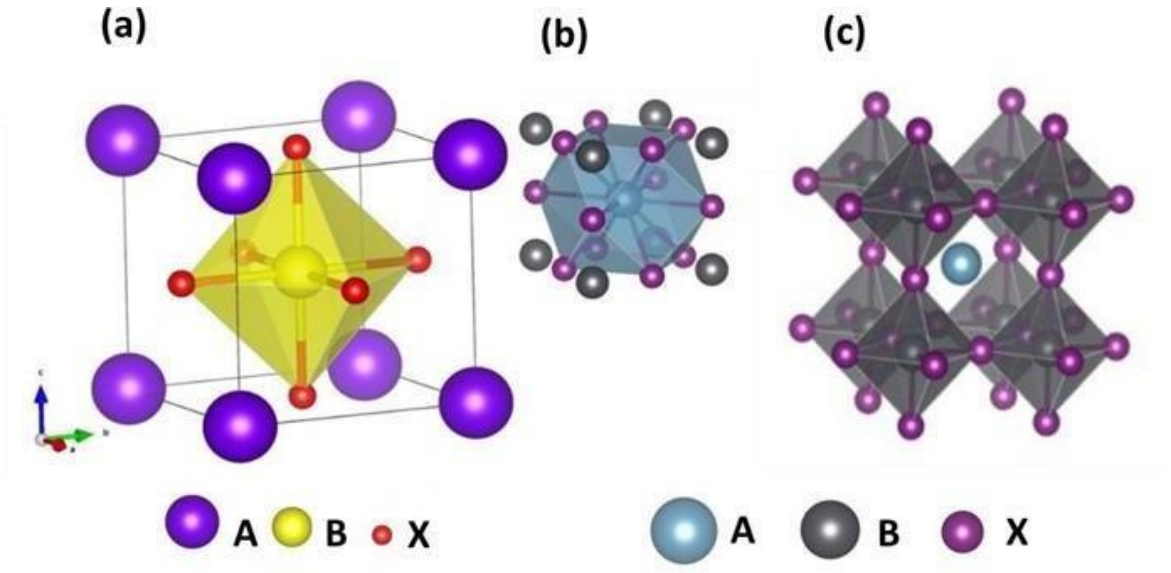

Figure I.5: (a) The general cubic structure of a perovskite. (b) Cubo-octahedral coordination around a cation A. (c) The octahedral coordination around a cation B.

b- Symmetry and chemical composition

Under ideal conditions, in order to maintain a more stable cubic structure and high symmetry of the ABX_3 perovskite, Goldschmidt proposed a tolerance factor (t) that should be close to 1 for oxidized perovskites and could be between 0.813 and 1.107 for halide hybrid perovskites [44,45]. The tolerance factor is defined according to this formula:

$$t = \frac{R_A + R_X}{\sqrt{2}(R_B + R_X)} \quad \text{(I-2)}$$

where R_A, R_B and R_X are the ionic radii of the corresponding ions in the ABX_3 structure.

To complement the tolerance factor criterion, another parameter was developed by Li et al. [46] to predict the formation of the perovskite structure. They used a ratio of the ionic radii of the B and X atoms called the "octahedral factor (μ)", given by the following relation:

$$\mu = \frac{R_B}{R_X} \quad \text{(I-3)}$$

This octahedral factor is well directly correlated with the BX_6 octahedron of the perovskite structure (figure I.5 c). According to this factor, perovskite formation occurs at values greater than 0.442, while below this value, the BX_6 octahedron will become unstable; Thus, the perovskite structure could not be formed [8].

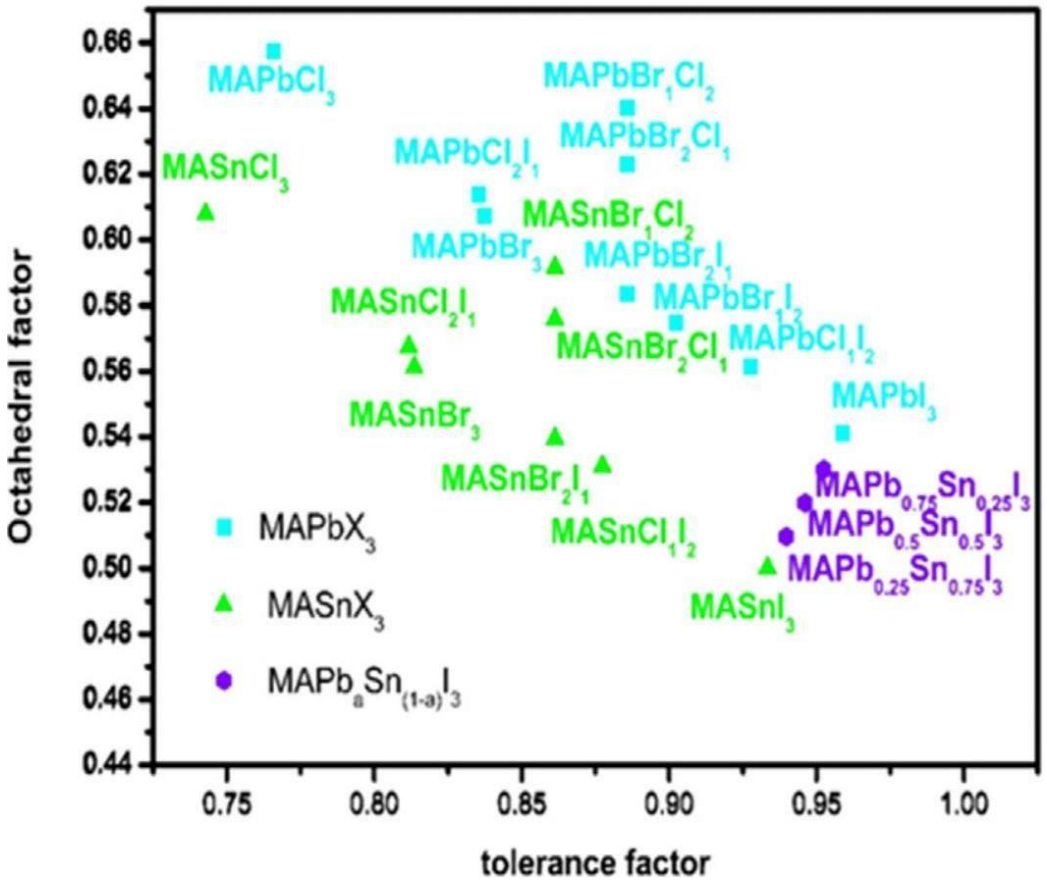

Figure I.6: The two tolerance and octahedral factors of some perovskites.

In general, cubic symmetry provides optimal electronic properties due to the high degree of ionic bonding and high symmetry [8]. According to figure I.6, if the tolerance factor (t) is in the range of 0.89-1.0, the most probable structure is cubic, with tolerance values (t) less than 0.89, the possible structures are tetragonal or orthorhombic of lower symmetries [7,47]. The three-phase crystal structures are illustrated in figure I.7.

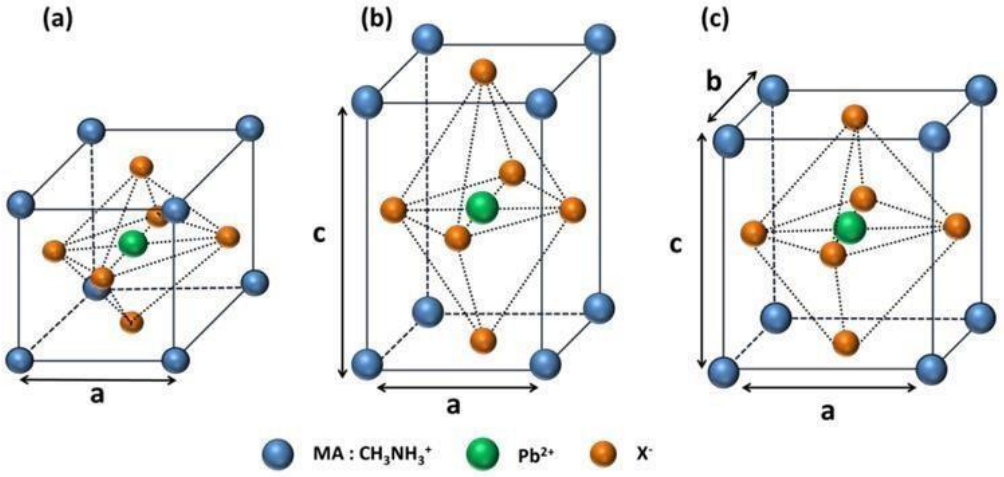

Figure I.7: Possible crystal structures of $MAPbX_3$ perovskites (X=I, Br, Cl): a) cubic, b) tetragonal and c) orthorhombic.

Despite these constraints, structural transitions in response to temperature and pressure are also an important aspect for any given perovskite. As an example, Table I.1 summarizes temperature-dependent structural data of ABX_3 based perovskites (A=MA, FA / B= Pb, Sn / X=I, Br, Cl) [7,48,49].

As presented in Table I.1, for the case of $MAPbI_3$ perovskite, it adopts a tetragonal structure at room temperature. However, this perovskite undergoes a structural transition from tetragonal to orthorhombic phase at T < 162.2 K or cubic at T > 327.4 K. Table I.2 also indicates that the symmetry of the perovskite structure increases with temperature, meaning that $MAPbBr_3$ and $MAPbCl_3$ perovskites form a cubic structure at room temperature [50,8]. In the case of $FAPbI_3$, $FASnI_3$ and $MASnI_3$ perovskites, Table I.1 shows no structural transition at high temperatures, but the noted change concerns the space groups.

Table I.1: Temperature-dependent structural data of some perovskites [8,50,51,52].

				lattice parameters (Å)			
Perovskites	**Temperature (K)**	**Crystal structure**	**Space group**	**a**	**b**	**c**	**Volume (Å)^3**
$MAPbCl_3$	>178.8	Cubic	Pm3m	5.675	5.675	5.675	182.2
	172.9-178.8	Tetragonal	P4/mmm	5.656	5.656	5.630	180.1
	<172.9	Orthorhombic	$P222_1$	5.673	5.628	11.182	357
$MAPbBr_3$	>236.9	Cubic	Pm3m	5.901	5.901	5.901	206.3
	155.1-236.9	Tetragonal	I4/mcm	8.322	8.322	11.832	819.4
	149.5-155.1	Tetragonal	P4/mmm	589.4	589.4	5.861	
	<144.5	Orthorhombic	$Pma2_1$	7.979	8.580	11.849	811.1
$MAPbI_3$	>327.4	Cubic	Pm3m	6.328	6.328	6.328	252.5
	162.2-327.4	Tetragonal	I4/mcm	8.855	8.855	12.659	992.60
	162.2	Orthorhombic	$Pma2_1$	8.861	8.581	12.620	959.5
$MASnI_3$	293	Tetragonal	P4mm	6.230	6.230	6.231	241.88
	200	Tetragonal	I4cm	8.757	8.757	12.42	953.2
$FAPbI_3$	293	Trigonal	P3m1	8.981	8.981	11.00	768.9
	150	Trigonal	P3	17.791	17.791	10.091	507.03
$FASnI_3$	340	Orthorhombic	Amm2	6.3286	8.9554	8.9463	507.03
	180	Orthorhombic	Imm2	12.512	12.512	12.509	1959.2

c- Chemical flexibility

The chemical flexibility of hybrid perovskites lends itself to a wide variety of substitutions on all three ionic components occupied by the A, B and X sites, in order to obtain several configurations with different properties. Here are some of the main substitutions of each site reported in the literature as presented below:

i) A-site

The A-site occupied by an organic cation has shown no direct contribution to the electronic properties due to the weak interaction and negligible overlap of electronic orbitals between the organic components and the inorganic B-X octahedra [53,54]. When the A-site of the perovskite structure is occupied by the small monovalent cations listed in Table I.1, such as: methylammonium (MA), formamidinium (FA), ethalemonium (EA), cesium (Cs), etc., a three-dimensional (3D) symmetry can be obtained [51]. If the A-cation is larger, the 3D symmetry can be perturbed, resulting in a two-dimensional (2D) or one-dimensional (1D) structure with the formulas A_2MI_4 and A_3MI_5, respectively. Therefore, the choice of the appropriate organic cation A is based on its ionic radius, since it must fit between the B-X octahedra to form the ABX_3 structure. From Table 2, it is clear that cations with ionic radii in the range of ~1.6 to ~2.5Å can form stable perovskite structures. For example, the organic cation of methylammonium has an ionic radius of 1.8Å which is well suited for formability with lead and iodine halide to form a $MAPbI_3$ perovskite [55]. However, substitution of MA with a large cation, such as formamidinium (FA), gives a higher symmetry than that of methylammonium [56]. Indeed, $FAPbI_3$ perovskite adopts a trigonal structure at room temperature with a favorable optical band gap (~1.43-1.48 eV, absorption at 840 nm) closer to the optimal band gap of 1.4 eV [57]. However, when the organic component is substituted by an inorganic component having a small size compared to MA, such as cesium (Cs), the tolerance factor becomes lower, hence a weak symmetry. This also leads to a higher band gap (1.73 eV) for $CsPbI_3$ compared to $MAPbI_3$ (1.57 eV).

Table I.2: Ionic radii of the most commonly used hybrid perovskite components

Site	**A**				**B**		**X**			
Ion	EA	FA	MA	Cs	Pb	Sn	I	Br	Cl	F
Ionic radii (Å)	2,3	2,53	1,8	1,67	1,19	1,1	2,2	1,96	1,81	1,33

ii) B-Site

The B-site is a metal cation located at the center of the perovskite structure, which can be occupied by the elements of group 14 of the periodic table with a divalent oxidation state (Pb^{2+}, Sn^{2+}, Ge^{2+}). Lead (Pb) is considered as a more commonly used element for photovoltaic applications, due to its superior performance and stability compared to tin [58]. The use of the latter in the $MASnI_3$ perovskite solar cell shows low photoconversion efficiencies (5 to 6%) due to its low stability in air [59]. Indeed, this instability of $MASnI_3$ perovskite is attributed to the oxidation of Sn^{2+} to more stable Sn^{4+} which is promoted by

humidity, thus producing a volatile SnI_4 compound [7]. However, $MASnI_3$ has a band gap of 1.3 eV allowing a wider light harvesting than that of $MAPbI_3$ (1.6 eV) [55]. Germanium (Ge) has been less studied compared to Pb and Sn, probably due to its highly unstable nature in the Ge^{2+} oxidation state [60]. Recently, several studies have been carried out on metal-part alloys to improve the stability and efficiency of perovskite based solar cells [61–64]. For example, Yuhei Ogomi et al reported that the performance of $MAPb_{1-x}Sn_xI_3$ based solar cells can be significantly improved by substituting 50% of the lead atoms for tin atoms. As a result, an efficiency of 4.18%, an open-circuit voltage of 0.42 V, a form factor of 0.50, and a short-circuit current of 20.04 mA/cm^2 were observed [65]. Additionally, an absorption of light up to the near infrared of ~1050 nm is obtained ($MASnI_3$), indicating a shift of 260 nm compared to the perovskite $MAPbI_3$ [66].

iii) X-site

The X-site is an anion occupied by chemical elements of group VIIA of the periodic table, called halide, such as: iodine, bromine, chlorine and fluorine. The halide anion is considered as the most substituted component in the ABX_3 matrix to provide good optoelectronic properties and excellent stability of the perovskite [10,67]. Traversing along group VIIA (from Cl to I) of the periodic table, the valence band shifts from 3p to 4p and 5p with a decrease in the electron binding energy, thus changes in the band gap upon halide substitution can be obtained [68]. For example, the optical gap of $CsPbI_3$ perovskite can be continuously modulated over the range 1.87 – 3.18 eV through a substitution of I → Br and Br → Cl [69], which allows for attractive coloration and especially bandgap engineering for tandem solar cell design. Furthermore, Silvia et al [70] have shown that chlorine (Cl) doping can significantly improve the diffusion length and carrier lifetime within the $MAPb(I_{1-x}Cl_x)_3$ perovskite layer, thus conferring higher solar cell efficiency, mainly in a planar configuration [71,72]. More recently, our study has shown that it is possible to significantly improve the UV stability of unencapsulated $MAPbI_3$ perovskite by incorporating an optimal chloride fraction of 20%.

I.7.3. Optical properties

As presented in figure I.8, ABX_3 halide hybrid perovskites exhibit higher optical absorption capacity and absorption coefficient, which enables their use in thin-film photovoltaic devices to harvest sufficient solar radiation to achieve higher efficiency. In addition, hybrid perovskites are direct bandgap semiconductor materials [73], which can be continuously tuned over an exceptionally wide range of the solar spectrum from 1.2 to 3.17 eV by varying the chemical composition of the three perovskite components $(MAPb(I, Br, Cl)_3)$ [74,75].

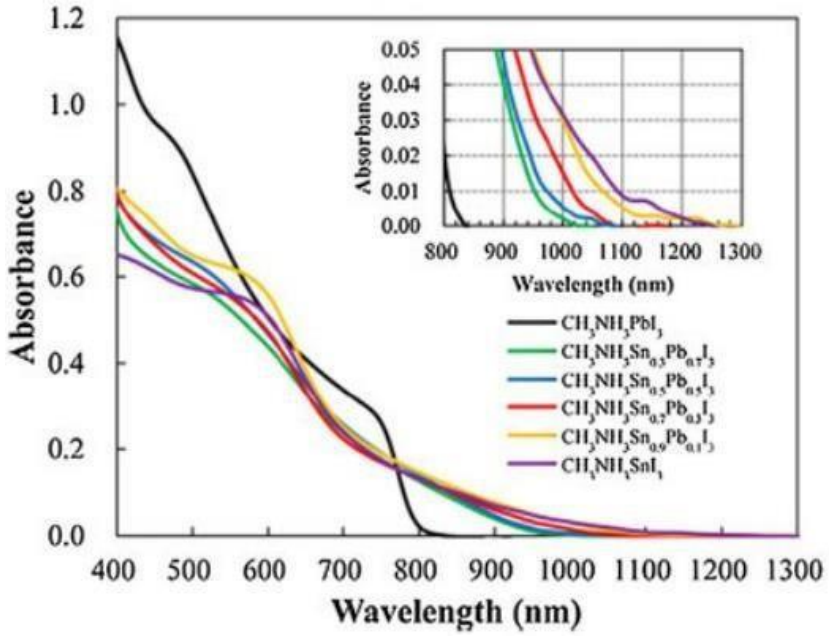

Figure I.8. Absorption spectra for $MAPb_{1-x}Sn_xI_3$ perovskites

As shown in figure I.9, $MAPbI_3$ perovskite exhibits a relatively high absorption coefficient ($> 10^5$ cm^{-1}) in the visible spectrum compared to semiconductors, such as: inorganic thin films (CdT, CIGS, GaAs …) and crystalline silicon (c-Si). In addition, perovskites are able to achieve high efficiencies with a sufficiently thin absorber layer. As an example, a $MAPbI_3$ solar cell with a thickness of 0.3 µm exhibits a maximum efficiency of 21%, while it is only 13% for GaAs solar cells. However, other inorganic absorbers, such as: CdTe, CIGS… must be around 2 µm to achieve similar efficiency [76,77].

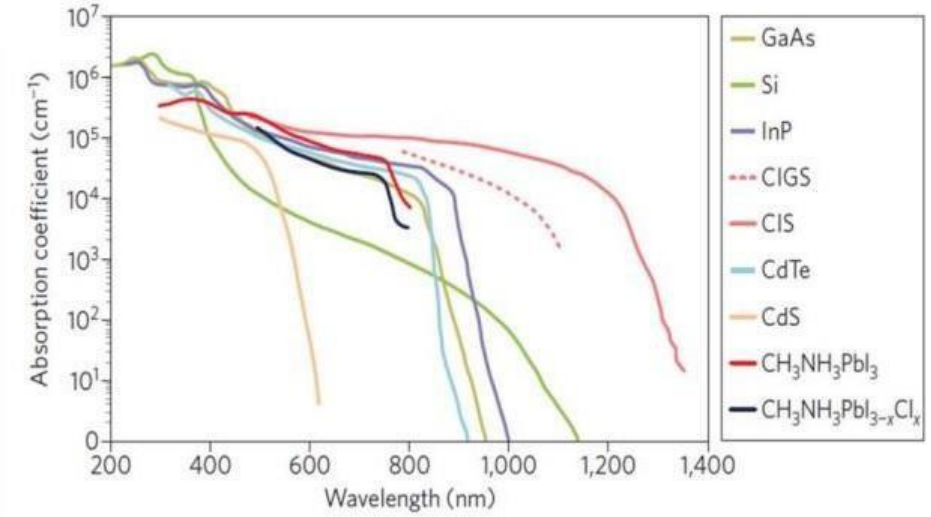

Figure I.9: Absorption coefficient of the $MAPbI_3$ and $MAPb(I_{1-x}Cl_x)_3$ perovskite compared to other absorbent layers

We present in figure I.10 below, the optical gap values of some ABX_3 perovskites reported in the literature. It can be noted that the lowest optical gap energy is 1.3 eV attributed to the $MASnI_3$ perovskite [78,79], while the $MASrI_3$ perovskite is characterized by a wider optical gap of 3.37 eV [41,80,81]. However, the $MAPbI_3$ and $FAPbI_3$ perovskites exhibit a band gap around 1.5 eV which is close to the optimal value of the single-junction solar cell (a-Si, GaAs…), and which guarantees a high absorption of photons up to 826 nm [82,83]. The optical gap energy values corresponding to $CsPbI_3$ and $EAPbI_3$ perovskites are about 1.73 and 2.2 eV respectively, showing an increase in the band gap induced by the change of the A cation [8,56]. Due to the larger ionic radius of I (2.2 Å) compared to Br (1.96 Å) and Cl (1.81 Å), the band gap of $MAPbBr_3$ and $MAPbCl_3$ broadens to 2.27 and 3.37 eV respectively [9]. This consecutive band gap range of halide hybrid perovskites could be used for tandem solar cell applications.

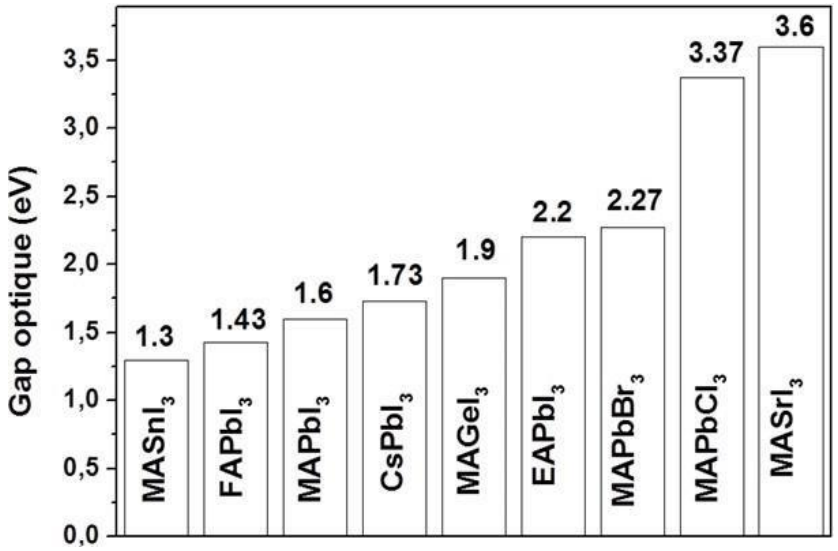

Figure I.10: Optical gap values of some ABX_3 perovskites

I.7.4. Electronic properties

One aspect of ABX_3 perovskite solar cells that helps explain their phenomenal performance is their excellent electronic properties, such as: long diffusion length [9], high charge carrier mobility, ultrafast charge generation [84], and low nonradiative carrier recombination rate [85]. In this section, we present the electronic properties of some ABX_3 halide hybrid perovskites.

a- Charge carrier diffusion length

The charge diffusion length (L_D) parameter is defined as an average distance that the charge is able to travel before recombining. The L_D diffusion length can be calculated from the diffusion coefficient D and the charge carrier lifetime τ using the following formula [86]:

$$L_D = \sqrt{D\tau} \quad \text{(I-4)}$$

L_D is a critical parameter for efficient operation of the solar cell as it has a direct influence on the charge collection efficiency.

According to the literature, several works have been undertaken on the improvement of the charge carrier properties of halide hybrid perovskites [70,71,87]. Recently, Guichuan et al. [55,87], by transient photoluminescence (PL) measurements, reported that the electron and hole diffusion lengths of $MAPbI_3$ are estimated to be ~130 and ~90 nm respectively. However, Samuel et al. found that the diffusion lengths are greater than 1 µm for both electrons and holes if the $MAPbI_3$ perovskite is doped with the chlorine halide anion $MAPb(I_{1-x}Cl_x)_3$ [71]. This indicates that the ETL layer should not be in mesoporous structure to achieve better collection of electrons photo-generated by the $MAPb(I_{1-x}Cl_x)_3$ perovskite. In addition, as demonstrated by Giles et al. [57], the diffusion lengths of $FAPbI_3$ based perovskites are relatively longer than those found in $MAPbI_3$ and shorter than those in $MAPb(I_{1-x}Cl_x)_3$ perovskites. Indeed, they estimated that electrons and holes may have a diffusion length of 177 and 812 nm, respectively. Furthermore, Gede et al. concluded that the $MAPbBr_3$ perovskite has a diffusion length of 201 nm. However, an improvement from 201 to 532 nm is obtained after deposition of a thin layer of aluminum oxide (Al_2O_3) of 4 nm, via a technique called "Atomic Layer Deposition (ALD)" [88].

Other authors have experimentally demonstrated that the $MAPbBr_3$ perovskite synthesized by the "Vapour assisted method" technique can exhibit diffusion lengths of order 1058 and 1083 nm for electrons and holes respectively [89].

Table I.3 gathers the parameters (diffusion coefficient "D", diffusion length "L_D" and lifetime "τ) of the perovskites discussed in the previous paragraph.

Table I.3: Diffusion coefficient (LD), diffusion length and lifetime (τ) values of some halide hybrid perovskites [57,71,87–90]

Perovskites	charge carriers	D ($cm^2.s^{-1}$)	L_D (nm)	τ(ns)
$MAPbI_3$	Electron / Hole	0.017 / 0.011	130 / 90	9.94 / 7.36
$MAPbBr_3$	Electron / Hole	0.2198 / 0.2301	1058 / 1083	50.92 / 50.97
$FAPbI_3$	Electron / Hole	0.004 / 0.091	177 / 812	78.32 / 72.45
$MAPbI_{3-x}Cl_x$	Electron / Hole	0.042 / 0.054	1069 / 1213	2720.86 / 2723.76
$MASnI_3$	Electron / Hole	0.045 /	30 / -	0.2 / -

I.8. Hybrid halide perovskite solar cells

I.8.1. The composition of hybrid perovskite solar cells

Photovoltaic solar cells based on hybrid perovskite are mainly constituted of five essential layers.

Firstly, the most important element is the hybrid perovskite absorbing layer, sandwiched in between the electron transport layer (ETL) and the hole transport layer (HTL). The sequence of HTL and ETL defines the device architecture [91]. When light penetrates the device through the ETL that is deposited above the hybrid perovskite material, the structure is called n-i-p. While in the inverse arrangement it is defined as p-i-n structure. Here p, i, and n define the HTL, perovskite layer, and the ETL respectively. These transporting layers are localized between two electrodes front contact (FC) and back contact (BC) as shown in figure I.11 Unlike silicon-based solar cells, perovskite layers do not need to be doped to allow charge exchange and the production of an electric current. The absorption of photons in hybrid perovskite leads to excitons creation (electron hole pairs) in the heart of the material. The ones on the surface are transported with the HTL and ETL then they join the electrodes, which leads to the production of an electric current. In 2012, and for the first time Etgar et al synthetized a mesoporous $CH_3NH_3PbI_3/TiO_2$ heterojunction and they demonstrated that $CH_3NH_3PbI_3$ can play the role of both light harvester and hole transporter in the PVCs [92]. On the other hand, Lee et al investigated a meso-superstructured $CH_3NH_3PbI_3/Al_2O_3$ [93]. They noticed that its efficiency is comparable to that of TiO_2 even though Al_2O_3 shows a wide band gap that will not allow it to extract electrons from the hybrid perovskite. Through these results researchers realized that the hybrid perovskite itself carried the electrons to the collector electrode.

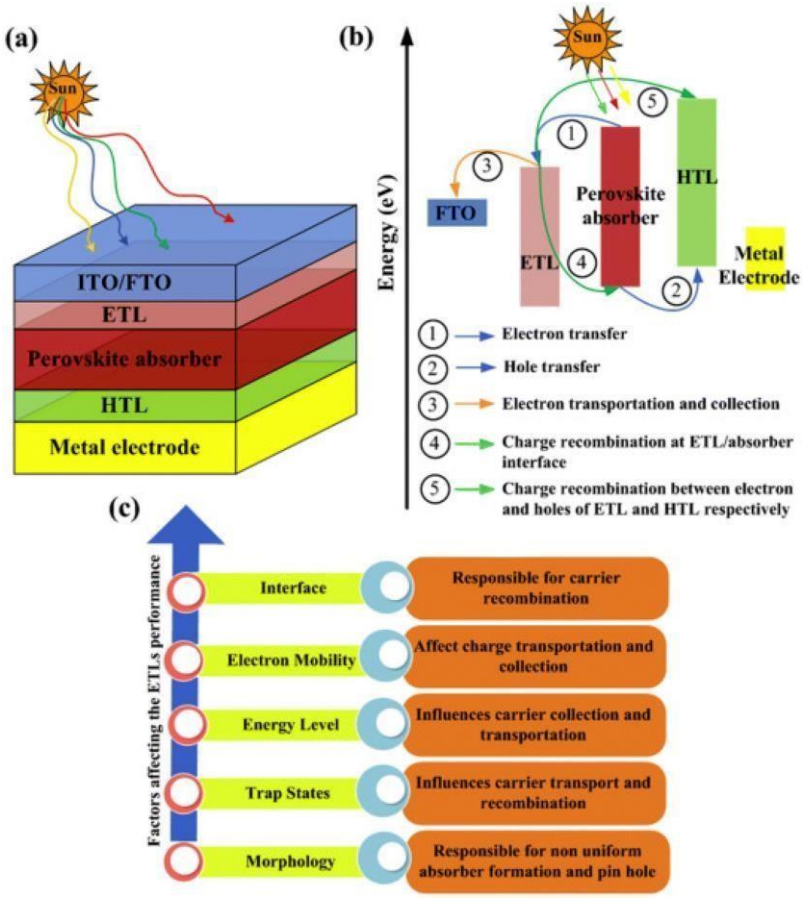

Figure I.11: (a) PSC assembly. (b) Graphic depiction of working and charge transference routes in ETLs of PSCs. (c) Factors influencing the ETL efficiency in PSCs

In this context, a paper has been published demonstrating that the charge carrier mobility in hybrid perovskite depends on different parameters such as the organic's cation orientation and the octahedral symmetry of the inorganic part [94]. Perovskite solar cells can be either mesoporous perovskite solar cells or planar perovskite solar cells [95]. Structures depicting both configurations p-i-n, and n-i-p mesoscopic/planar PSC of the device are shown in figure I.12. Mesoporous p-i-n solar cell structure based on hybrid perovskite was the first to be produced cell among a variety of perovskite cells that were constructed using TiO_2 as a hole-conducting material. It has various advantages namely, a much lower cost and an easier fabrication method [96]. The development of this photovoltaic device has consequently led to the appearance of new planar architecture. The high efficiency of this planar perovskite solar cell can be achieved by controlling the interfaces between the different layers making up the PSC and by varying the electron/hole transporting materials [97].

Nevertheless, planar architectures suffer more than mesoporous devices from the hysteresis behavior. The diminishment of this anomalous behavior is essential for fabricating long-term stable PSCs [98]. In particular, Heo et al were able to fabricate an inverted planar architecture of ITO/PEDOT:PSS/$MAPbI_3$/PCBM/Au offering less hysteresis behavior with a high efficiency [99]. Besides, a key success for the further improvement of the efficiency and long-term stable hybrid solar cells is the development of various synthetic and film deposition techniques to control the morphology and crystallinity of hybrid perovskites.

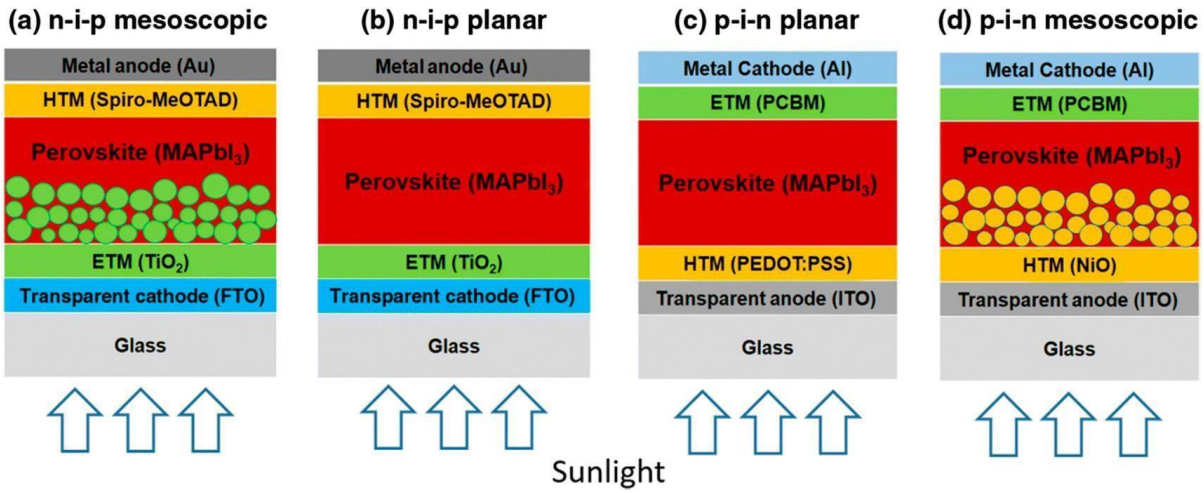

Figure I.12: Diagram displaying the four-layered assemblies of PSCs (a) n–i–p mesoscopic, (b) n–i–p planar, (c) p–i–n planar, and (d) p–i–n mesostructured

I.8.2. The manufacture of hybrid perovskite solar cells

The synthesis, as well as the deposition of hybrid perovskites, are very important elements for the device performance and stability enhancing as well as increasing the efficiency of the solar cell. Synthesis of hybrid perovskites is simple and less expensive compared with the synthesis of III-V or II-VI inorganic semiconductors. It is done by a soft chemistry at room temperature and is relatively unrestrictive [100]. One-step or two-step deposition process can be performed for the hybrid perovskite fabrication as depicted in figure I.13. To obtain 3D perovskites involving the one step method, the ammonium salt CH_3NH_3I and the inorganic salt PbI_2 will be dissolved, then the solution is followed by spin coating to form the molecular crystal [101]. For $CH_3NH_3PbI_3$ perovskite, the solvent used is γ-butyrolactone or dimethylacetamide [102]. However, this approach generally leads to uncontrolled morphological variations, which resulted in low reproducibility of photovoltaic performance. To achieve better control of crystal formation and growth, a sequential deposition method based on the two-step coating was developed [103]. Lead iodide PbI_2 was first loaded by spin coating dimethylformamide on the mesoporous titanium dioxide film and then exposed to a solution of CH_3NH_3I in isopropanol; after annealing the solution, the formation of the final perovskite pigment which penetrated the porous TiO_2 film is obtained. Furthermore, hybrid perovskite layers can also be created using MA gas as precursor [104]. In this process CH_3NH_2 gas in the presence of H_2O from air are exposed to a pristine PbI_2 thin film, resulting in the reaction of the MA molecules with the PbI_6^{4-} octahedral forming a high-quality, uniform $CH_3NH_3PbI_3$ [105]. For mixed halide hybrid perovskite, solvothermal synthesis method is highly advised as an approach for easy synthesis of this type of hybrid perovskite [106]. Further, the fabrication process of hybrid perovskite PVCs can be involved based on other techniques including, vapor assisted, solvent engineering, hot casting, and direct dropping. Recently, the synthesis of high-quality organic inorganic hybrid perovskite films using green solvent engineering has been adopted for a safe environment [107]. The vapor assisted synthesis method can help to achieve a steady enhancement of perovskite solar cells performance by a complete covering of the surface to avert low-resistance shunting paths

between the n and p type contacts [108]. Low-pressure vapor-assisted technique is used also in the formation of the multidimensional 2D/3D organometallic halide perovskite [109]. The presence of defects states in hybrid perovskite films affects the stability of the device which, in return, affects the growth of the power conversion efficiency. Future studies on the synthesis process of this material have to provide essential regard to the defect states and grain-boundary passivation of hybrid perovskite films for high-performance heterojunction solar cells.

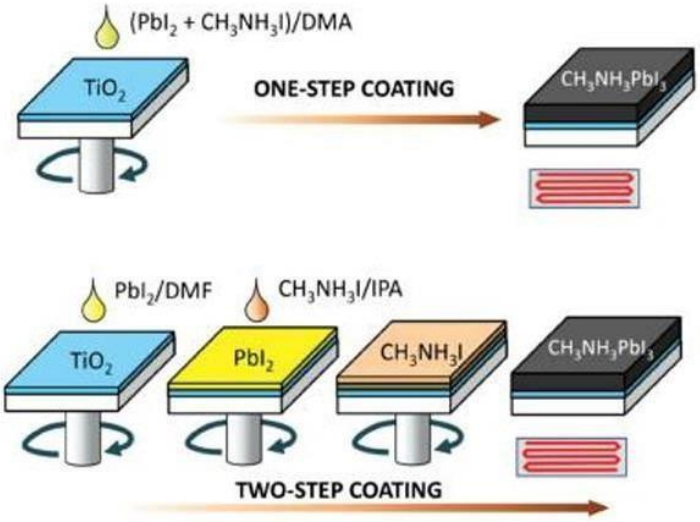

Figure I.13: One-step deposition and two-step deposition of solution processing technique

I.8.3. Evolution of the efficiency of the hybrid perovskite solar cells

Recently, perovskite solar cells represent a new class of conventional photovoltaic technologies. In 2009, Miyasaka et al. realized the first perovskite solar cell by replacing organic dyes (figure I.14.a), usually used as an absorber in the photoelectrochemical solar cell, with the perovskite absorber layer $MAPbI_3$ in a solar cell, called Graetzel cell (figure I.14.b) [110–112], which exhibited an efficiency of 3.9%. Subsequently, Park et al. [113] produced a solar cell based on perovskite nanoparticles in 2011; this achieved an efficiency of 6.5%. However, $MAPbI_3$ perovskite nanoparticles are very unstable in liquid electrolyte due to their rapid dissolution, leading to rapid performance degradation [111,114]. This degradation resulted in the replacement of the liquid electrolyte by a layer called SPIRO-OMeTAD, which acts as a solid hole transporter (HTL) (figure I.14.b). Consequently, this improved the stability of the perovskite solar cell with an efficiency of 9.7%.

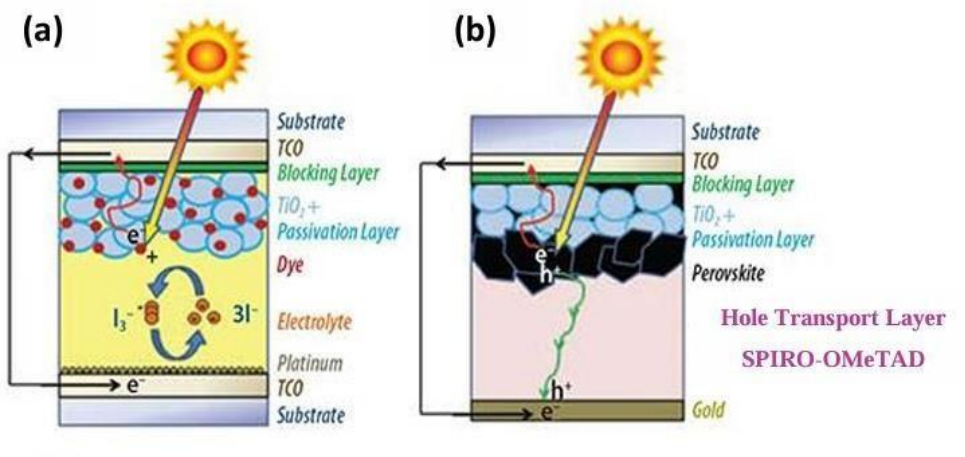

Figure I.14: Comparison between: a) Photosensitive pigment solar cell (Grätzel cells) and b) perovskite solar cell where the liquid electrolyte was replaced by the SPIRO-OMeTAD layer

In 2012, Snaith et al. observed an increase of a few millivolts in Vco via a replacement of the TiO_2 mesoporous layer (ETL) by an insulating layer based on alumina Al_2O_3, leading to an improvement in the efficiency of the solar cell to 10.9% [115]. As illustrated in figure I.15.a, this cell is called a "meso-superstructured solar cell" because the alumina Al_2O_3 layer only acted as a scaffold layer [116]. Indeed, the photoexcited electrons are supposed to be transported through the thin perovskite layer until they are collected by the planar TiO_2-coated electrode (figure I.15: a and b) [115], because electrons cannot be injected into Al_2O_3 [116].

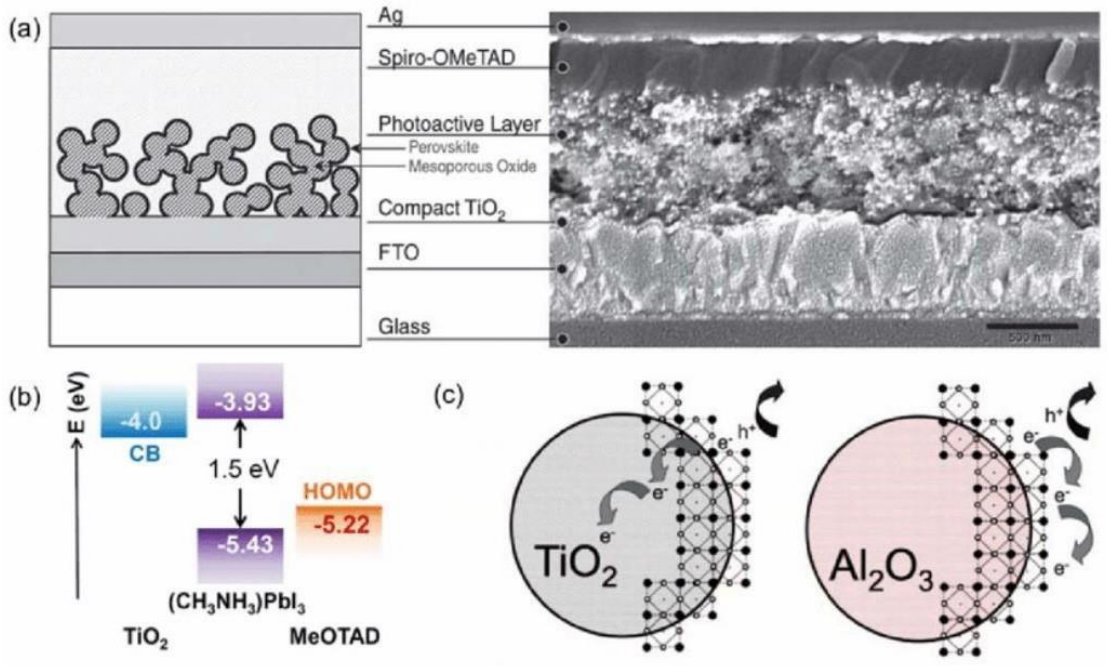

Figure I.15: Schematic illustrating of: (a) mesoporous perovskite solar cells (b) Relevant energy levels in the mesoporous TiO_2 perovskite solar cells and (c) charge transfer and charge transport in a perovskite TiO_2 solar cell and a non-injecting Al_2O_3 based solar cell

Another success of the efficiency of the perovskite solar cell was reported by Seok et al in 2013; They reported that the efficiency can reach 16.2% by using a halide alloy $MAPb(I_{1-x}Br_x)_3$ (10-15% of Br) with a polytriarylamine (PTAA) as a hole carrier [7]. At the end of November 2014, Seok et al. developed a solar cell with an efficiency of 20.1%. This efficiency improvement was achieved by a combination of two organic components based on formamidinium (FA) and methylammonium (MA) in the perovskite structure $(FAPbI_3)_{1-x}(MAPbBr_3)_x$ [111,117,118].
More recently, the National Renewable Energy Laboratory (NREL) officially reported that the efficiency of the perovskite-based solar cell is 26.7% by 2024 [119].

I.9. Stability of hybrid halide perovskites

In light of the outstanding properties and high efficiencies experienced by hybrid perovskite solar cells, their long-term use is hampered by their instabilities and rapid degradation under different exposures, such as: humidity [67], UV irradiation [85] and high temperature [120]. According to the literature [121,122–126], the most susceptible perovskites to degradation are ABX_3^-based, such as: (A = MA or FA; B = Pb or Sn and X = I or Br). In fact, the stability of these materials strongly depends on the engineering of the chemical composition. Moreover, this instability is usually manifested by changes in the structural, optoelectronic, morphological, and colorimetric properties, mainly attributed to their decomposition into the PbX_2 phase, causing a drastic degradation of the power conversion efficiency of perovskite solar cells [127,122].

Recently, many studies have been devoted to solving the problems related to perovskite stability which are considered as the main challenge for future research. In this section we present some approaches and progress reported in the literature on perovskite stability under the effect of: humidity, UV irradiation and high temperature.

I.9.1. Stability under humidity effect

According to the literature, among the most sensitive perovskites to humid atmosphere is $MAPbI_3$ based [128,129]. Indeed, some works [67,130] have shown that 20 days exposure under relatively high humidity (>55%) causes the efficiency of the $MAPbI_3$ based perovskite solar cell to drop by about 3%. The decomposition or degradation of the $MAPbI_3$ perovskite can be confirmed by the appearance of a PbI_2 diffraction peak in the DRX diagram. The mechanism of the possible decomposition of this perovskite is described according to the following equations (1 to 4):

$$CH_3NH_3PbI_{3\,(s)} \overset{H_2O}{\longleftrightarrow} PbI_{2\,(s)} + CH_3NH_3I_{(aq)} \quad (1)$$

$$CH_3NH_3I_{(aq)} \leftrightarrow CH_3NH_{2(aq)} + HI_{(aq)} \quad (2)$$

$$4HI_{(aq)} + O_{2\,(g)} \leftrightarrow 2I_{2(s)} + 2H_2O_{(l)} \quad (3)$$

$$2HI_{(aq)} \overset{h\nu}{\leftrightarrow} H_{2\,(g)} \uparrow + I_{2\,(s)} \quad (4)$$

Equation (1) shows that upon contact with moisture, the MA ion ($CH_3NH_3^+$) is released from the $MAPbI_3$ perovskite crystal due to its hygroscopic nature [131,132], leading to decomposition into PbI_2 and MAI. Then, MAI can decompose into aqueous methylamine ($CH_3NH_3^+$) and hydroiodic acid (HI) in the film (Equation 2). Similarly, HI could be transformed in two different ways, either into I_2 and H_2O via the redox reaction in the presence of oxygen (Equation 3), or into I_2 and H_2 via a photochemical reaction (Equation 4) induced by UV radiation [8,14,49]. Finally, the total decomposition of the perovskite makes the PbI_2 crystalline phase the final product of the reaction [131].

Recently, several approaches have been innovated to stabilize $MAPbI_3$ perovskite against humidity. Zheng et al. [132] demonstrated that efficient humidity stability of solar cell can be achieved via the insertion of a hydrophobic pentafluoro benzenethiol ($HS\text{-}C_6F_5$) molecular layer at the $MAPbI_3$/HTL interface; this layer can prevent the infiltration of H_2O molecules into the perovskite. In 2016, Yang et al. [133] proved that hydrophobic alkylammonium cations can be assembled on the surface of $MAPbI_3$ perovskite as an efficient water-resistant layer. This has largely contributed to successfully blocking any accessible leakage of water droplets or H_2O molecules, providing more effective protection of the perovskite under relatively high humidity (90 ± 5%) for 30 days. Another way to prevent degradation is reported by B. Li et al. [67]. They concluded that the incorporation of bromide atoms into the $MAPb(I_xBr_{x-1})_3$ matrix may play a critical role in improving the stability of the perovskite against humidity. The enhanced stability is mainly attributed to a structural transition from a tetragonal structure to a more stable and compact cubic structure.

I.9.2. Stability under temperature

It is well known that exposure of perovskite to high temperatures can also lead to degradation of its stability [134-136]. For example, as reported by Philippe [137], annealing of $MAPbI_3$ perovskite in vacuum at a temperature of 200 °C or higher can cause the N/Pb and I/Pb ratios to drop to 0 and 2, respectively. This shows that the resulting phase is composed of 100% PbI_2, thus indicating that $MAPbI_3$ perovskite is not stable at temperatures of the order of 200 °C. The decomposition reaction suggested by these authors [137] is as follows:

$$CH_3NH_3PbI_{3\,(s)} \leftrightarrow CH_3NH_{2\,(g)} \uparrow + HI_{(g)} \uparrow + PbI_{2\,(s)}$$

Furthermore, Zhun Yao et al. [138] demonstrated by thermogravimetric analyses that $MASnI_3$ based perovskite has superior thermal stability compared to $MAPbI_3$ because it thermally decomposes at a temperature of 240°C. According to the work of Dmesso et al. [139], the possible decomposition reaction of $MASnI_3$ is as follows:

$$CH_3NH_3SnI_{3\,(s)} \leftrightarrow CH_3NH_{2\,(g)} \uparrow + HI_{(g)} \uparrow + SnI_2$$

Sigalit Aharon et al. [140], made a study of the effect of annealing temperature on $FAPbI_3$, $MAPbI_3$ and $FA_{0.5}MA_{0.5}PbI_3$ perovskites. They concluded that the optimum temperature to achieve good morphology of $FA_{0.5}MA_{0.5}PbI_3$ perovskite is 175 °C. However, a degradation of the structure with a noticeable change in the color of $FAPbI_3$ and $MAPbI_3$ perovskite (figure

I.16) takes place at temperatures of 290 °C and 230 °C respectively. While $FA_{0.5}MA_{0.5}PbI_3$ perovskite starts to decompose at a temperature of 300 °C [141].

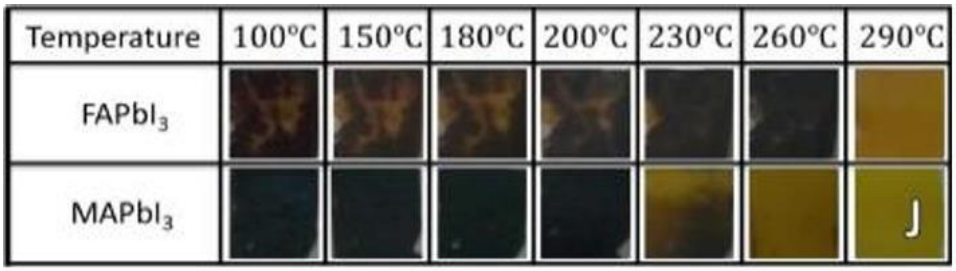

Figure I.16: Color variation of $FAPbI_3$ and $MAPbI_3$ perovskites as a function of temperature

In order to improve the thermal stability of perovskites, several approaches have been reported in the literature. For example, David et al. [142] showed that the $MAPb(I_{0.6}Br_{0.4})_3$ perovskite reveals a rapid degradation after 6 h of annealing at 130°. However, a substitution of MA by a $Cs_{0.17}FA_{0.83}$ alloy, with a fixed halide fraction, does not show any degradation or color change under the same processing conditions.

I.9.3. Stability under UV irradiation effect

In a $MAPbI_3$ perovskite solar cell, among the most commonly used photoanodes (ETL) is the one based on a compact/mesoporous layer of TiO_2. However, as reported by several researchers [52,143], TiO_2, with an optical gap of 3.20 eV, acts as a typical photocatalyst to oxidize water to produce hydroxyl radicals as well as to oxidize organic matter. Some studies [49,52], have shown that the solar cell based on $MAPbI_3$ perovskite and TiO_2 exposed to UV light for 12 hours, undergoes a drastic degradation in the $MAPbI_3/TiO_2$ interface. This degradation is likely attributed to the photocatalytic effect of the TiO_2 layer on the $MAPbI_3$ perovskite. Ito et al. [144] proposed a mechanism that can explain the process of perovskite degradation under UV. This mechanism is simplified by chemical equations (1 to 3) and schematized in figure I.17.

$$2I^- \leftrightarrow I_2 + 2e^- \quad (1)$$

$$3CH_3CH_3^+ \leftrightarrow 3CH_3NH_2 \uparrow + 3H^+ \quad (2)$$

$$I^- + I_2 + 3H^+ + 2e^- \leftrightarrow 3HI \uparrow \quad (3)$$

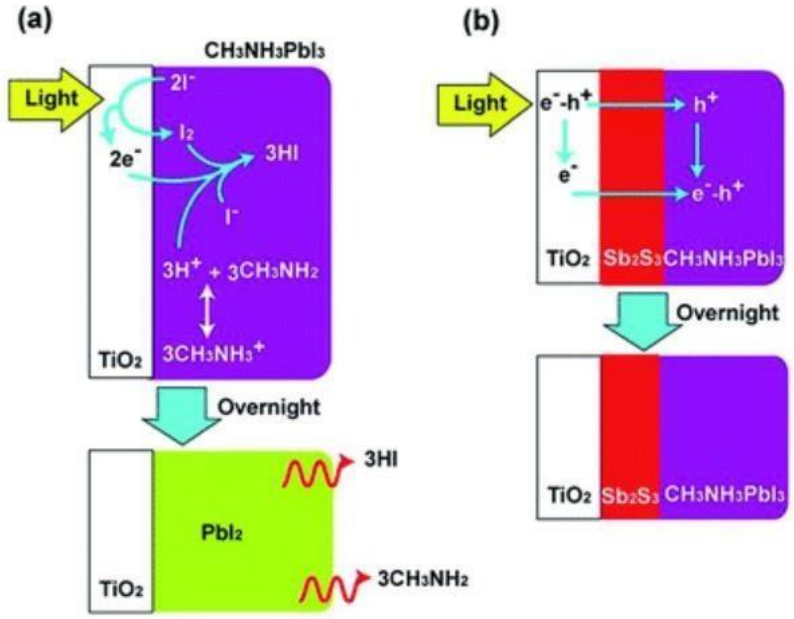

Figure I.17: Sketch maps of perovskite degradation against light exposure in the structure of (a) $TiO_2/CH_3NH_3PbI_3$ and (b) $TiO_2/Sb_2S_3/CH_3NH_3PbI_3$

Indeed, the perovskite crystal $CH_3NH_3PbI_3$ is composed of $CH_3NH_3^+$, Pb^{2+} and I^- ions. According to equation (1), after photoexcitation of the TiO_2 layer by UV irradiation, hole generation is obtained. These can extract electrons from I^- at the TiO_2/perovskite interface, causing distortion of the perovskite structure, thus leading to the formation of I_2 [143]. Although the dissociation constant (pKa) for the hydrolysis reaction of the methylammonium ion component ($CH_3NH_3^+ + H_2O \leftrightarrow CH_3NH_2 + H_3O^+$) is 10.8, the equilibrium tends to shift to the left, but the incessant elimination of hydrogen ion accompanied by the evaporation of CH_3NH_2, due to its low boiling point (17 °C) drives the reaction forward (Equation 2) [8]. Finally, the electrons extracted at the TiO_2 / $MAPbI_3$ interface can return to reduce I_2 and form the volatile component of HI (Equation 3) [8,49]. Therefore, the evaporation of CH_3NH_2 and HI leads to the appearance of the final component PbI_2 according to the following chemical equation [144]:

$$CH_3NH_3PbI_3 \leftrightarrow PbI_2 + CH_3NH_2 \uparrow + HI \uparrow \qquad (4)$$

In order to overcome the UV instability of $MAPbI_3$ perovskite in solar cell, Ito et al. [144] demonstrated that the insertion of a Sb_2S_3 based blocking layer at the $TiO_2/MAPbI_3$ interface can limit the photocatalytic effect of the TiO_2 layer on the perovskite. Indeed, this blocking layer was able to quench the reaction of I^- and I_2 on the TiO_2 surface, as shown in figure I.18.a. Therefore, the extraction and transport of electrons from the perovskite layer by TiO_2 is perfectly done without distortion of the $MAPbI_3$ perovskite structure. figure I.18.b shows the variation of the solar cell efficiency upon exposure to UV light for 12 h (AM1.5 - 100 mW cm^{-2}) with and without the use of the Sb_2S_3 blocking layer. Using this layer, figure I.18.b clearly shows that it is possible to significantly maintain the solar cell efficiency under long-term UV irradiation.

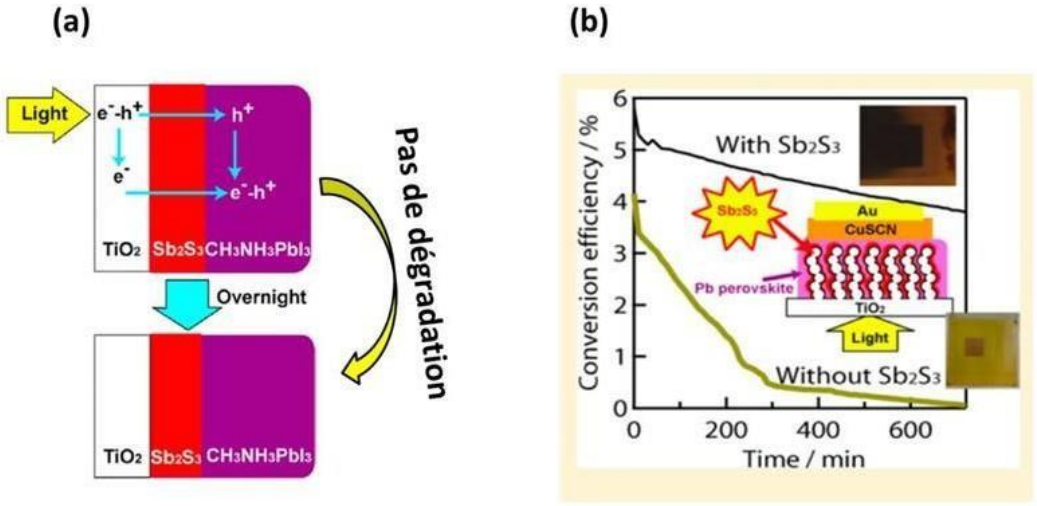

Figure I.18: a) Schematic of the insertion of a Sb_2S_3 blocking layer at the TiO_2/$MAPbI_3$ interface. b) Variation of the efficiency of the $MAPbI_3$ perovskite solar cell with and without the use of Sb_2S_3 during UV exposure [144]

Other studies [52,145] have shown that UV stability can be improved by adding a UV filter layer that absorbs UV light and transmits only visible light, thus effectively preventing UV rays from reaching the TiO_2 film. Furthermore, Snaith et al. [145] have demonstrated that the Al_2O_3 scaffold can be used as an alternative solution to replace the TiO_2 mesoporous to achieve better stability of perovskite at high levels of UV light exposure. Thus, among the objectives of our research work is to demonstrate the possibility of improving the UV stability of perovskite by incorporating an optimal chloride fraction.

I.10. Conclusion

This first chapter was devoted to the presentation of the state of the art of photovoltaic solar energy and more particularly on the hybrid halide perovskites ABX_3 used as absorbent layers in solar cells. Indeed, we presented in detail the structural, electrical and optical properties of the ABX_3 perovskite components which make it a very attractive material for photovoltaics. We have also seen in this part that the technology of hybrid perovskite solar cells has experienced an astonishing emergence due to their rapid evolution of efficiency from 3.1% to 24.2% since 2009 to 2019. This has mainly been achieved on the one hand thanks to the chemical flexibility of these ABX_3 hybrid perovskites which lend themselves to a wide variety of substitutions on all sites: A, B and X, which has made it possible to achieve several configurations with attractive optoelectronic properties. On the other hand, this rapid evolution has been achieved thanks to different solar cell architectures developed, such as: mesoporous and planar inverted or regulated. However, despite this incredible evolution of efficiency, we have cited in this chapter some problems of these hybrid halide perovskite materials related to their long-term instability under different exposures, such as: humidity, UV irradiation and high temperature. Furthermore, we have detailed some approaches developed in the literature on the improvement of this instability of hybrid perovskites.

Chapter II:

Synthesis procedures and characterization techniques

II.1 Introduction

Many techniques can be used to make thin films of different types of materials, such as: perovskites, transparent oxides and chalcogenides, etc. In fact, these deposition techniques fall into two categories:

i) Chemical processes that are based on chemical reactions in the liquid or vapor phase.

ii) Physical processes involving mechanical, electromechanical or thermodynamic executions to form a thin layer of solid.

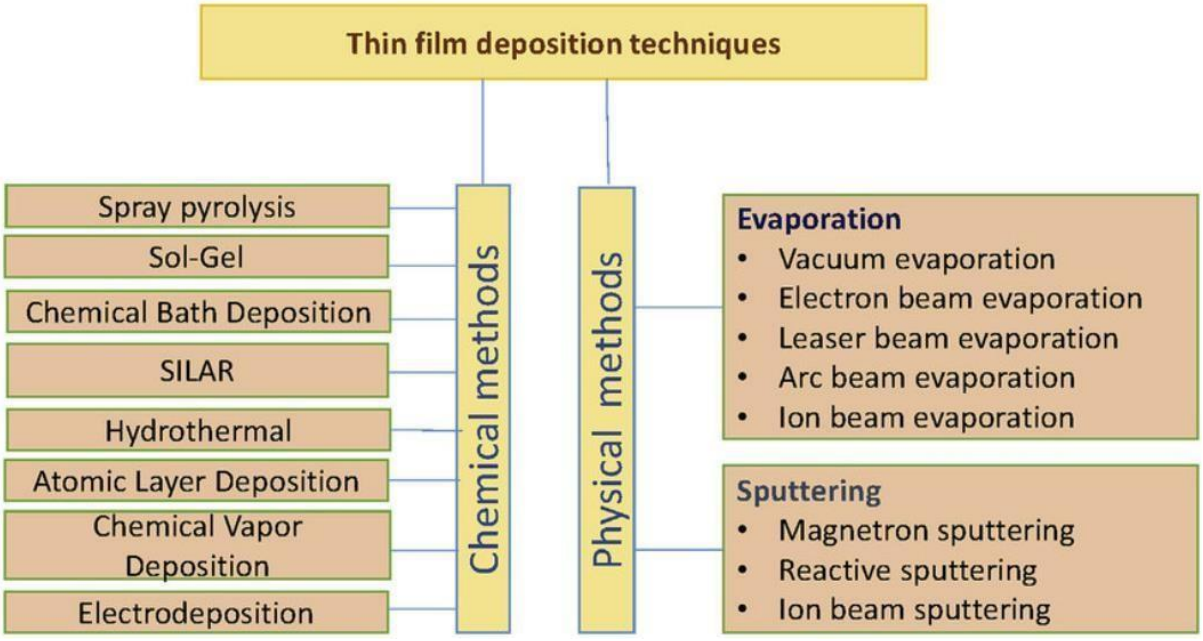

Figure II. 1: General techniques and processes for deposition of thin layers

In this chapter, we will present the synthesis and characterization techniques of thin layers based on hybrid perovskite $CH_3NH_3PbX_3$ (X=I, Br, Cl). The first part will be devoted to the description of the using synthesis processes in our studies used, namely: the gel-soil by centrifugation (spin-coatting) for synthesizing thin films of hybrid perovskites. Then we will also describe the processes performed on the developed thin films, specifically thermal blowing and UV irradiation. The second part is devoted to the exposition of the principal and interest of different characterization techniques that we have used to explore the structural, optical and morphological properties of the obtained thin films. Indeed, the characterization techniques used are: X-ray diffraction (XRD), scanning electron microscopy (SEM), UV-Vis spectrophotometry and the fourier transforms infra-red spectrophotometer (FTIR).

II.2. Synthesis procedures of hybrid perovskites $MAPbX_3$ (X=Cl, Br, I)

II.2.1. Substrates preparation

The thin film deposition of hybrid perovskites was carried out on glass substrates. Before each deposition, the glass substrates have undergone a thorough cleaning to remove any trace of

grease or dust for the purpose of achieving good adhesion of the deposit on the substrate. The process adopted for cleaning substrates is based on the following steps:

- Degreasing with detergent, then rinsing with distilled water.
- Wash in an ultrasonically activated acetone bath for 10 min.
- Wash in an ultrasonically activated ethanol bath for 10 min.
- Rinse in a bath of ultrasonically activated distilled water for 10 min.
- Drying in an oven at 60°C.

In this work, the spin-coating technique was used to deposit thin films of $MAPbX_3$ (X = Cl, Br, I). These can be performed by two different methods: Direct preparation method and Indirect preparation method.

II.2.2. Direct preparation method

The implementation of this method is divided into three stages, namely: (a) preparation of the perovskite powders, (b) dissolution of these perovskite powders and (c) deposition of the perovskite films.

a- Preparation of $MAPbX_3$ perovskite powder (X=I, Br, Cl)

This step consists firstly of preparing a solution A containing a mixture of 0.30 mole of hydrogen halide HX (X=I, Br or Cl) and 0.30 mole of methylamine CH3NH2 (33% wt. in absolute ethanol) in a round bottom at 0°C for 2 hours under magnetic agitation. Then another solution B containing 0.030 mole of lead nitrate ($Pb(NO_3)_2$) dissolved in 50 ml of distilled water was prepared. After, the two solutions (A and B) were heated separately to 80°C in the water bath, then solution (B) was added drop by drop to solution (A) under magnetic stirring of 700 tr/min. A few seconds later, the crystalline powders of perovskites were formed and precipitated, black for perovskite $MAPbI_3$, orange for perovskite $MAPbBr_3$ and white for perovskite $MAPbCl_3$. The liquid supernatant and the precipitated powder of the perovskite are then separated by centrifugation, followed by washing with absolute ethanol and then diethyl ether. Finally, the perovskite powders are dried overnight in an oven at 60°C.

The formation of the perovskite powders $MAPbI_3$, $MAPbBr_3$ and $MAPbCl_3$ can be described by the following chemical equations:

$$CH_3NH_2 + 3HI + Pb(NO_3)_2 \rightarrow CH_3NH_3PbI_3 + 2NO_3^- + 2H^+ \quad (1)$$

$$CH_3NH_2 + 3HBr + Pb(NO_3)_2 \rightarrow CH_3NH_3PbBr_3 + 2NO_3^- + 2H^+ \quad (2)$$

$$CH_3NH_2 + 3HCl + Pb(NO_3)_2 \rightarrow CH_3NH_3PbCl_3 + 2NO_3^- + 2H^+ \quad (3)$$

b- Dissolution of MAPbX3 perovskite powders (X=I, Br, Cl)

This step involves dissolving each powder in a dimethylsulfoxide (DMSO) solution to prepare the $MAPbX_3$ perovskite soils (X= Cl, Br, I). In addition, mixed perovskites based on the substitution of a fraction of I by Cl ($MAPb(I1\text{-}xClx)_3$) are prepared by varying the fraction x of the amount of material of each powder ($MAPbI_3$ or $MAPbCl_3$) according to the reaction (4). Then, to prepare thin films, these powders are dissolved in each DMSO solution. Finally, the soil solutions are agitated at room temperature overnight.

$$(1-x)MAPbI_3 + xMAPbCl_3 \rightarrow MAPb(I_{1-x}Cl_x)_3 \qquad (4)$$

c- The deposition of thin films perovskites MAPbX3 (X=I, Br, Cl)

This step is also called the Single-Step Deposition Technique. Indeed, to synthesize the $MAPbX_3$ perovskite thin films (X = Cl, I), 50 µL of the perovskite soil are taken and spread on the glass substrate by the spin-coating process at a rotational speed of 3000 tr/min for 30 seconds (figure II.2). At the end of the centrifugal coating process, $MAPbX_3$ (X = Cl, Br or I) perovskite films are dried in an oven at 60°C. They are characterized by colors ranging from black ($MAPbI_3$) to orange ($MAPbBr_3$) and white ($MAPbCl_3$) (figure II.3).

This color change suggests that the formation of the perovskite phase is achieved during the spin-coating step and is based on the evaporation of a large part of the DMSO.

Finally, to improve their crystallinity and densification, the synthesized films have been subjected at the same time to a thermal blowing of different temperature, this technique also allows to completely evaporate the traces of residual solvents (figure II.2). The perovskite films obtained are kept in a desiccator to avoid their degradation.

a)

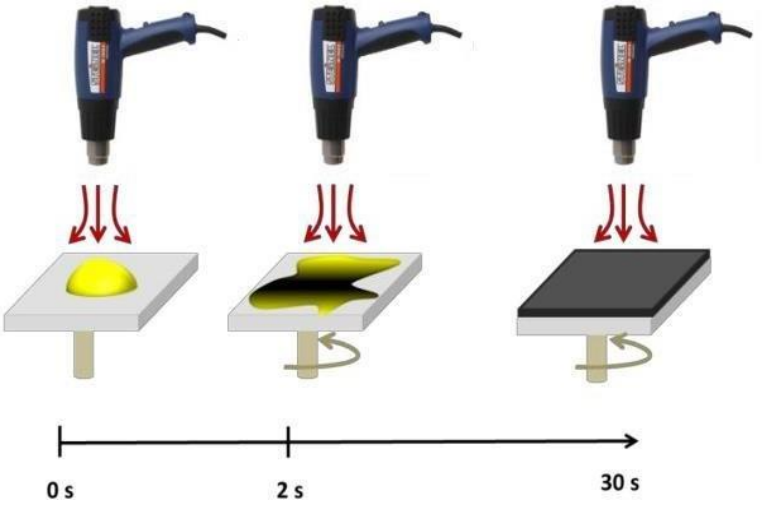

b)

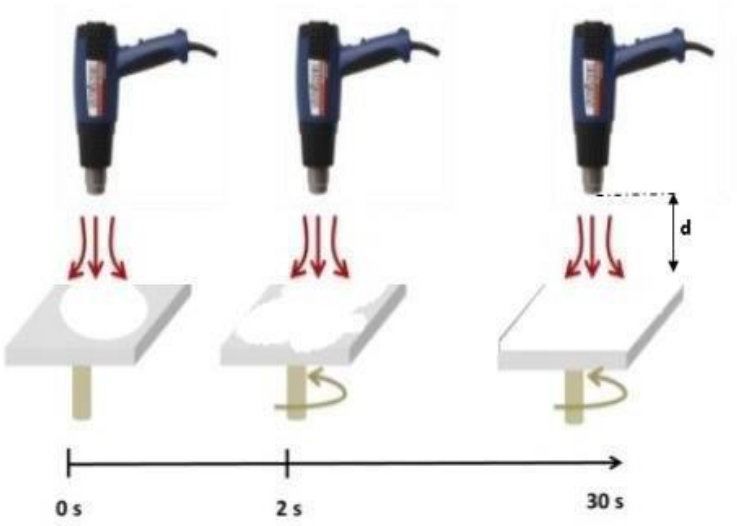

Figure II.2: Pattern of the deposition of perovskites by spin-coating a) $MAPbI_3$ b) $MAPbCl_3$ under thermal blowing.

II.2.3. Indirect preparation method

The indirect preparation method is implemented in three steps, namely (i) preparation of methylammonium halide salts, (ii) dissolution of soil from perovskites and (iii) deposition of perovskite films.

a- Preparation of the methylammonium halide salts MAX (X=I, Br, Cl)

To synthesize the methylammonium halide salts MAX or CH_3NH_3X (X=I, Br, Cl), a solution (A) containing a mixture of the reaction of a molar ratio of 1:1 of the hydrohalogeneic acid HX is first prepared (X = I, Br, Cl) and methylamine CH_3NH_2 (33% wt. in absolute ethanol) as described by equation (5), in a round-bottomed flask maintained at 0°C for 30 min under magnetic agitation. Then the MAX salts (X=I, Br, Cl) were recovered by placing solution (A) on a rotary evaporator to carefully remove solvents (ethanol and water) at 100°C. Finally, the resulting salts were washed several times with absolute ethanol and ether Diethyl, then vacuum dried at 60°C.

The formation of methylammonium halide salts MAX (X=I, Br, Cl) can be described by the following equation:

$$CH_3NH_2 + HX \rightarrow CH_3NH_2X \qquad (5)$$

b- Soil solution of MAPbX3 perovskites (X=I, Br, Cl)

The solution of perovskite soils requires first of all the lead halides PbX_2 (X=I, Br, Cl) which are commercially available with a purity of 99.999%.

Then, a molar ratio of 1:1 of MAX prepared beforehand and PbX_2 (X=Cl, Br, I) was dissolved in a solution with 45 wt% of DMF or DMSO, as described by equation (6). However, the preparation of mixed soil with $MAPb(I_{1-x}Br_x)_3$ or $MAPb(I_{1-x}Cl_x)_3$ is done by varying the fraction x of the amount of material in each MAX and PbX_2 (X=I, Cl or Br), according to the

reaction (7 and 8), dissolved in a 45 wt% solution of DMF or DMSO. Finally, the solutions are kept under magnetic agitation for 30 min.

$$MAX + PbX_2 \rightarrow MAPbX_3 \quad (6)$$

$$(1-x)(MAI + PbI_2) + x(MABr + PbBr_2) \rightarrow MAPb(I_{1-x}Br_x)_3 \quad (7)$$

$$(1-x)(MAI + PbI_2) + x(MACl + PbCl_2) \rightarrow MAPb(I_{1-x}Cl_x)_3 \quad (8)$$

c- The deposition of thin films perovskites MAPbX3 (X=I, Br, Cl)

The deposition and shaping of $MAPbX_3$ perovskite thin films can be carried out using the procedure explained in the previous paragraph, called Single-Step deposition technique. Nevertheless, there is another way to synthesize $MAPbX_3$ perovskite films, called the two-step deposition technique which consists first of depositing 40 µL of the dissolved PbX_2 solution in DMF at 70°C on the substrate. Secondly, the formed PbX_2 layer is immersed in a MAX solution dissolved in isopropanol. Finally, the perovskite film was annealed at 100°C for 30 min to evaporate the residual solvents.

Figure II.3 illustrates the cycle of thin films formation by this two-stage deposition technique.

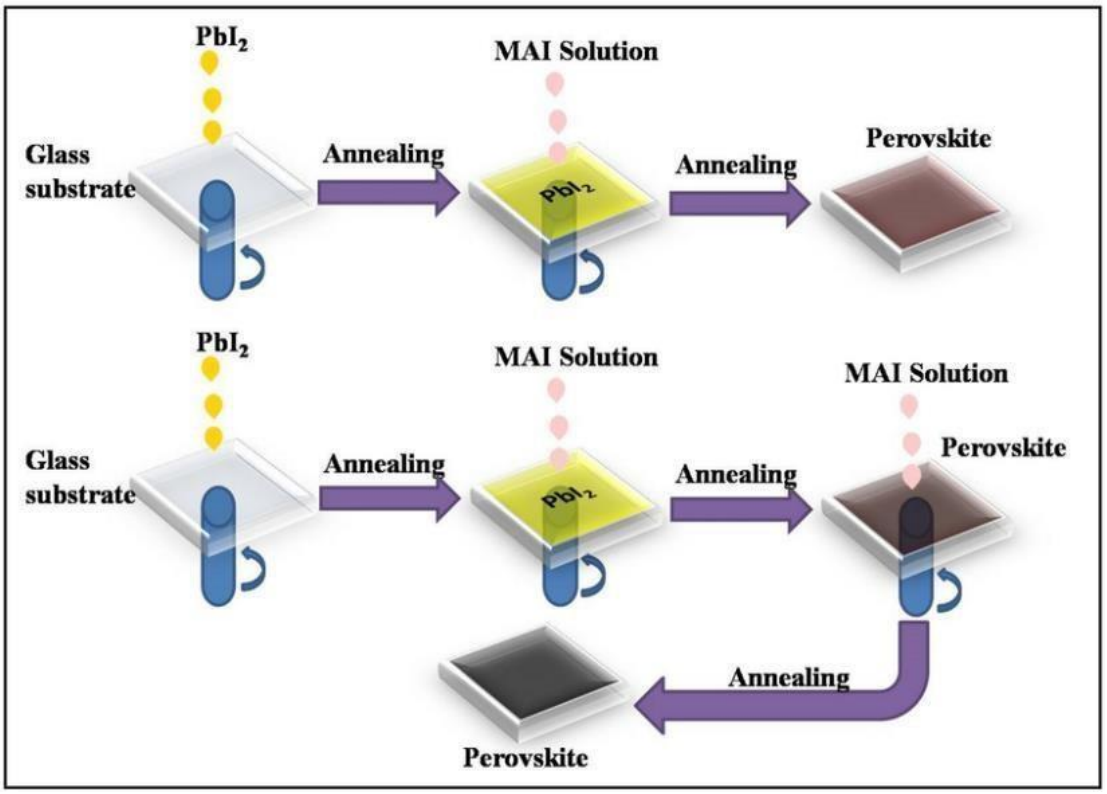

Figure II.3: Schematic of the deposition of perovskite films by two-step spin-coating

II.3. Thermal blowing and UV light techniques applied to synthesized films

II.3.1. Thermal blowing performed during the growth phase of $MAPbX_3$ perovskites

The study of the effect of thermal blowing performed at different temperatures and distances during the growth of $MAPbX_3$ perovskite films by spin-coating technique aims to improve the crystallinity and to control the compactness of the perovskite (figure II.2). The results of this study will be discussed in Chapter III. The thermal blowing during the spin process was carried out with a STEINEL Electronic «HG 2310 LCD» heat gun at a flow rate of 3.6 cfm (~ 101.91 l/ min) (figure II.4).

Figure II.4: STEINEL Electronic «HG 2310 LCD» heat gun.

II.3.2. UV irradiation performed on thin films of perovskites $MAPb(I_{1-x}Cl_x)_3$

The UV irradiation process performed on $MAPb(I_{1-x}Cl_x)_3$ perovskites was carried out to study the role of chlorine incorporation in the MAPI perovskite matrix to improve the stability of perovskite against UV radiation. The results of this study will be discussed in Chapter III (Part B). The UV irradiation was carried out with a CAMAG 4 UV lamp at a fixed wavelength of 392 nm with an intensity of about 350 $mWcm^{-2}$ (figure II.5). It should be noted that UV light (at wavelengths less than 400 nm) is only 4.61 $mWcm^{-2}$ under STC conditions: AM1.5, solar irradiation of 100 $mWcm^{-2}$ and a temperature of 25°C [45]. Therefore, the intensity of the UV device used in our study is 70 times higher than that of solar UV irradiation. The UV irradiation process was carried out at room temperature.

Figure II.5: UV irradiation device « CAMAG 4 ».

II.4. Characterization techniques

II.4.1. X-ray diffraction

X-ray diffraction (XRD) is a characterization technique used to study the crystallographic properties such as degree of crystallinity, orientations and size of the crystallites, lattice parameters, Etc.

The principle of this technique is to send a monochromatic x-ray beam onto a sample deposited on a flat sample holder at an angle θ to the incident beam, as shown in figure II.6. This X-ray beam will be scattered in all directions by the atoms of the sample. Indeed, the scattered rays will be interfered alternately in a constructive and destructive way depending on the angle 2θ. The constructive interference condition of scattered rays occurs when they have a phase difference of nλ (n is an integer), called «in phase». Whereas the condition of destructive interference occurs when the rays have a phase difference of nλ/2, called «completely out of phase». In addition, as shown in figure II.7, Diffraction peaks can be observed in certain specific directions when the difference in path between two rays reflected by two consecutive plants is equal to an integer n of wavelength λ. This leads to the Bragg law which reads:

$$2d_{hkl}sin\theta = n\lambda \qquad \text{(II-1)}$$

Where d_{hkl} is the interreticular distance of the planes of the family (hkl), θ is the angle of incidence taken from the surface of the planes (hkl), n is the diffraction order and λ is the wavelength of the X-rays.

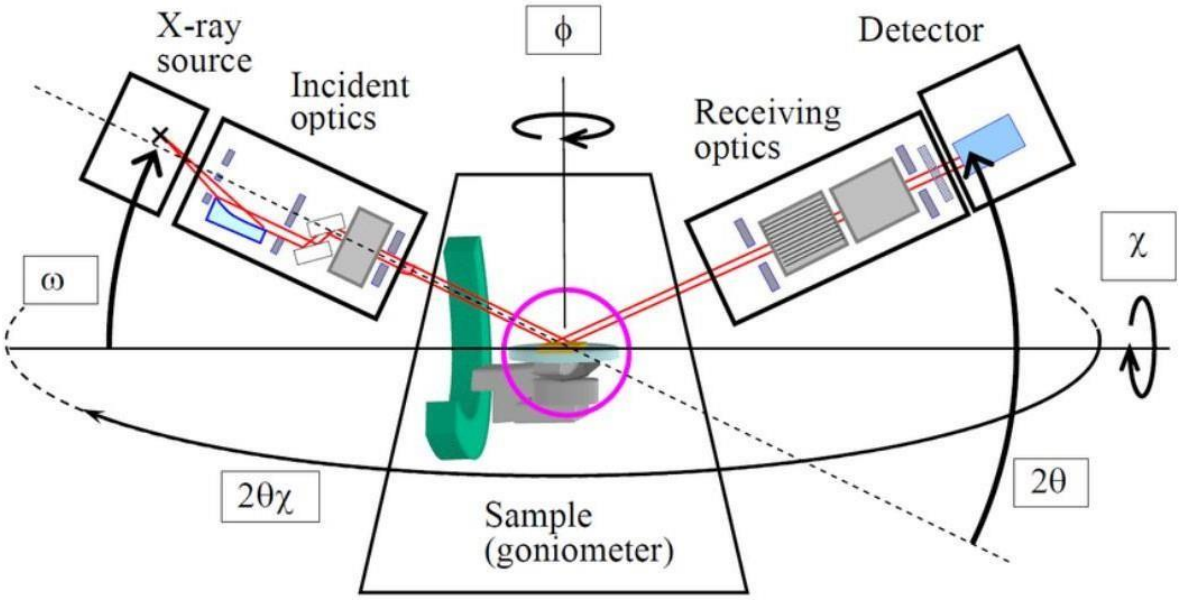

Figure II.6: Operating diagram of an X-ray diffractometer.

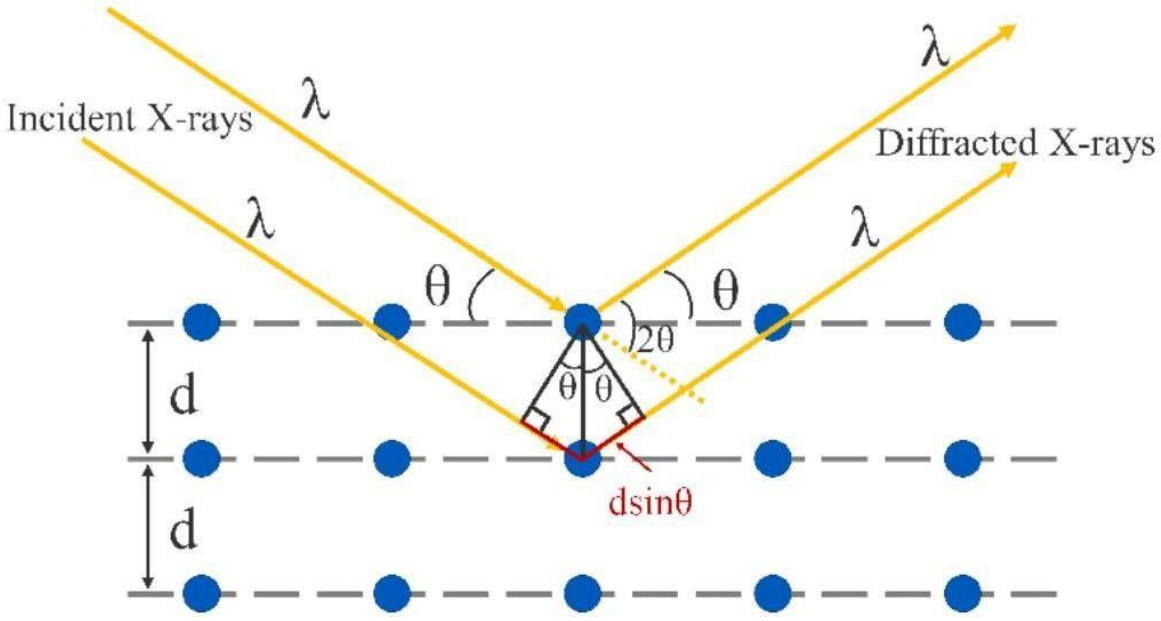

Figure II.7: Schematic representation of atomic planes in diffraction position.

X-ray diffraction patterns on thin layers of hybrid perovskites were performed by the X-ray Diffractometer (PANalytical Expert Pro) and the Diffractometer (PANalytical EMPYREAN) at CNRST, using a Cu K-alpha radiation source with a wavelength of 1.5406 Å. The figure II.8 shows the images of the used diffractometers.

a) **b)**

Figure II.8: X-ray diffractometers a) Panalytical Expert Pro and b) PANalytical EMPYREAN.

II.4.2. Scanning electron microscope (SEM)

The SEM scanning electron microscope is a technique that uses the principle of matter electron interactions to visualize and produce high-resolution images of the surface of a sample. The SEM images presented in this manuscript were taken by the CNRST-owned "QUATTRO S FEI" (figure II.9).

Figure II.9: Scanning electron microscope QUATTRO S FEI.

This SEM is equipped with an electron gun (FEG) which consists of the use of a metal cathode in the form of a very fine tip. A very intense electric field is thus produced at the tip end by applying a voltage of 2000 to 7000 V between the cathode and the anode. This will allow to remove the electrons from the tip with a very high efficiency by the tunnel effect. The electronic beam produced is accelerated by a very high potential difference of up to 30 kV. As shown in figure II.10, at the exit of the electron gun, the electron beam enters the electron column under a very high vacuum, including electromagnetic lens systems: condenser lenses, objective lenses and scanning coils (or deflector coils). This electromagnetic system allows, by successive interventions, to control the beam size, to focus and scan the beam on the sample in a small spot. Diaphragms, of optimal aperture diameter, are placed to reduce or exclude the electrons from the scattered beam.

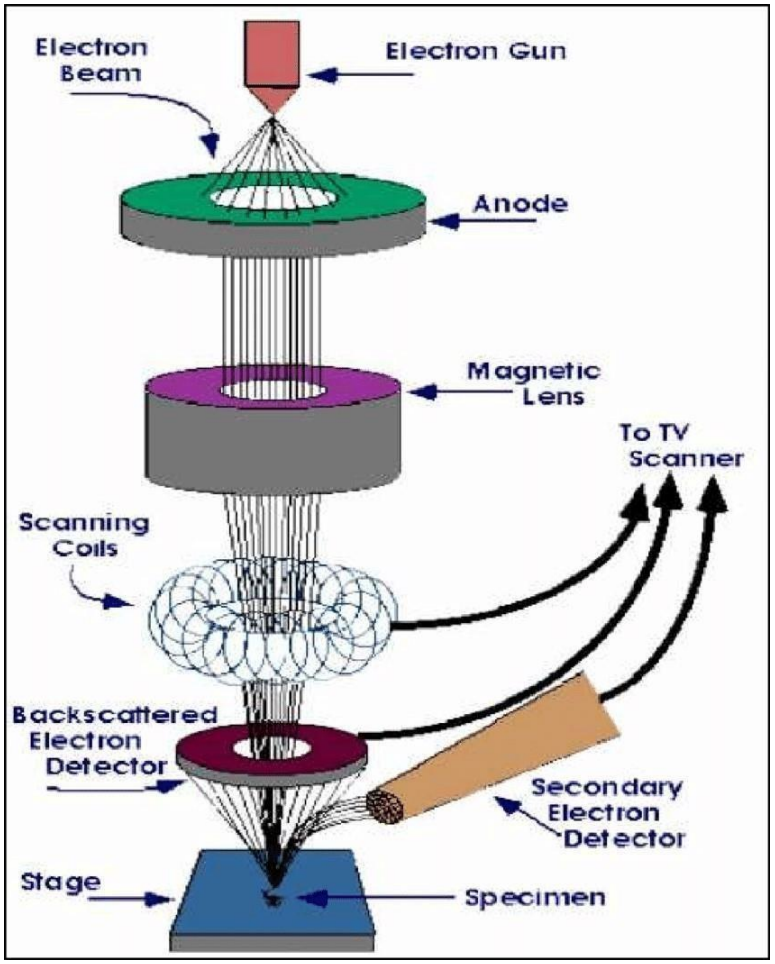

Figure II.10: Schematic of a scanning electron microscope.

The sample to be analyzed is glued to a sample holder by means of a conductive carbon tape placed at an optimum working distance of 10 mm, corresponding to the best resolution. The incident electron beam (called primary electrons) scans a rectangular area of the surface of the sample to be analyzed, line by point and line by line.

These primary electrons collide (interact) with the atoms of matter, while giving rise to various signals that carry information about the sample from which they are derived: secondary electrons, back-diffused electrons, auger electrons and X-rays (figure II.11). The secondary electrons are ejected from the sample surface in an inelastic manner. Therefore, these low-energy secondary electrons are attracted by a detector called (SED: secondary electron detector) to form a topographic image of the sample surface whose contrast is determined by the reliefs. Whereas the back scattered electrons, generated in a quasi-elastic way, which come from the deep levels of the atoms of the matter are detected by means of a detector called (BSED, back scattered electron detector) for the formation of a contrast image of chemical elements, i.e. areas containing light atoms (weak Z) appear darker. The SEM is coupled with an energy dispersive analysis spectrometer (EDS or EDX) which allows qualitative and semi-quantitative analyses of the analyzed sample.

When an incident electron ejects an electron from an inner layer of an atom, the electron is excited to a higher state, this returns to its ground state by an electronic transition, while ceding part of its energy by emitting an X-ray. The set of electronic transitions defines a discrete spectrum of lines whose energies are characteristic to the excited chemical elements. By analyzing the x-ray spectrum, we can identify the chemical nature of the atoms present.

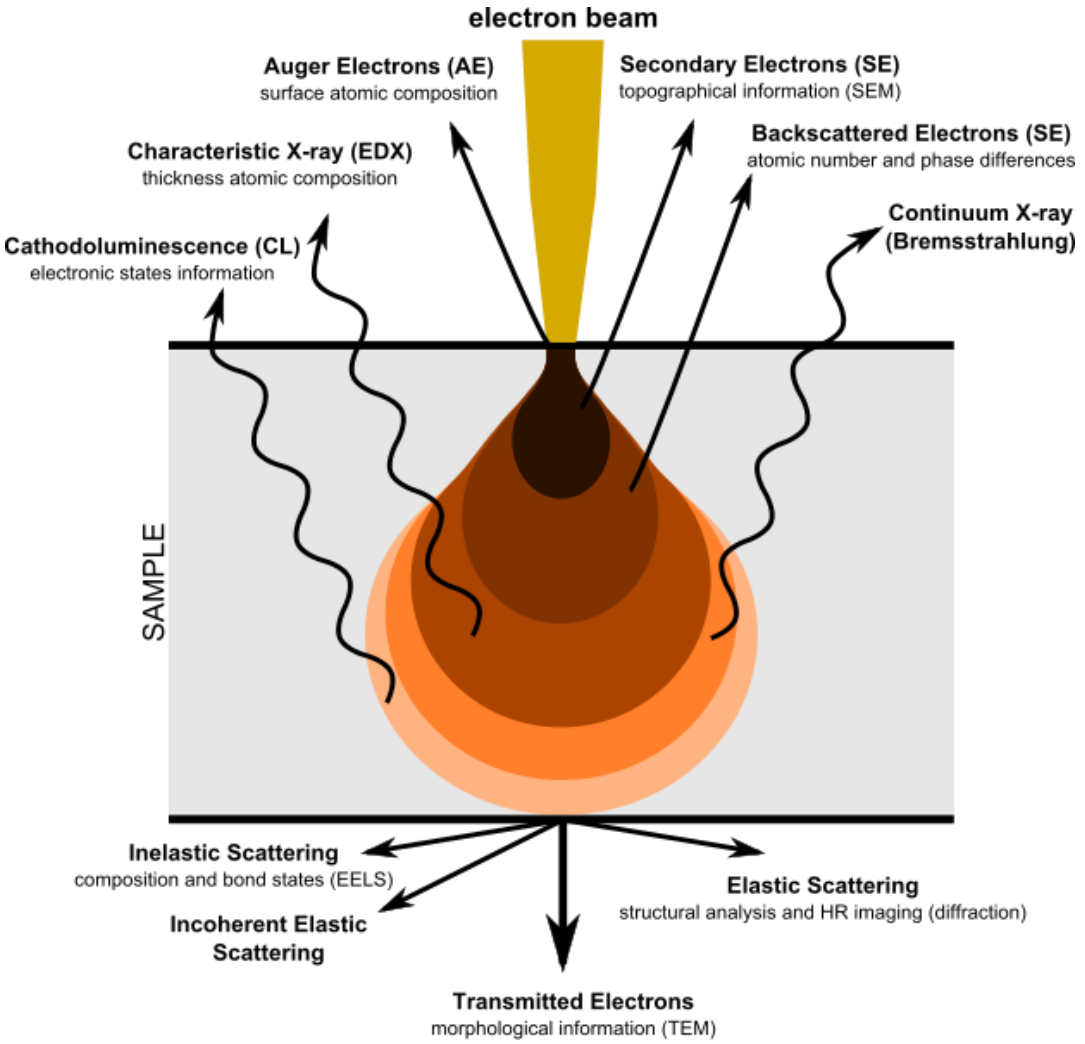

Figure II.11: Schematic of the analysis pear defining the generation volumes of the different types of electronic emission signals.

II.4.3. UV-Vis spectrophotometry

UV-Vis spectrophotometry is a technique that we used to measure optical properties: transmission, reflectance and absorbance of thin films or powders in the UV-Visible range. Measurements of these optical properties are made at room temperature using a CNRST-owned UV-Vis (Perkin Elmer Lambda 1050+) spectrophotometer with an integrative sphere covered with Barium Sulfate ($BaSO_4$) (figure II.12).

Figure II.12: Perkin Elmer Lambda 1050+ UV-Vis Spectrophotometer.

The principle of this UV-Vis spectrophotometry consists in using a light source which contains two lamps: one made of deuterium to cover the ultraviolet range (190-400 nm) and the other made of tungsten used for the range from 400 to 1100 nm (visible range). As shown in figure II.13, a monochromator selects a monochromatic ray, in the range of 190 to 1100 nm, directed at the sample placed in front of the aperture of the integrating sphere. Part of this radiation will be absorbed by the sample and another part will be transmitted and detected by the integrating sphere connected to a computer system to obtain the transmittance spectrum as a function of the wavelength.

The transmittance T is determined from the ratio of the measured beam intensity I to the incident beam intensity I_0:

$$T(\%) = \frac{I}{I_0} * 100 \qquad \text{(II-2)}$$

The part absorbed A by the sample is calculated automatically by the software "UV WinLab" according to the Beer-Lambert law:

$$A = \log\left(\frac{100}{T(\%)}\right) \qquad \text{(II-3)}$$

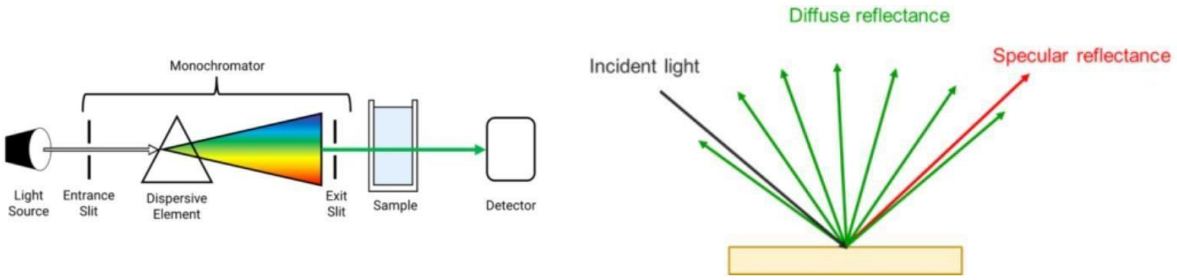

Figure II.13: Diagram of the UV-Vis spectrophotometer with an integrative sphere.

II.4.4. Fourier Transform Infrared Spectroscopy (FTIR)

Fourier Transform Infrared Spectroscopy, also known as FTIR Analysis or FTIR Spectroscopy, is an analytical technique used to identify organic, polymeric, and, in some cases, inorganic materials. The FTIR analysis method uses infrared light to scan test samples and observe chemical properties. Measurements of these optical properties were made at room temperature using a CNRST-owned FTIR (NICOLET iS50 FT-IR) spectrophotometer (figure II.14).

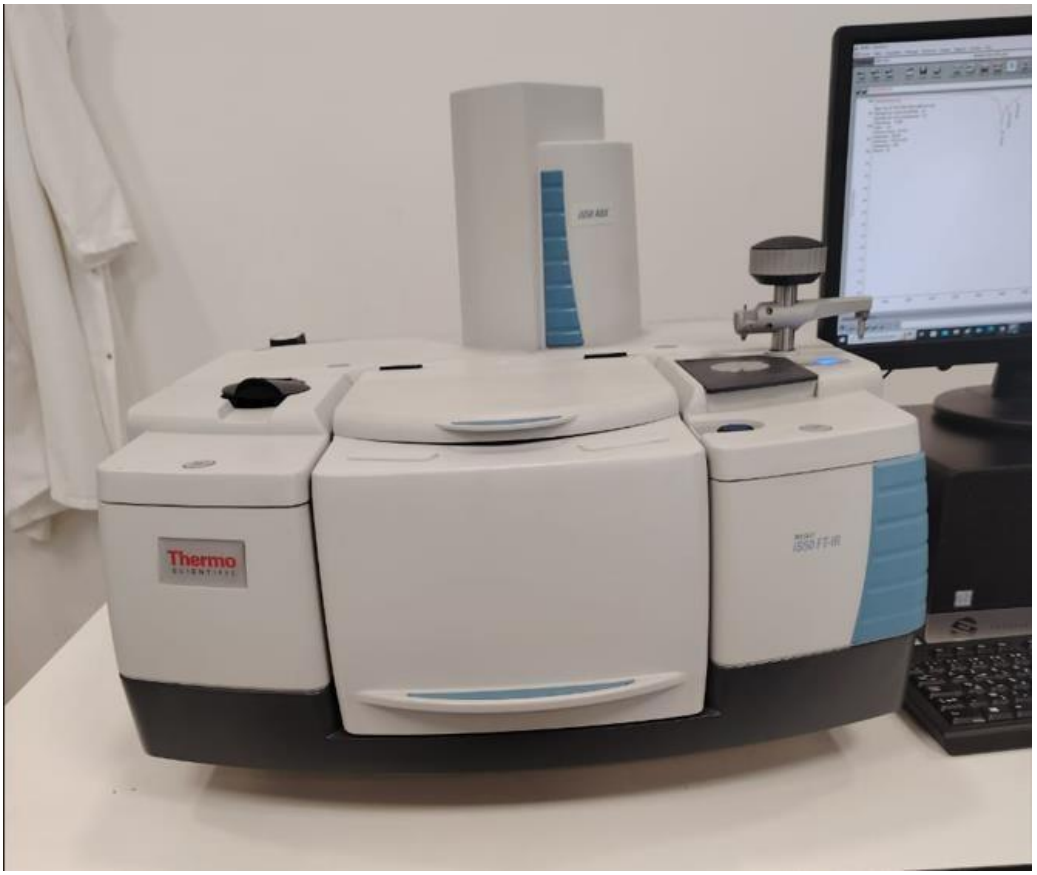

Figure II.14: NICOLET iS50 FT-IR Spectrophotometer.

The FTIR instrument sends infrared radiation of about 10,000 to 100 cm^{-1} through a sample, with some radiation absorbed and some passed through. The absorbed radiation is converted into rotational and/or vibrational energy by the sample molecules. The resulting signal at the detector presents as a spectrum, typically from 4000 cm^{-1} to 400cm^{-1}, representing a molecular fingerprint of the sample. Each molecule or chemical structure will produce a unique spectral fingerprint, making FTIR analysis a great tool for chemical identification.

FTIR spectroscopy is an established technique for quality control when evaluating industrially manufactured material, and can often serve as the first step in the material analysis process. A change in the characteristic pattern of absorption bands clearly indicates a change in the composition of the material or the presence of contamination. If problems with the product are identified by visual inspection, the origin is typically determined by FTIR microanalysis. This technique is useful for analyzing the chemical composition of smaller particles, typically 10 - 50 microns, as well as larger areas on the surface.

FTIR analysis is used to:

- Identify and characterize unknown materials (e.g., films, solids, powders, or liquids)
- Identify contamination on or in a material (e.g., particles, fibers, powders, or liquids)
- Identify additives after extraction from a polymer matrix
- Identify oxidation, decomposition, or uncured monomers in failure analysis investigations

Today, however we have the ability to not only use transmission techniques, but reflectance techniques as well. Because of the ability to focus and manipulate the incident beam with optics, we generally rely on variations of ATR (Attenuated Total Reflectance) techniques to introduce and observe the energy. ATR involves using a phenomenon of internal reflectance to propagate the incident energy.

ATR has largely surpassed transmission and is now the primary measurement technique used as this method involves minimal sample preparation and is non-destructive. To use ATR, the sample is simply placed on top of a crystal which is typically made of diamond, germanium, or zinc selenide. The IR light is directed through the crystal where it is partially absorbed by the sample. The IR light then passes through the crystal again and is detected (figure II.15).

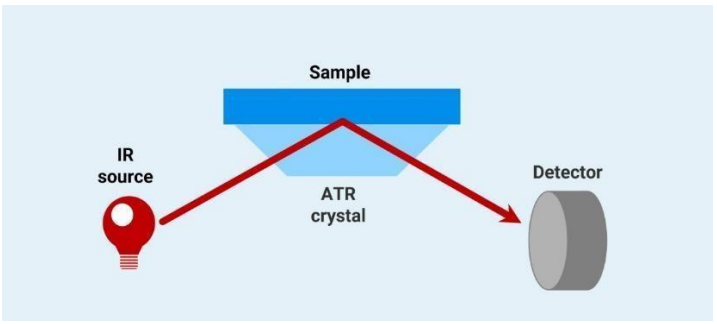

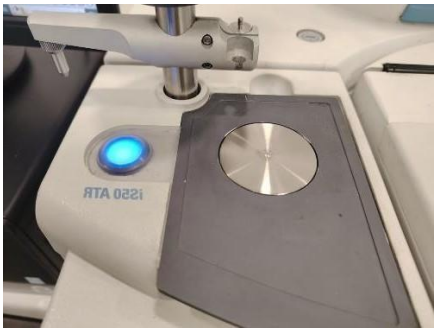

Figure II.15: ATR IR spectroscopy.

II.5. Conclusion

In this second chapter, we describe the synthesis procedures adopted for the preparation of thin films based on hybrid perovskites $MAPbX_3$. Indeed, the techniques of spin coating was used to synthesize the perovskite films. We then presented the different processes applied to the synthesized thin films, such as: UV irradiation and thermal blowing. The second part of this chapter was devoted to the description of the principal and interest of the different characterization techniques used to study structural (X-ray diffraction), morphological (SEM) and optical properties (UV-Vis spectrophotometry and FTIR spectrophotometry) of our samples. The following chapter III is mainly intended for the exposure of experimental results.

Chapter III:

Experimental results and discussions

III. Introduction

Hereafter, this chapter gathers the fruit of our work and projects the experimental results which will be divided in two parts: the first one where the effect and advantages of temperature and distance of hot airflow on the quality of $MAPbCl_3$ thin films grown by Sol-gel deposition was studied. The applied Hot airflow impacts the structural, morphological and optical properties of the of the prepared films, according to the experimental results, the temperature and airflow position clearly affect the physical characteristics of the perovskite. Increasing the airflow temperature from 50°C to 150°C, for instance, improves the produced films' continuity and crystallinity overall. The direct band gap energy also shifted from 2.98 to 2.94 eV. For low distances (5 cm), continuous $MAPbCl_3$ layers with good homogeneity (germination process) were thus produced. At this distance, SEM images reveal a high homogeneous nucleation, with the airflow temperature reaching 100°C and the surface almost completely covered. These latter settings (5 cm/100°C) are thought to be ideal for producing continuous $MAPbCl_3$ films of superior quality. Meanwhile, the stability issue remains a persistent difficulty known with perovskite-based solar cells which is brought on by their vulnerability to deterioration from moisture and UV light. Where comes the motivation for the next study, depicted in the second part, where the Chloride incorporation was investigated as a solution to improve the stability in the MAPI hybrid perovskite. The degradation of $CH_3NH_3PbI_3$ perovskite thin films is investigated, along with the effects of UV light on their optical, morphological, and structural properties. The primary result of this investigation shows that integrating a sufficient concentration of chloride into the perovskite structure can enhance the stability of $MAPbI_3$ under UV radiation. Indeed, experimental data unequivocally confirm that a chloride doping concentration of greater than 20% greatly enhances the stability of $CH_3NH_3Pb(I_{1-x}Cl_x)_3$ perovskite. The XRD study also makes it abundantly evident that a structural change from the tetragonal to the more stable cubic phase is directly responsible for the observed improvement in UV stability.

Part A

The effect of temperature and distance of hot airflow on the quality of $MAPbCl_3$ thin films grown by Sol-gel deposition

III.A.1. Introduction

The $MAPbCl_3$ perovskite, which exhibits a strong stability in ambient atmosphere [146], has been successfully used as a hole carrier layer for efficient organic light-emitting diodes, thanks to its transparent property in the visible domain [147]. In addition to that, doping the perovskite is also an effective solution to improve the crystallinity, the stability and to adjust the bandgap of the material [148].

In order to synthesize the perovskite thin films, there are various methods, for instance: the vapor-assisted solution processing [149], the vacuum deposition [150] and the atomic layer deposition [151].

The spin-coating technique associated to the hot airflow step has been recently used to synthesize successfully homogeneous and compact $MAPbI_3$ layers [152].

In this part of the third chapter, we will present the experimental results and their discussions concerning perovskites to hybrid halides. Indeed, we are interested in the characterization of $MAPbCl_3$ perovskite hybrids in thin layers and powder that we have synthesized. The process is the synthesis technique that was presented in the previous chapter. For this, we used several characterization methods such as: XRD, SEM and UV-Vis spectrophotometry. We show through the characterizations that the $MAPbCl_3$ perovskite adopts a cubic structure. The films obtained are dense and homogeneous, with high absorbance and an optical gap of about 2.94 eV. In the present work, we study the advantage and effect of hot air flow parameters (temperature and distance) on the physical properties of $MAPbCl_3$ thin films. For this, many $MAPbCl_3$ films were synthesized by spin-coating by varying the parameters of the hot air flow, namely temperature and distance. Thus, the effect of these two parameters on morphological, structural and optical properties was examined. Experimental analyses show a significant improvement in crystallinity, surface coverage and optical absorbance of thin films when the temperature and distance from the hot air flow are optimized.

III.A.2. Sol-gel deposition under hot air flow: towards better quality of $MAPbCl_3$ perovskite films

III.A.2.1. XRD analysis

The XRD pattern of the prepared $MAPbCl_3$ powder, presented in figure III.1.b, matches well the pure perovskite defined in the JCPDS card N° 96-723-1906 (figure III.1.a), which consists of a cubic crystal system (a=5.675 Å) and a Pm3m as space group.

(a)

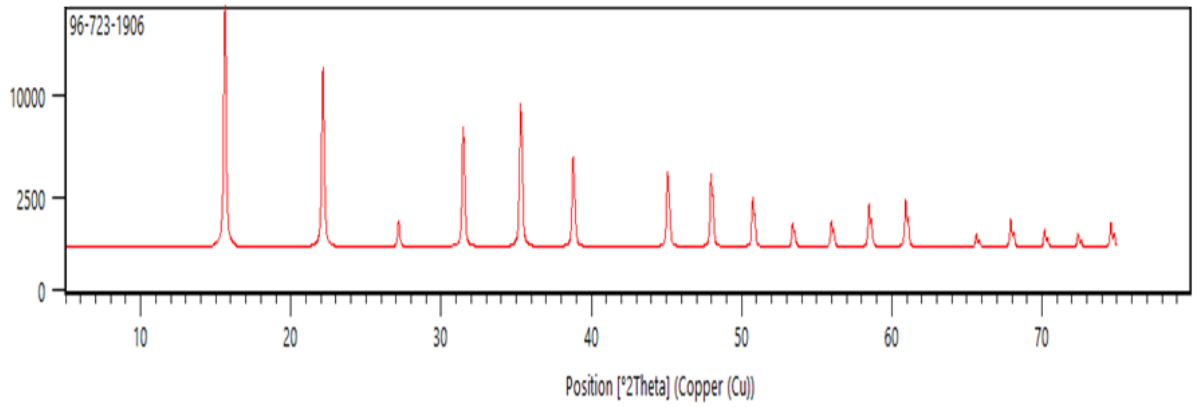

(b)

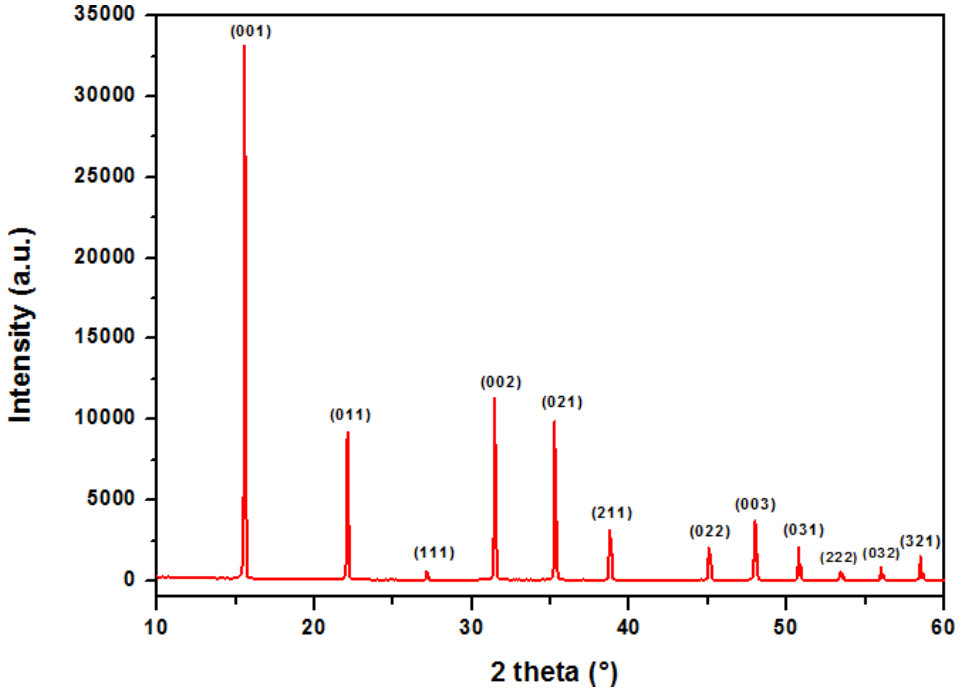

Figure III.1: (a) The standard XRD patterns of $MAPbCl_3$**, (b)** the X-Ray diffractogram of $MAPbCl_3$ synthetized powder.

III.A.2.2. The airflow temperature effect

The XRD diffractograms of the unheated and the heated $MAPbCl_3$ thin films at various airflow temperatures (50°C-150°C) are presented in figure III.2. For each temperature, only three principal peaks are observed and indexed as (001), (002) and (003) indicating a strong orientation in the c-axis direction. As the airflow temperature increases from 50°C to 150°C, the diffraction peaks become increasingly intense and sharp, with a decrease in the Full Width at Half Maximum (figure III.3), indicating the improvement of the crystallinity. Notice that, when the hot airflow temperature reaches 150°C, another peak appears at the angular position of 19.85°, which is attributed to the (002) $PbCl_2$ phase. This result shows that 100°C is the best airflow temperature to synthesize pure and homogeneous $MAPbCl_3$ perovskite without any secondary phase formation.

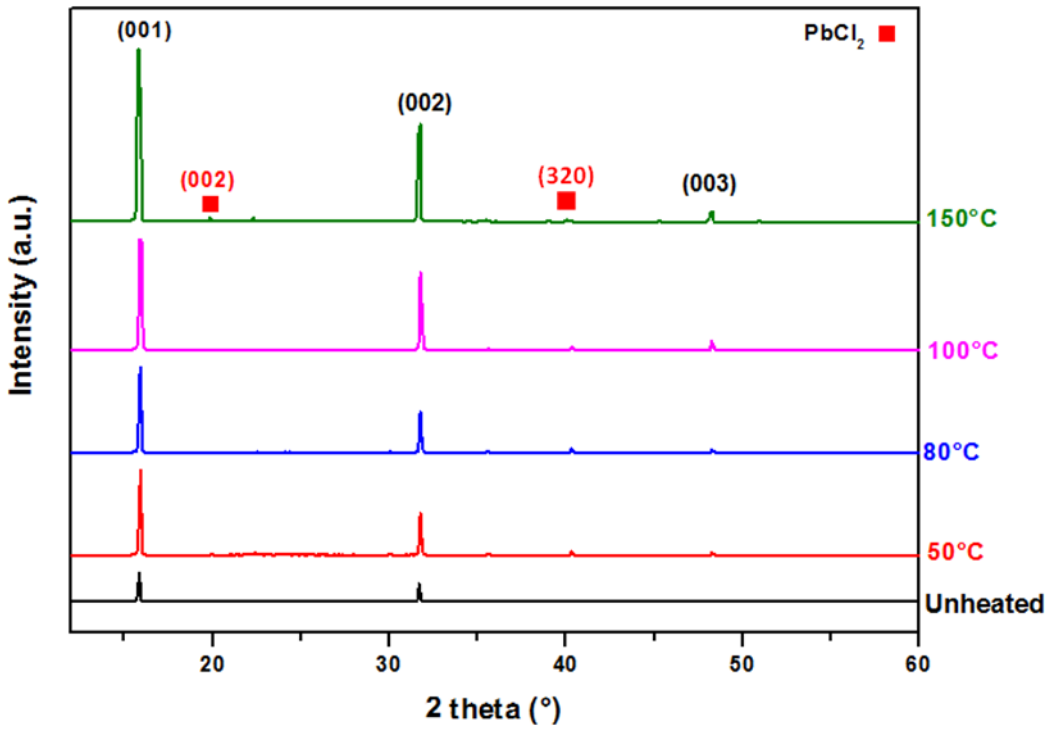

Figure III.2: The X-Ray diffractograms of the unheated and heated $MAPbCl_3$ films at different temperatures (50°C-150°C), the distance of the hot air flow was fixed at 5cm.

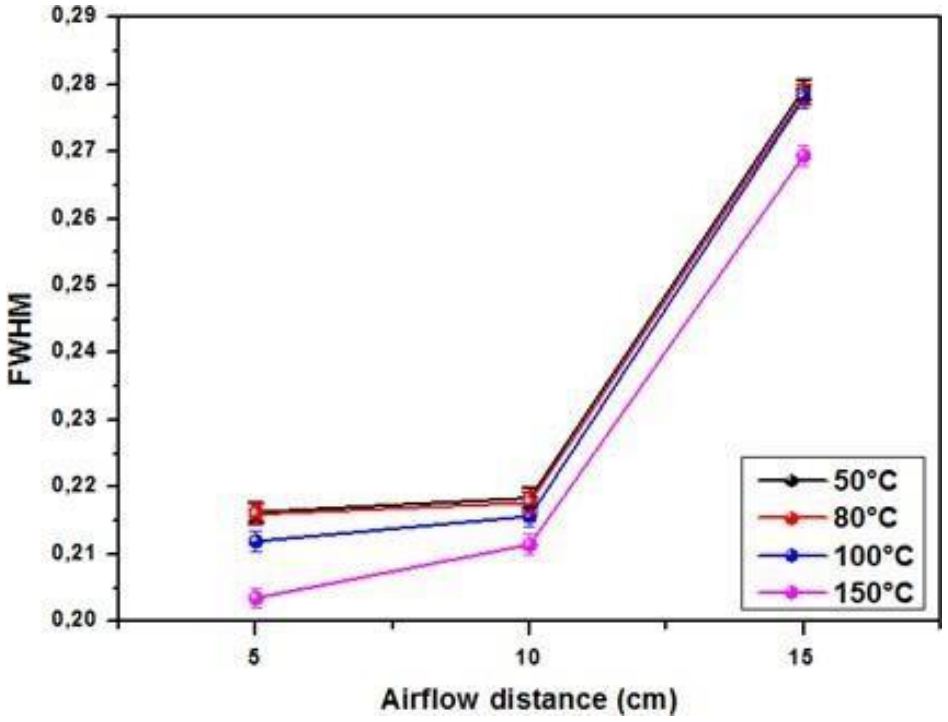

Figure III.3: Variation of the (001) peak FWHM versus the airflow distance at various temperatures.

III.A.2.3. The hot airflow distance effect

In this study, the airflow temperature was fixed at the optimized value of 100°C and the distance has been varied from 5cm to 15cm. The X-ray diffraction patterns presented in figure III.4, show that the best crystallinity, which manifested by the highest intensity peaks, is obtained when the airflow distance is equal to 5cm. This observed phenomenon could be explained by the fact that, at low distance, the hot airflow enhances the mobility of the chemical species at the substrate surface and as a result the grains growth kinetic is enhanced [153].

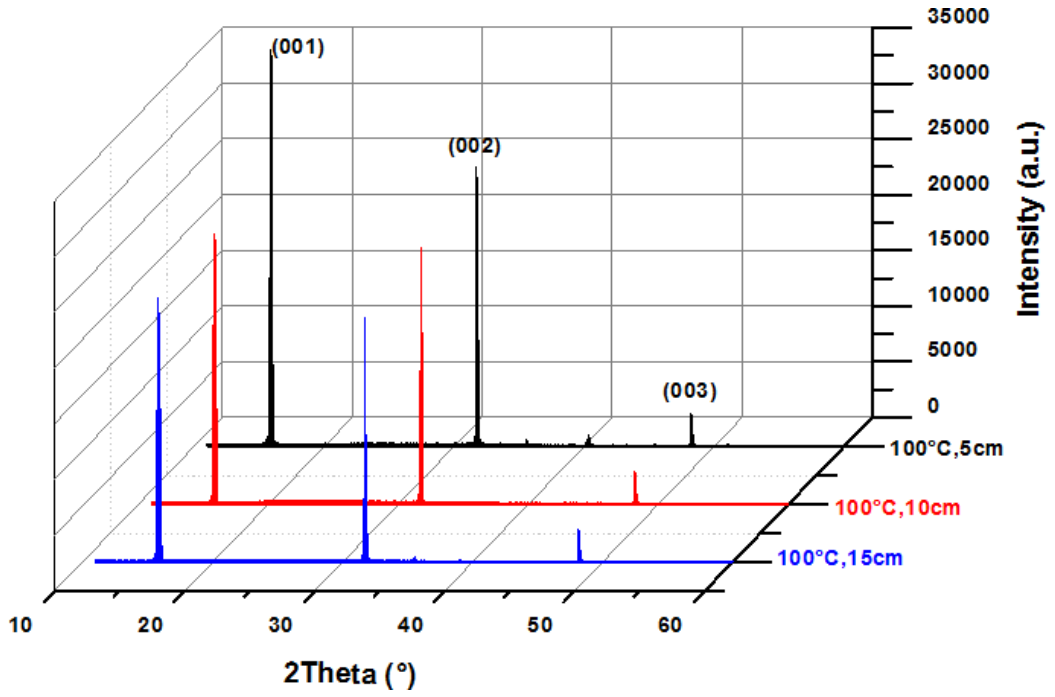

Figure III.4: X-Ray diffractograms of the heated $MAPbCl_3$ films using airflow at 100°C for different distances.

The crystallite size (D) is estimated using the Scherrer formula [154]:

$$D = \frac{K\lambda}{\beta \cos\theta} \qquad \text{(III-1)}$$

where D is the average crystallite size, λ is the x-ray wavelength, β is the width of the x-ray peak on the 2θ axis, normally measured as full width at half maximum (FWHM) after the error due to instrumental broadening has been properly corrected (subtraction of variances), θ is the Bragg angle, and K is the so-called Scherrer constant [155]. Further, microstrain in the crystallite or nanocrystal also affects the width β. More discussion can be found in [156].

The variation of the obtained crystallite size as a function of the airflow distance for different temperatures is illustrated in figure III.5. It's clear that the airflow distance affects strongly the crystallite size. The latter becomes larger when the distance is decreased and/or the temperature is raised. To more explain the observed effect, the high growth kinetic of the crystallite, observed at high temperature (and/or low distance), could be originated from a higher evaporation rate of the DMSO solvent making the supersaturation degree of the perovskite solution to be increased. Consequently, this enhances the formation of the nucleation sites which closely connect tightly each other to form large crystallite sizes [152, 157].

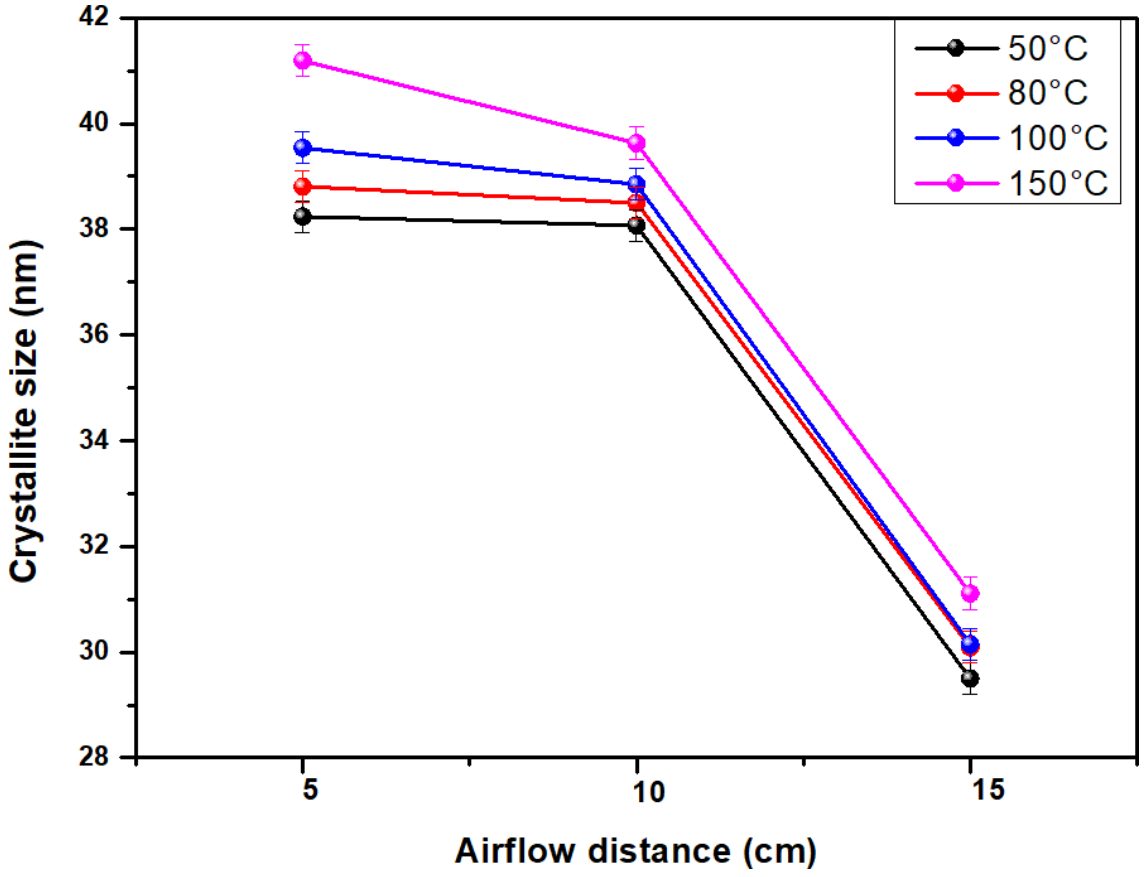

Figure III.5: Variation of the $MAPbCl_3$ crystallite size, estimated from (001) peak, as a function of the airflow distance for different temperatures.

III.A.2.4. The SEM surface analysis

The following SEM characterizations of thin films, elaborated without and under airflow at different temperatures and distances, are presented in the figure III.6. These micrographs show grains of rectangular shape in conformity with the $MAPbCl_3$ cubic structure, as revealed by the XRD study. However, a non-continuity of the phase associated to a lack of homogeneity is observed in the unheated sample (micrograph a). Both the homogeneity and continuity are strongly improved as the airflow temperature is increased and/or the distance is reduced. Besides, at 150°C, the SEM micrographs indicate a fusion of the grains which is attributed to the apparition of a $PbCl_2$ secondary phase as revealed by the XRD results.

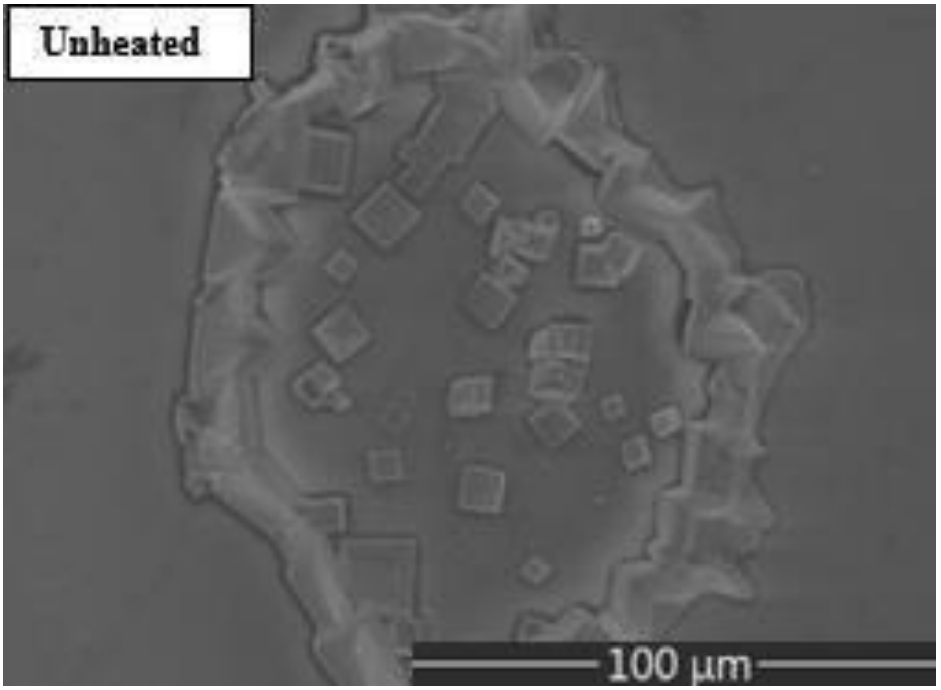
Unheated
100 µm

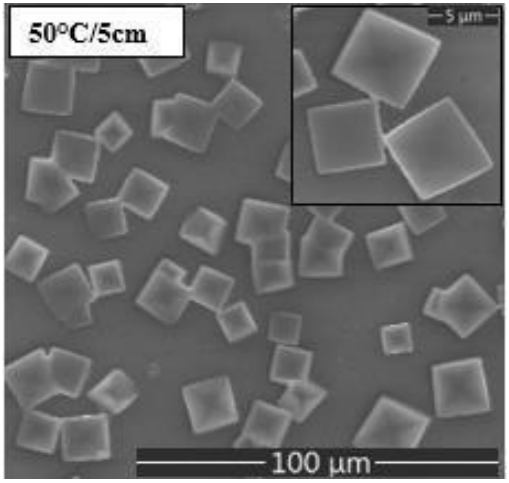
50°C/5cm
5 µm
100 µm

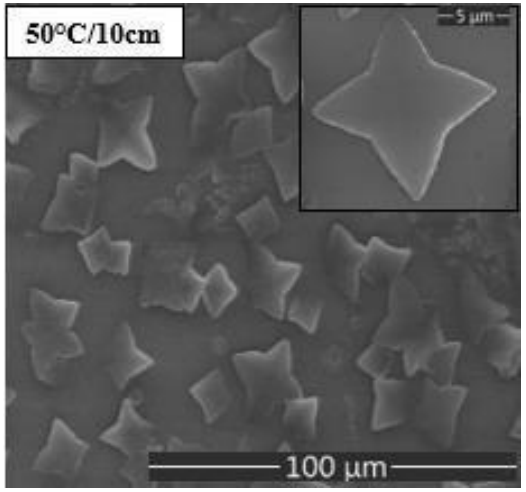
50°C/10cm
5 µm
100 µm

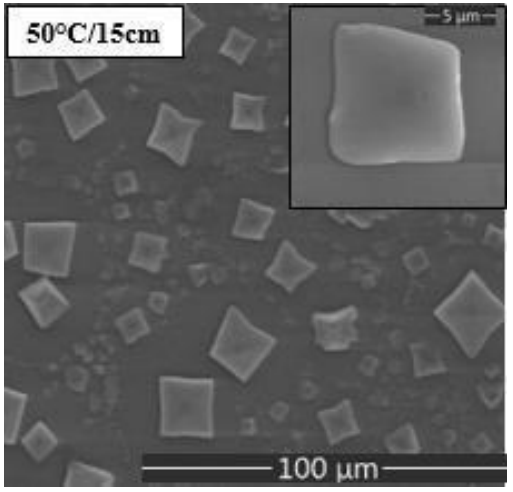
50°C/15cm
5 µm
100 µm

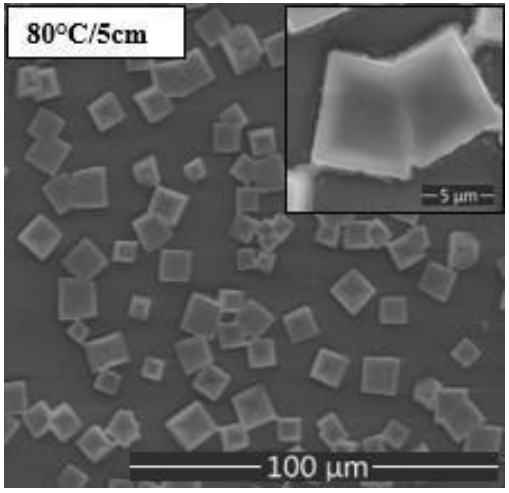
80°C/5cm
5 µm
100 µm

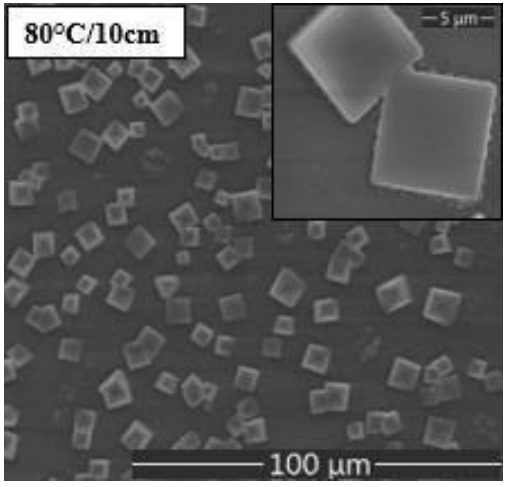
80°C/10cm
5 µm
100 µm

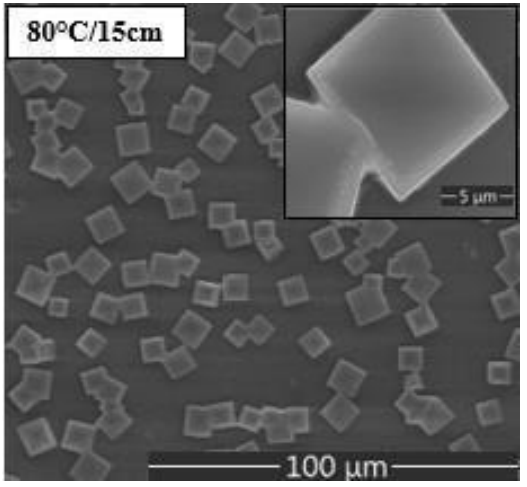
80°C/15cm
5 µm
100 µm

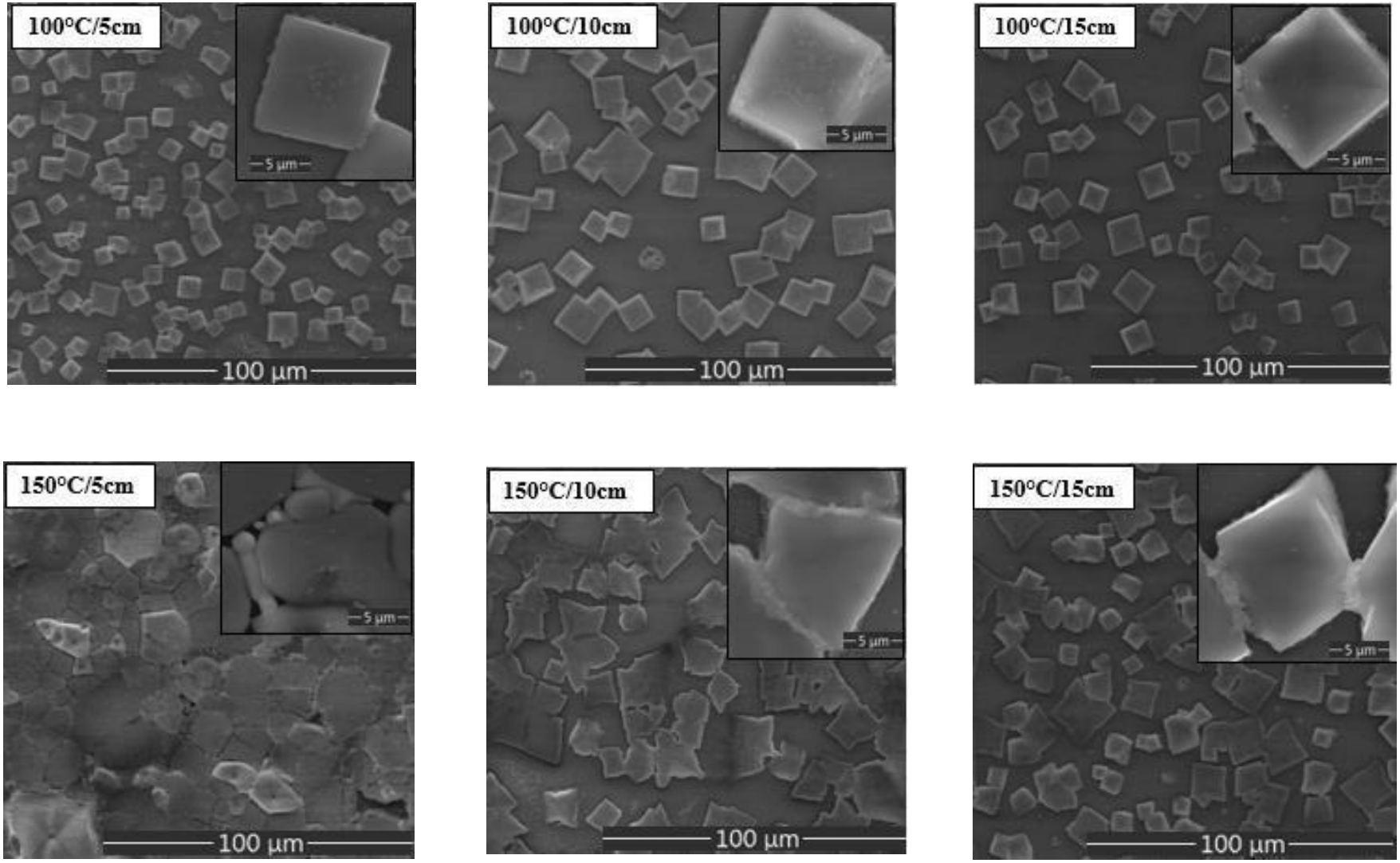

Figure III.6: The SEM micrographs of unheated and heated $MAPbCl_3$ thin films at different airflow temperatures and distances.

Subsequently, figure III.7 illustrates the variation of the surface coverage, deduced from the SEM micrographs, as a function of the airflow temperature and distance. One can notice that regardless the distance, when the temperature is increased from 50 to 150°C, the surface coverage becomes strongly improved (from 71% to 92%), attesting of a nucleation rate enhancement. The same behavior but less marked is also observed when decreasing the airflow distance.

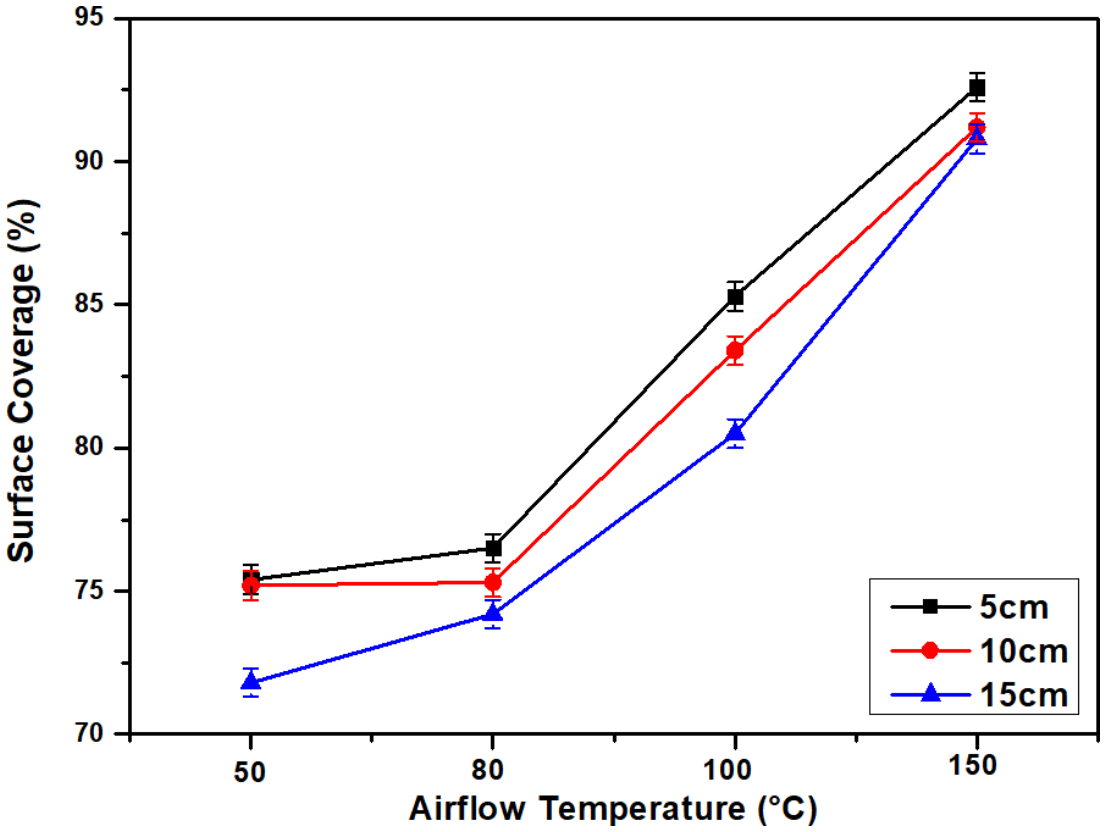

Figure III.7: The surface coverage estimated by the ImageJ software as function of the airflow temperature.

III.A.2.5. The optical characterization

The optical properties of the prepared $MAPbCl_3$ powder and films are determined from the absorption measurements. The bandgap energy *(Eg)* is extracted from the absorption measurements using the Tauc's equation [158]:

$$(\alpha h\nu) = A\,(h\nu - Eg)^{1/2} \qquad \text{(III-2)}$$

Where $h\nu$ represents the photon energy and A is a constant.

The Plotting of $(\alpha hv)^2$ versus the photon energy (hv) gives a straight line in a specific region. The extrapolation of this straight line will intercept the (hv) axis to give the value of the direct optical gap energy (Eg).

Thereafter, the measured UV-VIS absorbance spectrum of the $MAPbCl_3$ powder, illustrated in figure III.8, exhibits a high absorbance at low wavelengths and the band gap value is estimated to 2.79 eV.

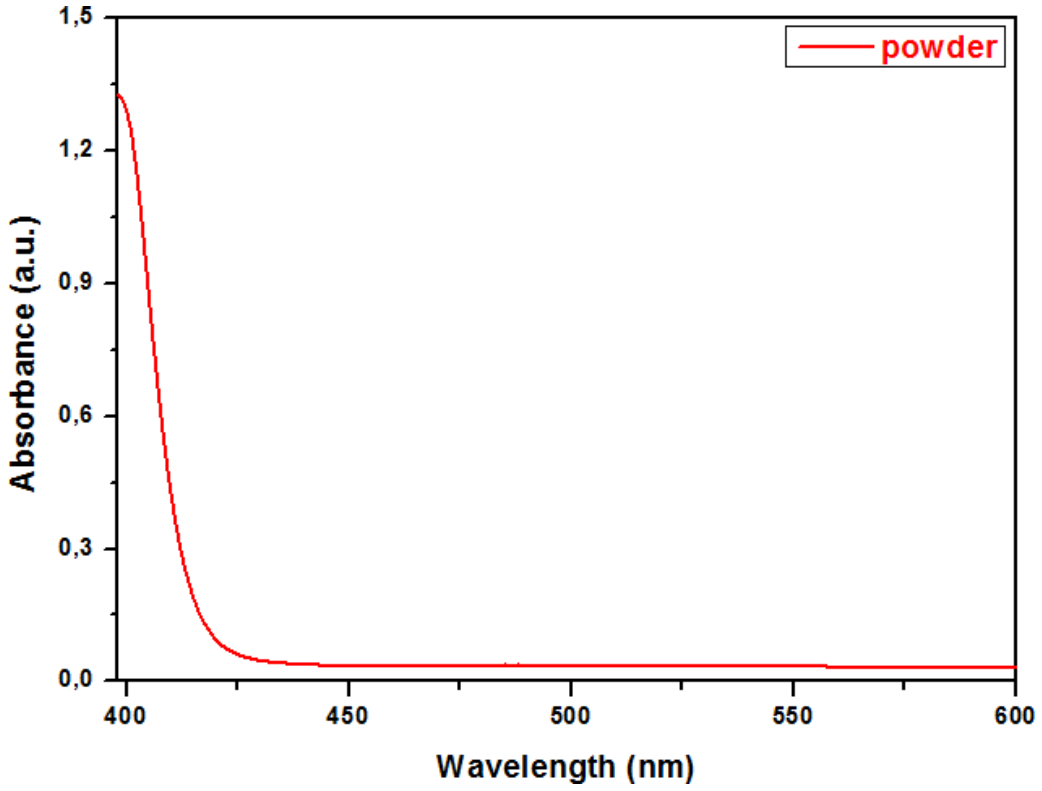

Figure III.8: UV-Vis absorbance spectrum of the obtained $MAPbCl_3$ powder.

The absorbance spectra, illustrated in figure III.9, show a significant improvement of the absorbance in the studied region when increasing the temperature and/or reducing the distance. This observed effect is directly attributed to the improvement of the surface coverage and the crystallinity. In fact, SEM micrographs presented at figure III.7 show a clear increase of the surface coverage (from 71% to 92%) when the temperature is increased from 50 to 150°C. In another hand, figure III.3 indicates a net decrease of the (001) peak FWHM, as the airflow temperature varies from 50°C to 150°C, which attests of a clear improvement of crystalline quality of the obtained films. Both these two effects are the origin of the observed absorbance improvement.

Note also that, when the temperature increases up to 150°C, a dramatic absorbance reduction between 300 and 396 nm can be observed with an absorption edge at 315 nm, indicating the $PbCl_2$ phase formation. In fact, when the hot airflow temperature becomes higher than 150°C, the ultra-rapid evaporation of the DMSO solvent (the boiling point is 189°C) leads to an immediate crystallization followed by a relative sublimation of the MACl organic compound (the MACl sublimation point is about 227°C) during the hot airflow process. As a consequence, a partial decomposition of perovskite structure to $PbCl_2$ phase occurs [159, 160]. This latter result is in good agreement with the XRD results previously presented.

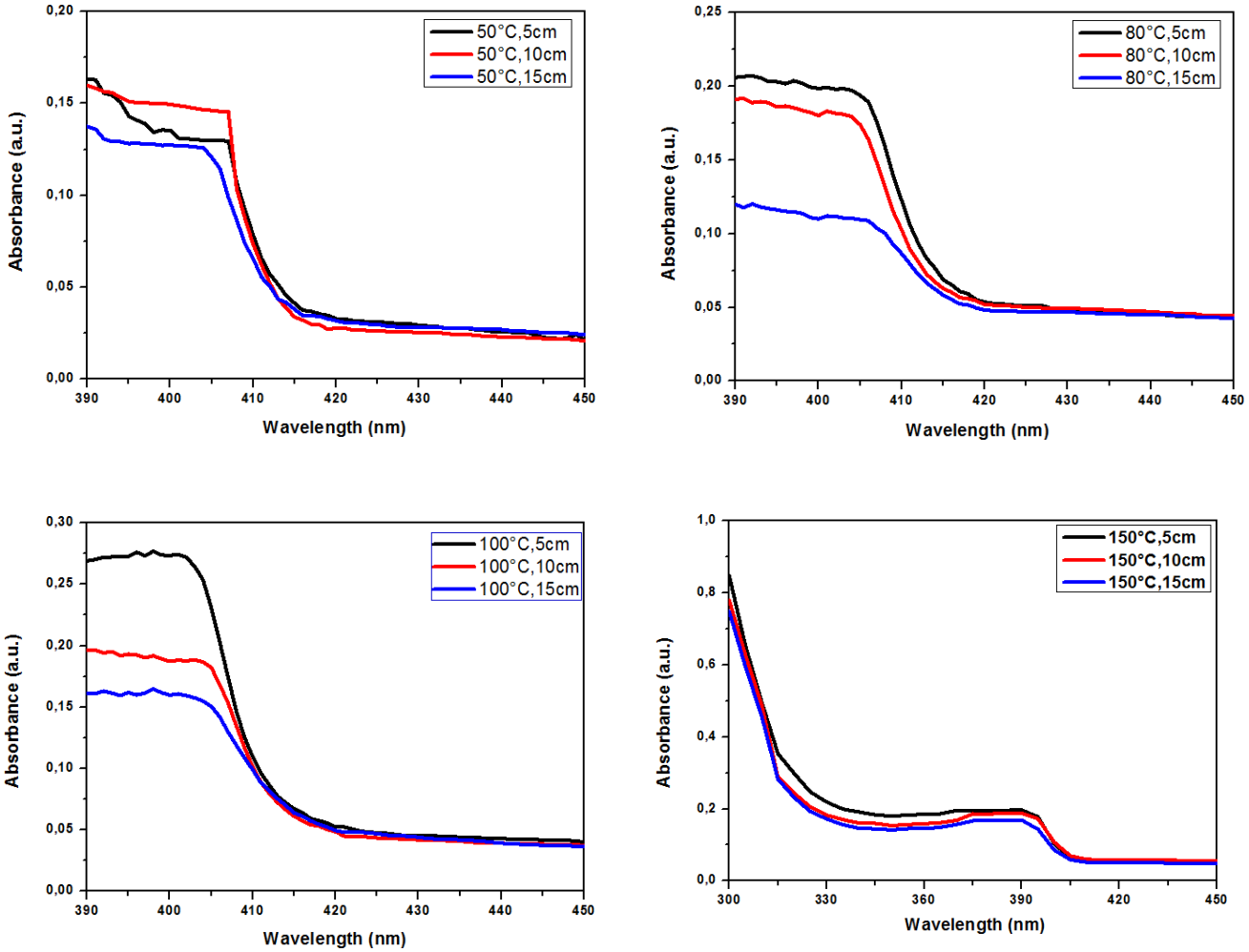

Figure III.9: UV-Vis absorption spectra of $MAPbCl_3$ films using the airflow at different temperatures (50°C-150°C) at various distances (5cm-15cm).

To more elucidate the dependence of the physical properties on the hot airflow parameters; the figure III.10.a illustrates the variation of the band gap energy value and crystallite size as a function of the airflow temperatures at a fixed distance (5cm). From these graphs, it's clear that as the air flow temperature is varied from 50 to 150°C, the band gap energy decreases from 2.98 to 2.94 eV while the crystallite size increases from 38 to 41 nm. Consequently, the smallest gap energy (2.94 eV) value is obtained for the highest crystallite size (41 nm) indicating that a clear blue shift in the band gap energy appears as the particles diameter become smaller. This behavior is inversely proportional in figure III.10.b where one varies the distance of the flux, increasing the distance, the size of the crystals decreases while the gap increases. This obtained cross experimental curve, is a clear illustration of the quantum confinement phenomenon, known as the exciton Bohr radius, which corresponds to a principal shift in optical and electronic properties [161].

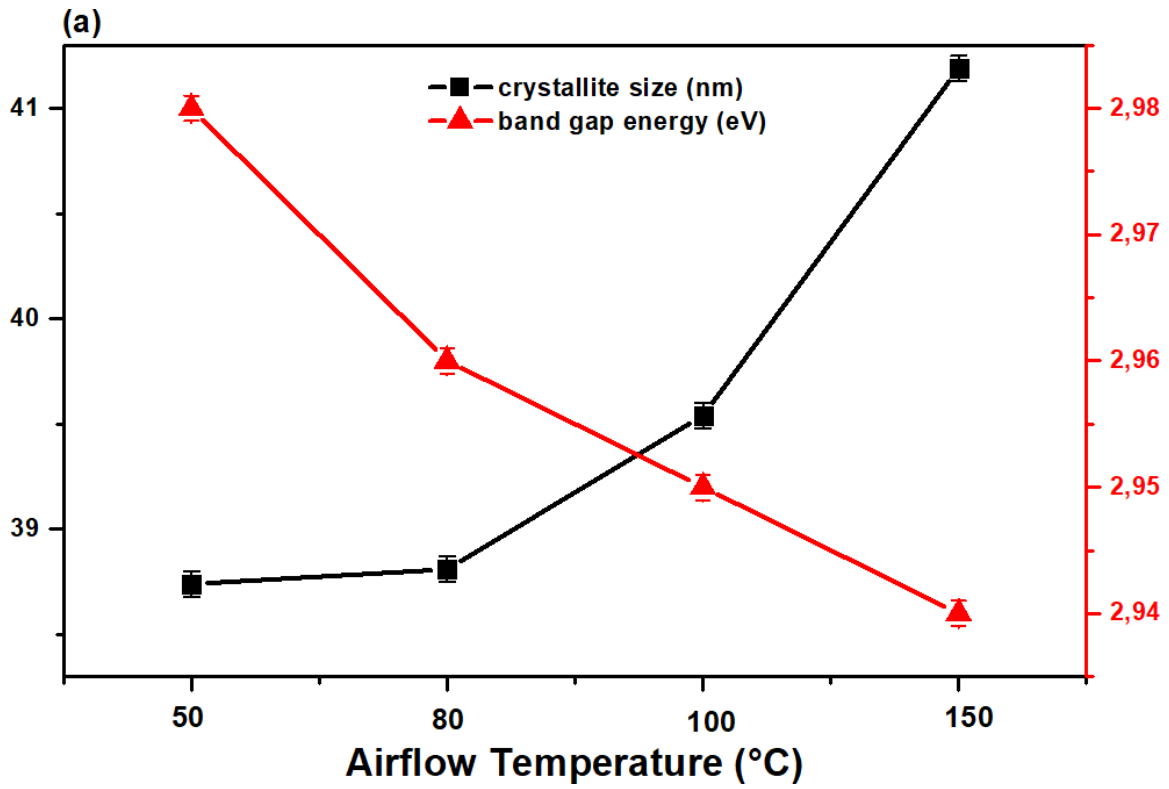

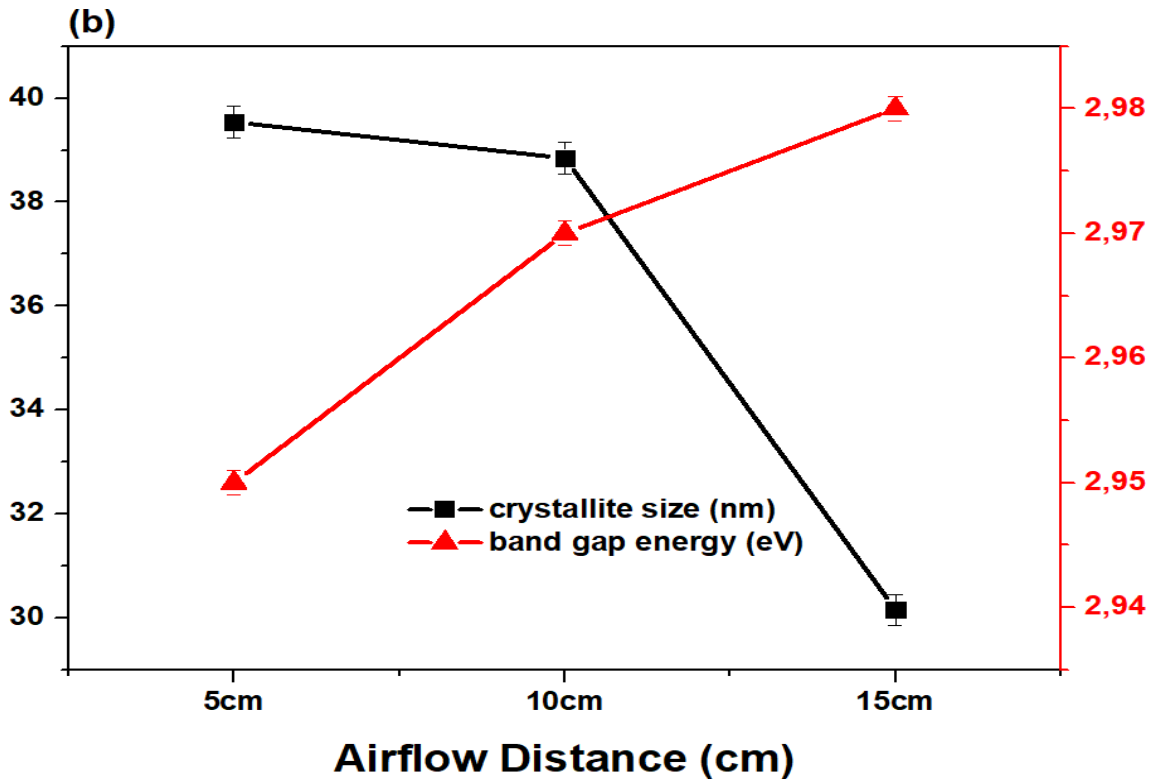

Figure III.10: a) Variation of the band gap energy and the crystallite size versus the temperature at 5cm, **b)** Variation of the band gap energy and the crystallite size versus the distance at 100 °C.

III.A.3. Conclusion

Stable $MAPbCl_3$ perovskite thin films were synthetized using a hot airflow step performed during the spin-coating process. The effect of the airflow position and temperature on the structural, morphological and optical properties of the prepared films has been studied. The experimental results show that increasing the airflow temperature from 50°C to 150°C and/or reducing the distance from 15 to 5 cm results in a net improvement of the continuity and crystallinity of the films. At 150°C the observed partial decomposition of the perovskite is attributed to an excessive evaporation of the DMSO solvent. These results show that the temperature 100°C and the distance 5cm are the best airflow parameters to synthesize pure and homogeneous $MAPbCl_3$ perovskite without any secondary phases. The reduction of the band gap energy is firmly related to the increase of the crystallite size, as confirmed by the cross experimental curve, which is a clear illustration of the quantum confinement phenomenon.

Part B

Chloride incorporation for the stability improvement of the $CH_3NH_3PbI_3$ hybrid perovskite

III.B.1. Introduction

The methylammonium lead halide perovskites $CH_3NH_3PbX_3$ (with CH_3NH_3 denoting MA and X representing a halogen) offer considerable potential for improving solar cell efficiency. In this context, halide perovskites like $MAPbCl_3$, $MAPbBr_3$, $MAPbI_3$, and composite-halide $MAPb(I_{1-x}Br_x)_3$ play pivotal roles as noteworthy contributors to the field [162]. On the other hand, hybrid perovskites have excellent properties, which include low recombination rate, strong absorption in the visible region, tunable bandgap, low effective mass and, most importantly, low manufacturing costs [163–169].

In this context, $MAPbI_3$ is a hybrid perovskite which is widely used in the industry. Unfortunately, these perovskites are notorious for losing their stability when exposed to air, moisture, UV irradiation and/or high temperatures. These issues are the subject of current research, which aims to develop a more straightforward synthetic technique that can be produced on a large scale to produce a stable, highly efficient and affordable perovskite-based solar cell [170,171].

We are particularly interested in the effect of the incorporation of chloride atoms into the $MAPb(I_{1-x}Cl_x)_3$ perovskite matrix on morphological and optical structural properties and also on stability against UV irradiation. We show that it is possible to make this perovskite more stable when chloride is incorporated into the matrix with a rate greater than 20%. We worked at a temperature of 100°C and a distance of 5 cm from the air flow imposed during the centrifugation coating process [172].

III.B.2. Results and Discussions

III.B.2.1. XRD analysis of $MAPbI_3$ and $MAPbCl_3$ films

The X-ray diffraction patterns of unencapsulated $MAPbI_3$ and $MAPbCl_3$ films, before and after 12 hours UV exposition, are displayed in figure III.11. Before UV irradiation, the XRD pattern for $MAPbI_3$ (figure III.11.a) reveals three major peaks, corresponding to the (110), (200), and (220) plans, at 14.20°, 20.18°, and 28.48°. These patterns support the JCPDS Card No. 97-025-2413 [173] primary tetragonal phase of $MAPbI_3$ perovskite. On the other hand, according to JCPDS card N° 96-723-1906 [172], (figure III.11.b) shows that the fresh sample $MAPbCl_3$ has two significant peaks at 15.90° and 31.88° that fit well with the (001) and (002) planes, respectively, and suggest the presence of a cubic phase.

Simultaneously, following a 12-hour exposure of $MAPbI_3$ films to UV irradiation, figure III.11.c displays striking alterations in both the XRD patterns and the sample color (turning from black to yellow). The findings show that exposure to UV light causes a structural decomposition from a tetragonal $MAPbI_3$ perovskite to a hexagonal PbI_2, which is in a good agreement with previous reported work [85]. On the other hand, figure III.11.d shows the XRD patterns of $MAPbCl_3$ after 12 hours of UV exposure. Noting that no obvious change in the structure or colors has been noticed. For that, $MAPbCl_3$ perovskite demonstrated higher stability against UV irradiation. In fact, the cubic structure of $MAPbCl_3$ is recognized to be extra stable and denser compared to the tetragonal structure of $MAPbI_3$, which helps to explain the observed differences in behaviors of the two examined structures. We think that the observed stability of $MAPbCl_3$ perovskite is directly related to the strength of the Pb-I and Pb-Cl bonds being different. Indeed, the Pb-Cl bond is tougher and more stable than the Pb-I bond because Cl has a higher electronegativity (3.16) than I (2.66).

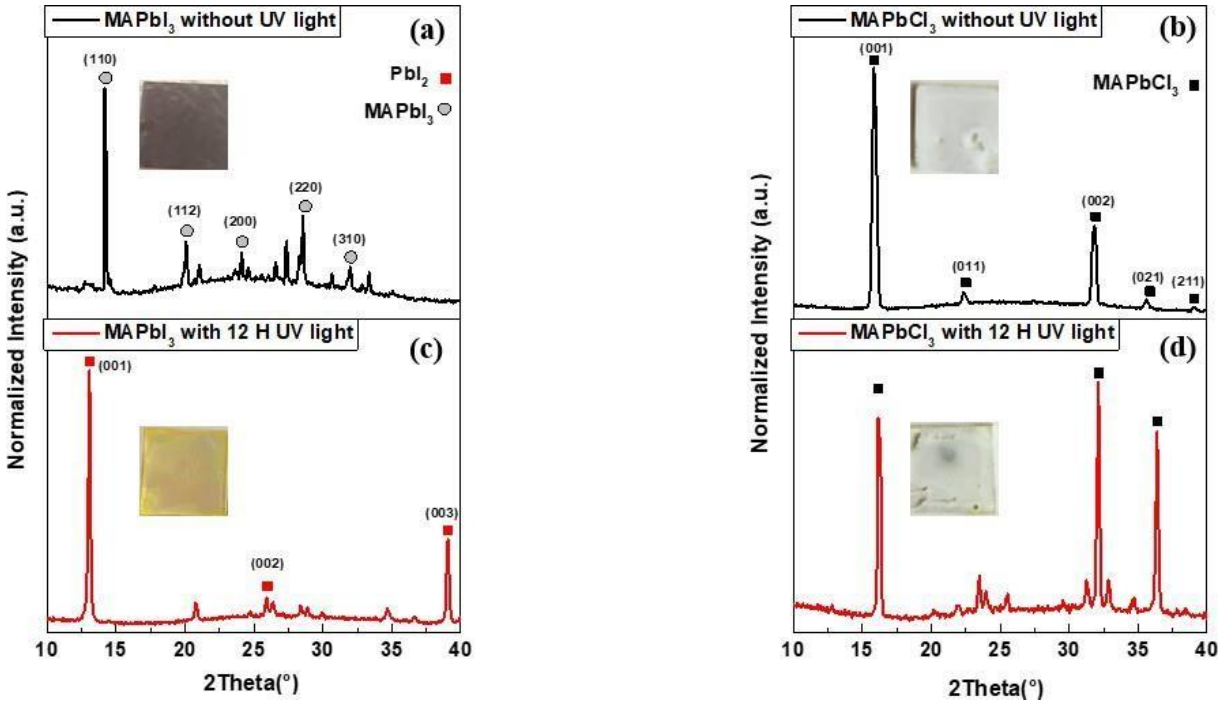

Figure III.11: XRD patterns and colors of the as-deposited $MAPbI_3$ (a) and $MAPbCl_3$ (b) perovskites before and after 12 hours exposure to the UV irradiation (c) and (d).

III.B.2.2. XRD analysis of $MAPb(I_{1-x}Cl_x)_3$ films

The structural change in the MAPI perovskite caused by partial iodine substitution with chloride under UV irradiation is the topic of interest in this paragraph. In order to illustrate this, figure III.12 displays the XRD patterns of the $MAPb(I_{1-x}Cl_x)_3$ perovskite before and after a 12-hour UV exposure, for x= 0%, 10%, 15%, 20%, 30%, 40%, 50%, and 100%. To enhance clarity, the XRD patterns of $MAPb(I_{1-x}Cl_x)_3$ films are exclusively displayed inside the 2θ interval, which extends from 12° to 17° and highlights the primary structural alteration. Figure III.12.a, which represents the XRD study of $MAPb(I_{1-x}Cl_x)_3$ that was not exposed to UV light, makes it clear that when the chloride ratio rises from 0 to 30%, the diffraction patterns change towards higher angles. This type of shift has a well-established relationship with the I and Cl elements differing ionic radii [174]. There is a morphotropic structural shift from tetragonal (I4/mcm) to cubic (Pm3m) structure when the chloride fraction exceeds 30%, and this transition is linked to a greater reduction of the lattice parameter.

In fact, figure III.12.b displays the XRD analysis of $MAPb(I_{1-x}Cl_x)_3$ perovskite (x=0%, 10%, 15%, 20%, 30%, 40%, 50%, and 100%) after 12 hours of UV exposure. When the chloride ratio is less than 20%, these XRD patterns clearly demonstrate that the PbI_2 phase predominates, showing an induced perovskite deterioration that is directly proportional to the chloride ratio. Nevertheless, no peak associated with the PbI_2 phase is seen in the XRD patterns when the chloride ratio exceeds 20%, indicating that the produced perovskite becomes more stable and does not degrade. It should be noticed that at 30% of chloride content the structural dominance changes from tetragonal phase to the more stable cubic phase. These results show, unequivocally, that 20% of chloride is considered as the optimal content value for producing a $MAPb(I_{1-x}Cl_x)_3$ perovskite more resistant to UV irradiation.

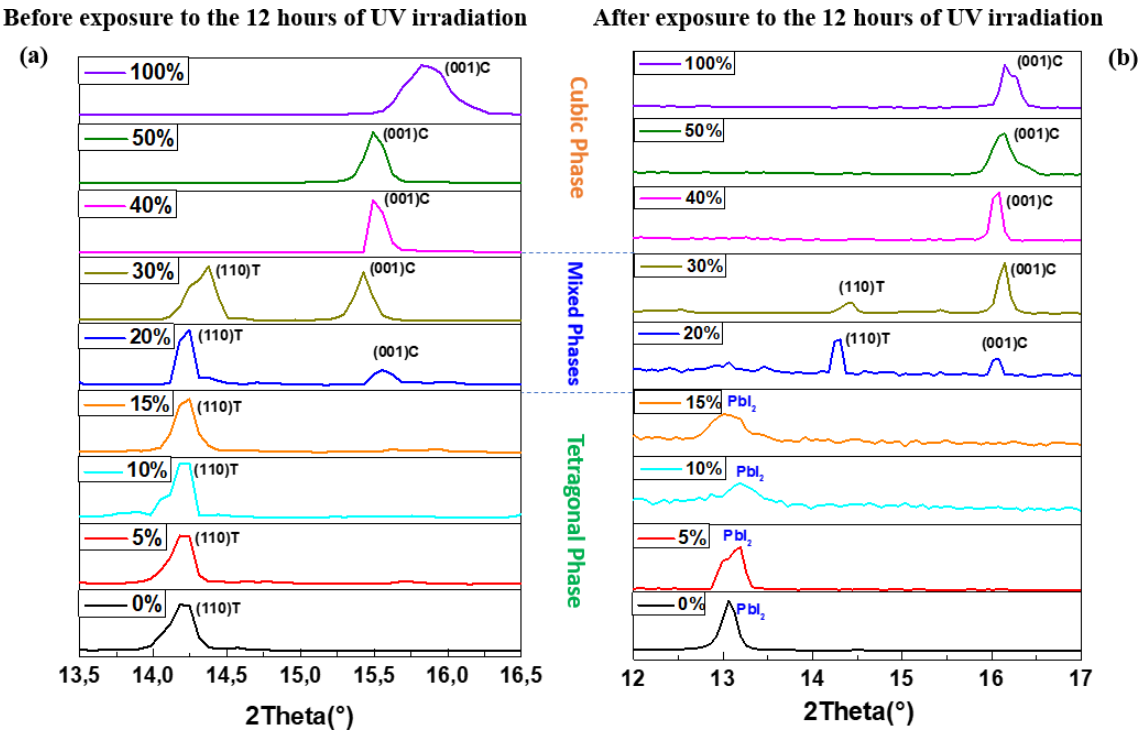

Figure III.12: XRD diffractograms of $MAPb(I_{1-x}Cl_x)_3$ films deposited with different chloride ratios (0, 5, 10, 15, 20, 30, 40, 50 and 100 %), before (a) and after (b) exposure to the 12 hours of UV irradiation.

III.B.2.3. SEM surface analysis

The SEM investigation is conducted to examine the influence of Cl incorporation on perovskite morphology. For that, figure III.13 presents top view SEM images of the $MAPb(I_{1-x}Cl_x)_3$ perovskite thin films deposited on glass substrates with different fractions (x=0%, 10%, 15%, 20%, 30%, 40%, 50%, and 100%), before and after 12 hours of exposure to UV irradiations. The $MAPb(I_{1-x}Cl_x)_3$ films have a denser and homogenous morphology with crystal-like fibers in the case of $MAPbCl_3$ (figure III.13.q), the micrograph shows grains of rectangular shape in conformity with the $MAPbCl_3$ cubic structure. Additionally, changing the chloride portion from 5% to 50% results in a change in the grain morphology and size (figure III.13.c, e, g, i, k, m and o). Noticing that SEM micrographs show the dependence of the grain size on Cl content (x). In Fact, the resulting films exhibit varying morphology, size, and form depending on the amount of chloride present. Commonly, as the composition x increases, the aggregation of gains increases accordingly.

However, following UV exposure, the samples show a comparatively low degradation, as seen in (figure III.13.b, j, l, n, p and r), compared with (figure III.13.d, f and h), which is

indicated by the existence of fiber-like crystals attributed to the presence of PbI_2 phase. More significantly, when the chloride fraction is between 20 and 50%, no appreciable alterations in the surface and/or grain morphology were noticed (figure III.13.j, l, n and p). Once again, our findings demonstrate that the perovskite may be produced in this chloride fraction range with a better UV stable shape.

Alternatively, after exposure to UV irradiation, the specimens with Cl contents (x=0, 0.2, 0.3, 0.4, 0.5, and 1) demonstrated comparatively minimal degradation, as depicted in figure III.13.b, j, l, n, p, and r, in contrast to those with chlorine contents (x=0.05, 0.1, 0.15) depicted in figure III.13.d, f, and h. This disparity is evident through the presence of crystal-like structures resembling fibers. More importantly, no remarkable changes in the surface and/or the grain morphology were observed when the chloride fraction is between 20 and 50% (figure III.13.j, l, n and p). Once again, these results show that a better UV stable morphology of the perovskite can be achieved within this chloride fraction range.

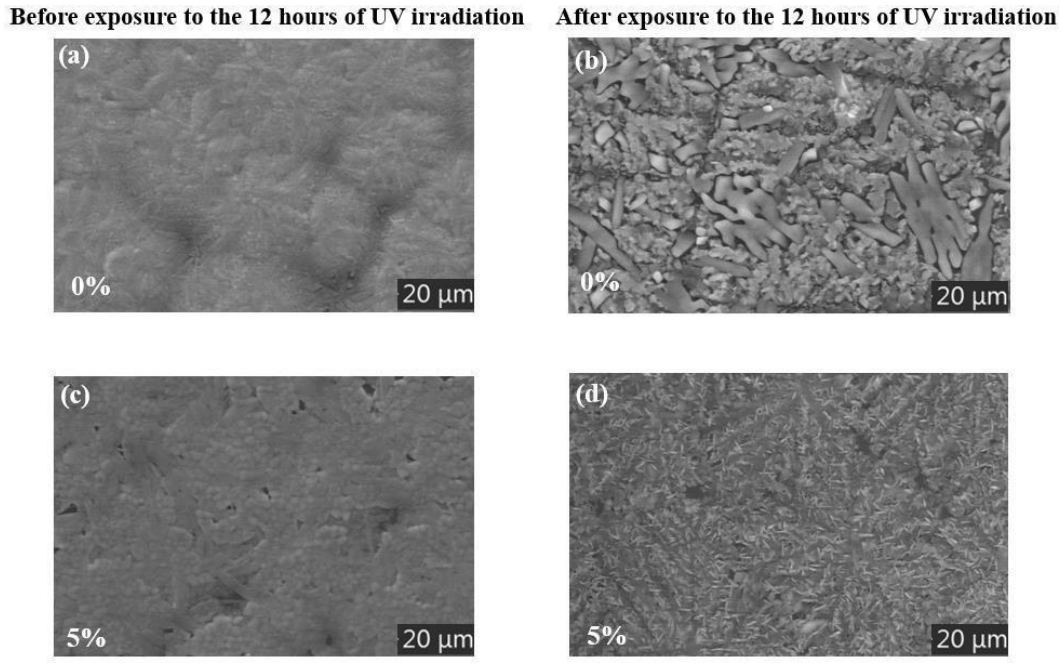

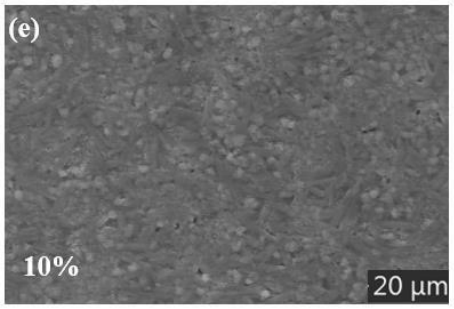
(e)
10%
20 µm

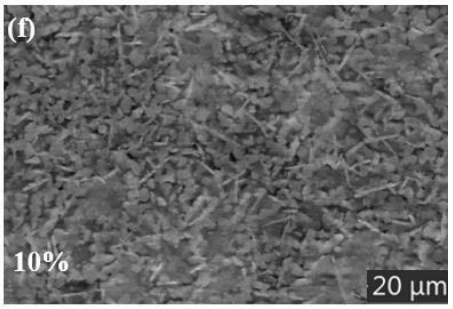
(f)
10%
20 µm

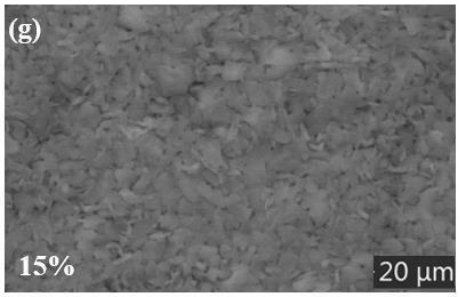
(g)
15%
20 µm

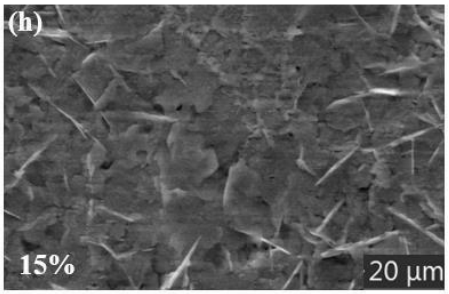
(h)
15%
20 µm

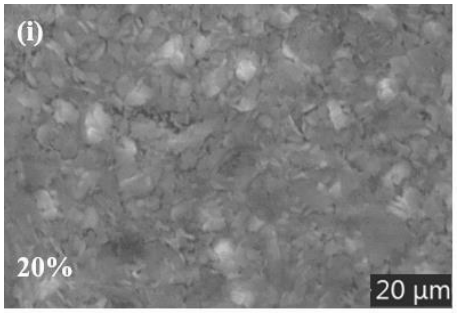
(i)
20%
20 µm

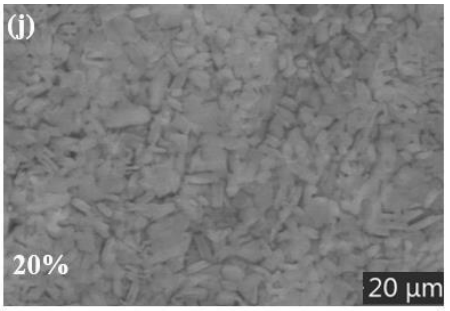
(j)
20%
20 µm

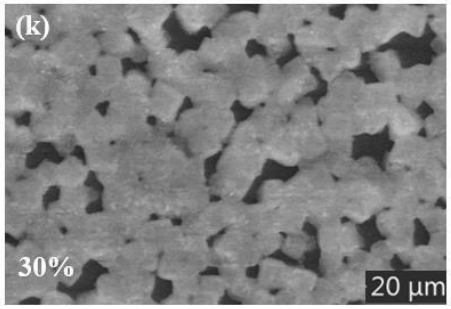
(k)
30%
20 µm

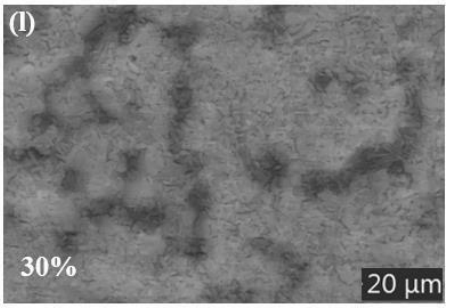
(l)
30%
20 µm

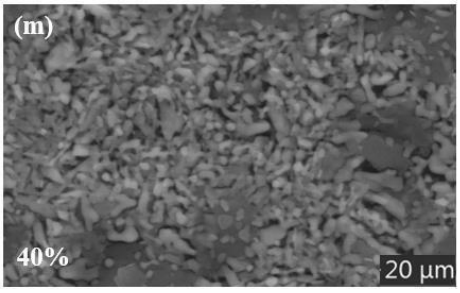
(m)
40%
20 µm

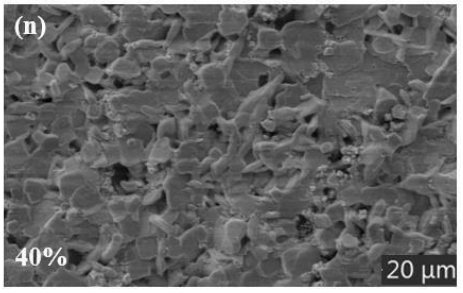
(n)
40%
20 µm

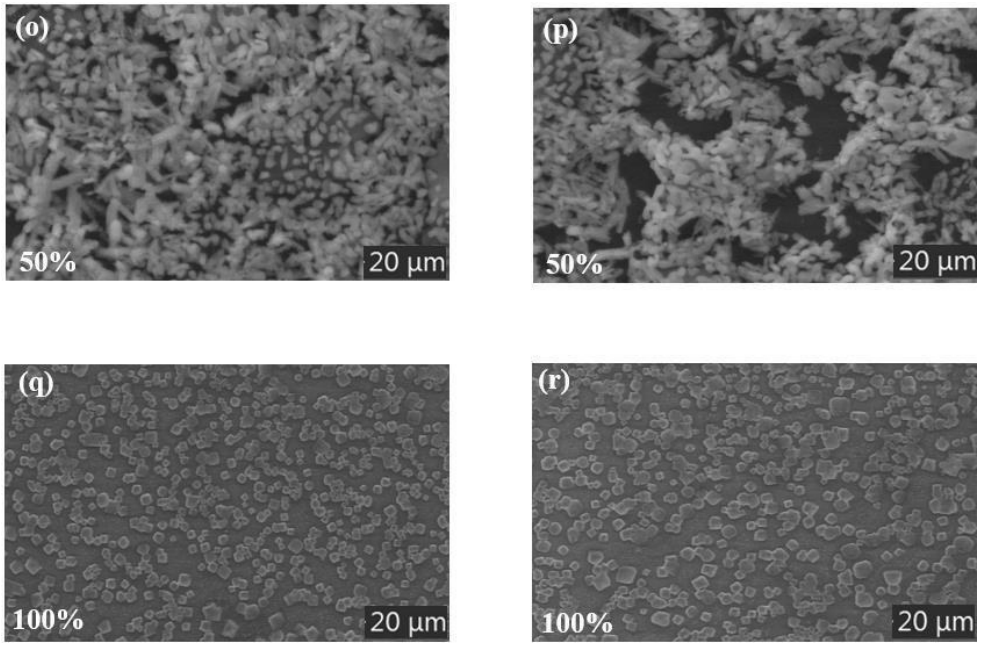

Figure III.13: SEM images of $MAPb(I_{1-x}Cl_x)_3$ perovskite films prepared with different Cl content x ($0\% \leq x \leq 100\%$) before (a, c, e, g, i, k, m, o and q) and after (b, d, f, h, j, l, n, p and r) 12 hours of the UV exposure.

III.B.2.4. Optical characterizations

In order to evaluate the degradation effect on the optical properties of the perovskite films under the UV irradiation, figure III.14. (a, b, c and d) present the Uv-Vis absorption of samples of $MAPb(I_{1-x}Cl_x)_3$ before and after 1, 2 and 12 hours of UV exposure. In that way, as the Cl content increases, the absorbance edge shifts to short wavelength values, indicating the increase of the band gap energy related to the prepared perovskite thin films. Note that, the onset band gap of mixed Chloride iodide perovskite thin films is located in intermediate values between 1.56 eV ($MAPbI_3$) and 2.93 eV ($MAPbCl_3$), meaning that the band gap can be tuned by varying the composition of the ratio I/Cl (figure III.15). The structural deformation brought on by the shift in Pb-I bond stress following the Cl inclusion, as well as the UV irradiation effect, are both responsible for this rise in band gap energy. Interestingly, no noteworthy change in the absorbance spectra is seen after one hour of UV irradiation when the chloride component is above 20%. Consequently, by substituting a 20% percentage of the chloride atoms for the iodine atoms, $MAPb(I_{1-x}Cl_x)_3$ can be made to have greater optical stability.

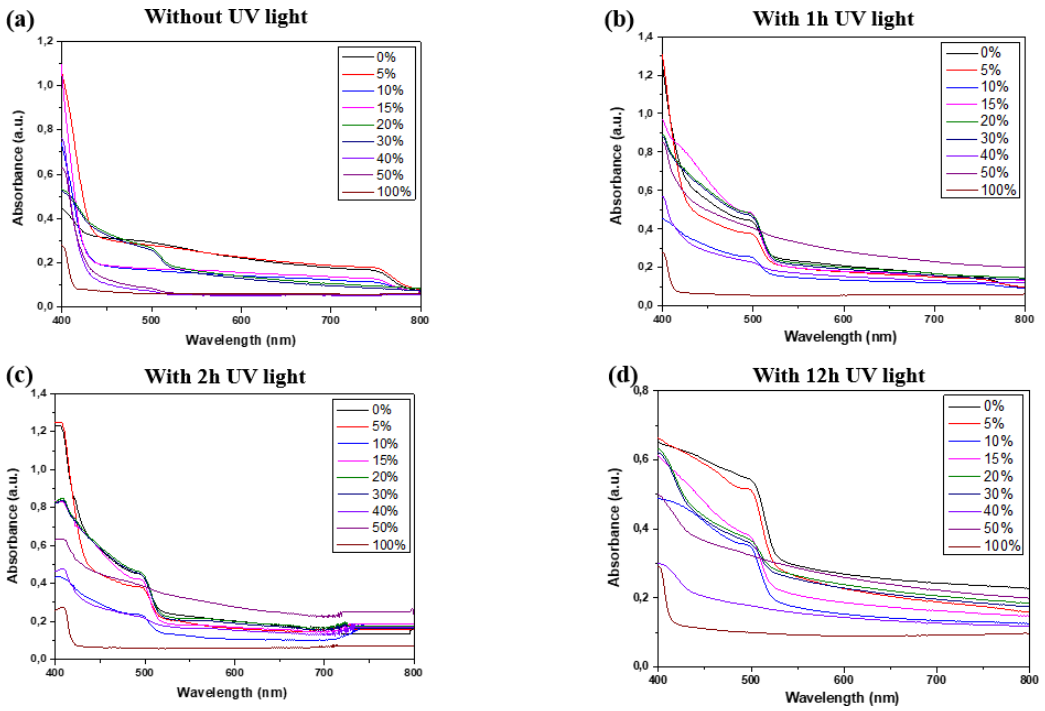

Figure III.14: UV−VIS absorption spectra of $MAPb(I_{1-x}Cl_x)_3$ before (a), after 1 hour (b), 2 hours (c) and 12 hours (d) of exposure to the UV irradiation.

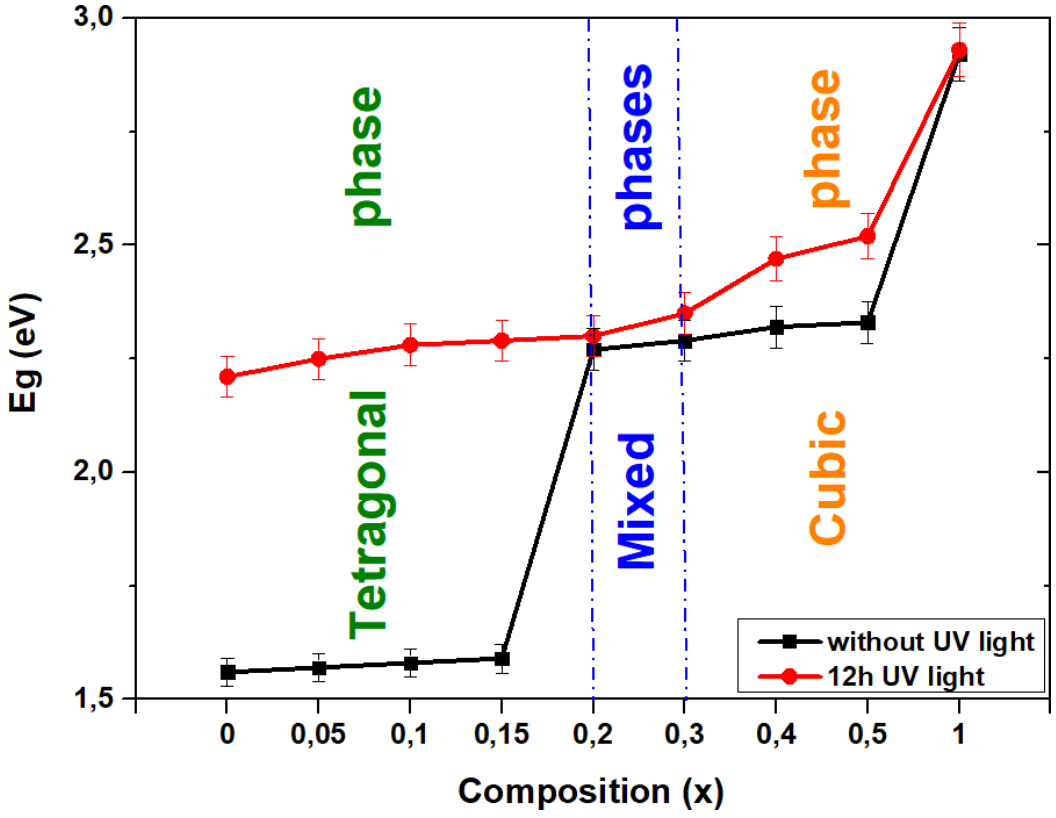

Figure III.15: Variation of the absorption edge with the chemical composition of chloride for $MAPb(I_{1-x}Cl_x)_3$ ($0\% \leq x \leq 100\%$) before and after exposure to the UV irradiation.

III.B.2.5. Fourier transforms infra-red spectrophotometer

The FTIR spectroscopy was used to study the influence of light exposure, as it is sensitive to the presence of hydroxyl groups, which play a crucial role in the photovoltaic process by limiting charge injection and transfer, as well as energy transfer from perovskite crystallites to OH vibrational states. Figure III.16 shows a comparison of IR spectra between a freshly prepared sample and a degraded sample exposed to 12 hours of UV irradiation.

The comparison of IR spectra between freshly prepared and degraded samples demonstrates a decrease in the intensity of the band corresponding to the stretching vibrations of hydroxyl group. This may indicate desorption or dissociation of hydroxyl group within the sample. Consequently, the dissociation of H_2O molecule under the influence of light can compromise the efficiency and stability of the absorptive layer due to the formation of defects [175]. A more pronounced peak, corresponding to asymmetric N–H bending vibrations, is observed with a shift in position from 1568 cm^{-1} to 1590 cm^{-1}. Besides, pronounced peaks at 905 cm^{-1}, corresponding to rocking oscillations of $CH_3NH_3^+$, are also observed, indicating the degradation of the perovskite film. Noticing that a strong changes in the absorption intensity of the characteristic frequencies corresponding to the NH and CH functional groups were revealed in the range (3136 cm^{-1} and 3200 cm^{-1}) after UV exposure. We attribute these changes to the degradation, of the perovskite structure, which affects especially the NH and CH functional groups [176].

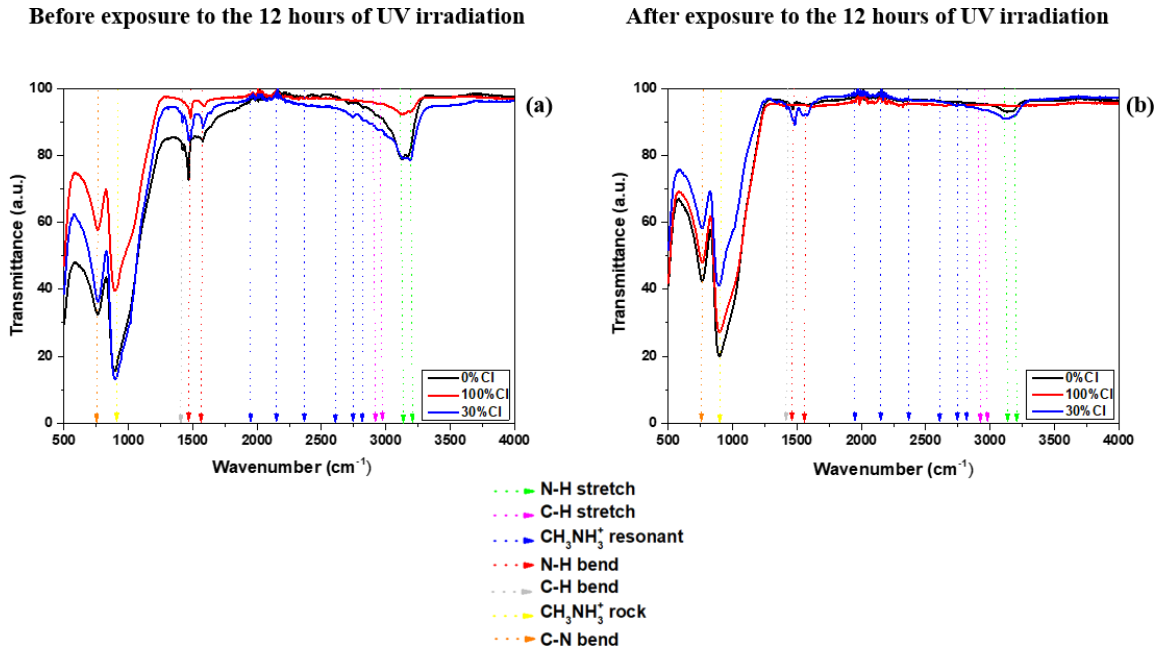

Figure III.16: IR spectra of $MAPb(I_{1-x}Cl_x)_3$ (x= 0%, 30% and 100%) freshly prepared (a) and after exposure to the UV irradiation (b).

III.B.3. Conclusion

In conclusion, this research centered on the degradation of $CH_3NH_3PbI_3$ perovskite thin films and precisely investigated the effects of UV irradiation on their structural, morphological, and optical properties. The key discovery of this study highlights the potential for enhancing the stability of $MAPbI_3$ against to UV light through a strategic introduction of chloride atoms into the perovskite structure. In fact, our experimental results clearly show that, once the chloride doping concentration is above the 20% threshold, $CH_3NH_3Pb(I_{1-x}Cl_x)_3$ perovskite films become significantly more stable. By means of XRD analysis, we have clarified that this improved stability is directly linked to a structural change from the more robust cubic phase to the tetragonal phase. On the other hand, the FTIR analysis of the $CH_3NH_3Pb(I_{1-x}Cl_x)_3$ perovskite at different level contents show clearly that the UV degradation affects especially the NH and CH functional groups. The main finding of this work is to show that it is possible to improve the stability of the perovskite against UV irradiation by a judicious choice of the chlorine content.

General Conclusion

General Conclusion

This thesis work is structured around two main axes. In a first axis, we developed a synthesis process to deposit the thin films of $MAPbCl_3$ which is to establish a hot air flow during the growth of the film $MAPbCl_3$ by the soil gel (spin-coating) process. The experimental results show that the properties of the $MAPbCl_3$ perovskite strongly depend on the temperature of the hot air flow. We have shown that 100°C is the optimal temperature and 5 cm is the optimum distance which allows a high coverage area (92%), good crystallinity with better optical absorption. In a second axis, we studied physical properties, UV stability and the compactness of thin films based on hybrid perovskites $MAPb(I_{1-x}Cl_x)_3$. Thin layers based on the perovskites $MAPb(I_{1-x}Cl_x)_3$ were also developed by the sol-gel (spin-coatting). Various characterization techniques have been deployed to evaluate the structural and microstructural properties, as well as the optical properties of the samples obtained.

In the first chapter we have presented some general concepts on solar energy and the state of the art of hybrid perovskite components used for photovoltaic applications. The first chapter was devoted to a bibliographical study on the latest developments reported on the physical properties of thin films of hybrid perovskites used in solar cells. In the second chapter, we presented the procedures for synthesis and characterization of thin layers based on $MAPbX_3$ perovskites. We described in a first part all the synthesis processes that we used: the soil gel by centrifugation (spin-coatting) and the hot air flow added to the process. In a second part, we presented a description of the post-deposition processes, namely: thermal blowing and UV irradiation, carried out on the thin films developed. The last part was devoted to the presentation of the different characterization techniques used.

In the first part of the third chapter, we presented first the properties of $MAPbCl_3$ perovskite elaborated in powder and thin film. The results of structural characterizations obtained confirm that the perovskite $MAPbCl_3$ has a cubic structure belonging to the space group (Pm3m). The morphological analysis of the surface of the samples shows that the powder $MAPbCl_3$ consists of interlaced cubic crystals. However, the morphological characterization of the thin-film perovskite deposition showed that the $MAPbCl_3$ film is denser and more homogeneous with a compactness of about 92%. Experimental results show that film continuity and crystallinity are generally improved when the air flow temperature is increased

from 50°C to 150°C and/or the distance is reduced by 15 to 5 cm. The observed partial degradation of perovskite to 150°C is attributed to an overabundance of solvent evaporation from DMSO. These results show that a temperature of 100°C and a distance of 5 cm are the best flow parameters for synthesizing a pure, homogeneous $MAPbCl_3$ perovskite without secondary phase. The reduction of gap energy is strongly related to the increase in size of the crystallites, as confirmed by the cross-experimental curve that clearly illustrates the phenomenon of quantum confinement.

In the second part of chapter III, the study of the instability of the perovskite $MAPbI_3$ vis-à-vis UV irradiation is also presented in this part of chapter III. The problem of UV instability was solved by the incorporation of chloride atoms in the $MAPbI_3$ perovskite matrix. An experimental study based on structural, morphological and optical characterizations clearly shows that the photo-degradation of perovskite is strictly related to its crystalline structure. Indeed, a better UV stability is observed for the $MAPbCl_3$ perovskite with a cubic structure. Noting that the $MAPbI_3$ perovskite has a tetragonal structure which is very sensitive to UV. The XRD results of $MAPb(I_{1-x}Cl_x)_3$ perovskites show that as the chloride fraction increases, there is an emergence of a structural transition from the tetragonal structure (I4/mcm) to the cubic structure (Pm3m) when the chloride fraction reaches 20%. This transition is accompanied by a clear improvement in the UV stability of the $MAPbI_3$ perovskite. These results can be directly exploited in the manufacture of solar cells based on the UV-stable and better yielding $MAPb(I_{1-x}Cl_x)_3$ perovskite.

List of publications

- **Asmae EL-YAHYAOUI**, Boujemaa JABER , Larbi LAANAB, Mohammed EL MAHI, El Mostapha LOTFI, “The effect of temperature and distance of hot airflow on the quality of $MAPbCl_3$ thin films grown by sol–gel deposition”, J Mater Sci: Mater Electron (2023) 34:252

- **Asmae EL-YAHYAOUI**, Boujemaa JABER , Larbi LAANAB, El Mostapha LOTFI, “Chloride incorporation for the stability improvement of the MAPI hybrid perovskite”, J Mater Sci: Mater Electron (2024) 35:798

- **Asmae EL-YAHYAOUI,** Boujemaa JABER , Larbi LAANAB, El Mostapha LOTFI, “Synthesis and characterization of MASnCl3 Perovskite: structural, morphological and Optical Study”, Journal of Materials Science: Materials in Electronics (2024)

- K. Oukacha, **A. El-Yahyaoui**, L. Laanab, S. El Hajjaji, B. Jaber, “Optimazation of cobalt doping content for the synthesis of high-performance photocatalytic Co-ZnO nanoparticles”, Journal of Inorganic and Organometallic Polymers and Materials (2024)

References

[1] Adrian E. Raftery, Hana Ševčíková, International Journal of Forecasting 39 (2023) 73-97.

[2] Hillard Huntington, Brantley Liddle, Energy Economics 111 (2022) 106082.

[3] N. Abas, A. Kalair, N. Khan, Futures 69 (2015) 31-49.

[4] B.M. Soucase, I. Guaita Pradas, K.R. Adhikari, Numerical Simulations on Perovskite Photovoltaic Devices, Perovskite Mater. - Synth. Characterisation, Prop. Appl. (2016).

[5] Leon Wang, Leigh Wang, Yang Li, John Wang, Decision Analytics Journal, 7 (2023) 100237.

[6] J.A. Church, N.J. White, Sea-Level Rise from the Late 19th to the Earlyaz 21st Century, Surv. Geophys. 32 (2011) 585–602.

[7] G.K. Singh, Solar power generation by PV (photovoltaic) technology: A review, Energy. 53 (2013) 1–13.

[8] M.A. Green, A. Ho-Baillie, H.J. Snaith, The emergence of perovskite solar cells, Nat. Photonics. 8 (2014) 506–514.

[9] Q. Chen, N. De Marco, Y. Yang, T. Bin Song, C.C. Chen, H. Zhao, Z. Hong, H. Zhou, Y. Yang, Under the spotlight: The organic-inorganic hybrid halide perovskite for optoelectronic applications, Nano Today. 10 (2015) 355–396.

[10] J.S. Manser, J.A. Christians, P. V. Kamat, Intriguing Optoelectronic Properties of Metal Halide Perovskites, Chem. Rev. 116 (2016) 12956–13008.

[11] M. Ouafi, B. Jaber, L. Atourki, R. Bekkari, L. Laânab, Improving UV stability of MAPbI3 perovskite thin films by bromide incorporation, J. Alloys Compd. 746 (2018).

[12] Https://www.nrel.gov/pv/assets/pdfs/pv-efficiencies-07-17-2018.pdf, Full-Text, (2015) 2020.

[13] H. Yu, F. Wang, F. Xie, W. Li, J. Chen, N. Zhao, The Role of Chlorine in the Formation Process of "CH3NH3PbI3-xClx" Perovskite, Adv. Funct. Mater. 24 (2014) 7102–7108.

[14] Z. Song, S.C. Watthage, A.B. Phillips, M.J. Heben, Pathways toward high-performance perovskite solar cells: review of recent advances in organo-metal halide perovskites for photovoltaic applications, J. Photonics Energy. 6 (2016) 22001.

[15] D. Wang, M. Wright, N.K. Elumalai, A. Uddin, Stability of perovskite solar cells, Sol. Energy Mater. Sol. Cells. 147 (2016) 255–275.

[16] Y. Zhao, K. Zhu, Organic–inorganic hybrid lead halide perovskites for optoelectronic and electronic applications, Chem. Soc. Rev. 45 (2015) 655–689.

[17] M.D. McGehee, Perovskite solar cells: Continuing to soar, Nat. Mater. 13 (2014) 845–846.

[18] C.R Kagan, D.B Mitzi and C.D. Dimitrapoulos. Organic-inorganic Materials as semiconducting channels in thin-film Field-effect Transistors. Science 286, 945-947 (1999).

[19] D.B. Mitzi, K. Chondroudis, and C.R. Kagan. Organic – Inorganic Electronics. IBM J. Res. Dev. 45, 29–45 (2001).

[20] M.M Lee, J. Teusher, T. Miyasaka, T. N Murakami and H. J Snaith. Efficient hybrid solar cell based on meso-superstructured organometal Halide perovskite. Science 338, 643-647, (2012).

[21] G. Xing, N. Mathews, S. Sun, S.S. Lin, Y. M. Lam, M. Grätzel, S. Mhaisalkar, T. Ch. Sum. Long range balanced electron and hole transport lengths in organic-inorganic CH3NH3PbI3. Science 342, 344-347 (2013).

[22] Q. Dong, Y. Yuan, Y. Shao, Y. Fang, Q. Wang, J. Huang, Abnormal crystal growth in CH 3 NH 3 PbI 3−x Cl x using a multi-cycle solution coating process, Energy Environ. Sci. 8 (2015) 2464–2470.

[23] S. Song, M.T. Hörantner, K. Choi, H.J. Snaith, T. Park, Inducing swift nucleation morphology control for efficient planar perovskite solar cells by hot-air quenching, J. Mater. Chem. A. (2017).

[24] E. Kabir, P. Kumar, S. Kumar, A.A. Adelodun, K. Kim, Solar energy : Potential and future prospects, 82 (2018) 894 900.

[25] S.Y. Abdelouadoud, Vers une méthode automatique d'estimation de la distribution spectrale du rayonnement solaire. Cas du ciel clair. Applications à la lumière du jour, photosynthèse et ultraviolet, (2015).

[26] A. CHALEIL, Développement d'une source de rayonnement X par diffusion Compton inverse sur l'accélérateur ELSA et optimisation à l'aide d'un système d'empilement de photons, Thèse l'Université Paros Sud. (2016).

[27] D. SOUBANE, Élaboration et Caractérisation des Films Absorbeurs I-II-VI2 {CuInSe2, CuInS2, CuIn(Se,S)2 et Cu(In,Ga)Se2}, Film Buffer I-VI CdS et Nano Fenêtre Optique ZnO, Destinés à la Fabrication des Cellules Solaires à Faible Coût de Revient, Univ. IBN ZOHR. (2007).

[28] C. Howell, RENEWABLE ENERGY AND ENERGY EFFICIENCY SCIENCE PROECTS IN RENEWABLE, Natl. Renewble Energy Laboratoy. (2007).

[29] https://fr.scribd.com/document/101019894/PV-History, (n.d.).

[30] J.M. Navarro, Cellules Photovoltaïques Organiques Transparentes Dans Le Visible, (2008).

[31] C. Semassou, Aide a la décision pour le choix de sites et systemes energetiques adaptes aux besoins du Benin, (2011) 244.

[32] G.K. Singh, Solar power generation by PV (photovoltaic) technology: A review, Energy. 53 (2013) 1–13.

[33] D. Lincot, The new paradigm of photovoltaics : From powering satellites to powering humanity, Comptes Rendus Phys. 1 (2017) 1–10.

[34] Russell S. Ohl, LIGHT-SENSITIVE ELECTRIC DEVICE INCLUDING SILICON, (1948).

[35] Ohl, R. S. Light-Sensitive Electric Device. US2402662A, June 25, 1946.

[36] Best Research-Cell Efficiency Chart. https://www.nrel.gov/pv/cell-efficiency.html.

[37] D. Reaux, Cellules photovoltaïques à hétérojonctions de silicium (a-Si H / c-Si) : modélisation des défauts et de la recombinaison à l ' interface, (2017).

[38] Q. Dong, Y. Yuan, Y. Shao, Y. Fang, Q. Wang, J. Huang, Abnormal crystal growth in CH3NH3PbI3−xClx using a multi-cycle solution coating process, Energy Environ. Sci. 8 (2015) 2464–2470.

[39] S. Song, M.T. Hörantner, K. Choi, H.J. Snaith, T. Park, Inducing swift nucleation morphology control for efficient planar perovskite solar cells by hot-air quenching, J. Mater. Chem. A. (2017).

[40] N.K. Noel, A. Abate, S.D. Stranks, E.S. Parrott, V.M. Burlakov, A. Goriely, H.J. Snaith, Enhanced photoluminescence and solar cell performance via Lewis base passivation of organic-inorganic lead halide perovskites, ACS Nano. 8 (2014) 9815–9821.

[41] T.J. Jacobsson, M. Pazoki, A. Hagfeldt, T. Edvinsson, Goldschmidt ' s Rules and Strontium Replacement in Lead Halogen Perovskite Solar Cells : Theory and Preliminary Experiments on CH NH SrI Goldschmidt ' s Rules and Strontium Replacement in Lead Halogen Perovskite Solar Cells : Theory and Preliminary Experi, (2015).

[42] J. Choi, S. Song, M.T. Hörantner, H.J. Snaith, T. Park, Well-Defined Nanostructured, Single-Crystalline TiO2 Electron Transport Layer for Efficient Planar Perovskite Solar Cells, ACS Nano. 10 (2016) 6029–6036.

[43] W. Ke, G. Fang, J. Wang, P. Qin, H. Tao, H. Lei, Q. Liu, X. Dai, X. Zhao, Perovskite Solar Cell with an Efficient TiO2 Compact Film Perovskite Solar Cell with an Efficient TiO 2 Compact Film, (2014).

[44] Z.M.A. Bundhoo, Renewable energy exploitation in the small island developing state of Mauritius: Current practice and future potential, Renew. Sustain. Energy Rev. (2017).

[45] Z. Cheng, J. Lin, Layered organic–inorganic hybrid perovskites: structure, optical properties, film preparation, patterning and templating engineering, CrystEngComm. 12 (2010) 2646–2662.

[46] C. Li, X. Lu, W. Ding, L. Feng, Y. Gao, Z. Guo, Formability of ABX 3 (X = F, Cl, Br, I) halide perovskites, Acta Crystallogr. Sect. B Struct. Sci. 64 (2008) 702–707.

[47] N.K. Elumalai, A. Uddin, Hysteresis in organic-inorganic hybrid perovskite solar cells, Sol. Energy Mater. Sol. Cells. 157 (2016) 476–509.

[48] A. Poglitsch, D. Weber, Dynamic disorder in methylammoniumtrihalogenoplumbates (II) observed by millimeter wave spectroscopy, J. Chem. Phys. 87 (1987) 6373.

[49] G. Niu, X. Guo, L. Wang, Review of recent progress in chemical stability of perovskite solar cells, J. Mater. Chem. A. 3 (2015) 8970–8980.

[50] G. Niu, X. Guo, L. Wang, Review of Recent Progress in Chemical Stability of Perovskite Solar Cells, J. Mater. Chem. A. 3 (2015) 8970–8980.

[51] C.C. Stoumpos, C.D. Malliakas, M.G. Kanatzidis, Semiconducting tin and lead iodide perovskites with organic cations: Phase transitions, high mobilities, and near-infrared photoluminescent properties, Inorg. Chem. 52 (2013) 9019–9038.

[52] S.-W. Lee, et al Kim, UV Degradation and Recovery of Perovskite Solar Cells, Sci. Rep. 6 (2016) 38150.

[53] I. Borriello, G. Cantele, D. Ninno, Ab initio investigation of hybrid organic-inorganic perovskites based on tin halides, Phys. Rev. B - Condens. Matter Mater. Phys. 77 (2008) 1–9.

[54] Y. H. Chang and C. H. Park, First-Principles Study of the Structural and the Electronic Properties of the, J. Korean Phys. Soc. 44 (2004) 889–893.

[55] M.I.H. Ansari, A. Qurashi, M.K. Nazeeruddin, Frontiers, opportunities, and challenges in perovskite solar cells: A critical Photochem.

[56] S. Pang, H. Hu, J. Zhang, S. Lv, Y. Yu, T. Qin, H. Xu, Z. Liu, G. Cui, J. Accepted, NH 2 CH = NH 2 PbI 3 : An Alternative Organolead Iodide Perovskite Sensitizer for Mesoscopic Solar Cells, Chem. Mater. (2014).

[57] G.E. Eperon, S.D. Stranks, C. Menelaou, M.B. Johnston, L.M. Herz, H.J. Snaith, Formamidinium lead trihalide: a broadly tunable perovskite for efficient planar heterojunction solar cells, Energy Environ. Sci. 7 (2014) 982.

[58] P. Umari, E. Mosconi, F. De Angelis, Relativistic GW calculations on CH3 NH3 PbI 3 and CH3 NH3 SnI3 Perovskites for Solar Cell Applications, Sci. Rep. 4 (2014) 1–7.

[59] S.D. Stranks, H.J. Snaith, Metal-halide perovskites for photovoltaic and light-emitting devices, Nat. Nanotechnol. 10 (2015) 391–402.

[60] C.C. Stoumpos, L. Frazer, D.J. Clark, Y.S. Kim, S.H. Rhim, A.J. Freeman, J.B. Ketterson, J.I. Jang, M.G. Kanatzidis, Hybrid germanium iodide perovskite semiconductors: Active lone pairs, structural distortions, direct and indirect energy gaps, and strong nonlinear optical properties, J. Am. Chem. Soc. 137 (2015) 6804–6819.

[61] F. Hao, C.C. Stoumpos, D.H. Cao, R.P.H. Chang, M.G. Kanatzidis, Lead-free solid-state organic–inorganic halide perovskite solar cells, Nat. Photonics. 8 (2014) 489–494.

[62] S.F. Hoefler, G. Trimmel, T. Rath, Progress on lead-free metal halide perovskites for photovoltaic applications: a review, Monatshefte Fur Chemie. 148 (2017) 795–826.

[63] P.P. Sun, Q.S. Li, S. Feng, Z.S. Li, Mixed Ge/Pb perovskite light absorbers with an ascendant efficiency explored from theoretical view, Phys. Chem. Chem. Phys. 18 (2016) 14408–14418.

[64] S.M. Jain, D. Phuyal, M.L. Davies, M. Li, B. Philippe, C. De Castro, Z. Qiu, J. Kim, T. Watson, W.C. Tsoi, O. Karis, H. Rensmo, G. Boschloo, T. Edvinsson, J.R. Durrant, An effective approach of vapour assisted morphological tailoring for reducing metal defect sites in lead-free, (CH3NH3)3Bi2I9bismuth-based perovskite solar cells for improved performance and long-term stability, Nano Energy. 49 (2018) 614–624.

[65] Y. Ogomi, A. Morita, S. Tsukamoto, T. Saitho, N. Fujikawa, Q. Shen, T. Toyoda, K. Yoshino, S.S. Pandey, S. Hayase, CH3NH3SnxPb(1−x)I3 Perovskite Solar Cells Covering up to 1060 nm, Phys. Chem. Lett. ACS. (2014).

[66] F. Hao, C.C. Stoumpos, R.P.H. Chang, M.G. Kanatzidis, Anomalous band gap behavior in mixed Sn and Pb perovskites enables broadening of absorption spectrum in solar cells, J. Am. Chem. Soc. 136 (2014) 8094–8099.

[67] J.H. Noh, S.H. Im, J.H. Heo, T.N. Mandal, S. Il Seok, Chemical management for colorful, efficient, and stable inorganic-organic hybrid nanostructured solar cells, Nano Lett. 13 (2013) 1764–1769.

[68] A. Walsh, Principles of Chemical Bonding and Band Gap Engineering in Hybrid Organic − Inorganic Halide Perovskites, (2015).

[69] Q.A. Akkerman, V.D. Innocenzo, S. Accornero, A. Scarpellini, A. Petrozza, M. Prato, L. Manna, Tuning the Optical Properties of Cesium Lead Halide Perovskite, J. Am. Chem. Soc. (2015).

[70] S. Colella, E. Mosconi, P. Fedeli, A. Listorti, F. Gazza, F. Orlandi, P. Ferro, T. Besagni, A. Rizzo, G. Calestani, G. Gigli, F. De Angelis, R. Mosca, MAPbI 3-x Cl x Mixed Halide Perovskite for Hybrid Solar Cells: The Role of Chloride as Dopant on the Transport and Structural Properties, Chem. Mater. 25 (2013) 4613–4618.

[71] S.D. Stranks, G.E. Eperon, G. Grancini, C. Menelaou, M.J.P. Alcocer, T. Leijtens, L.M. Herz, A. Petrozza, H.J. Snaith, Electron-Hole Diffusion Lengths Exceeding 1 Micrometer in an Organometal Trihalide Perovskite Absorber, Science (80). 342 (2013) 341–344.

[72] C. Quarti, E. Mosconi, P. Umari, F. De Angelis, Chlorine Incorporation in the CH3NH3PbI3 Perovskite: Small Concentration, Big Effect, Inorg. Chem. 56 (2017) 74–83.

[73] R.E. Brandt, V. Stevanovid, D.S. Ginley, T. Buonassisi, Identifying defect-tolerant semiconductors with high minority carrier lifetimes: beyond hybrid lead halide perovskites, MRS Commun. 5 (2015) 1–11.

[74] N.N. Lal, Y. Dkhissi, W. Li, Q. Hou, Y.B. Cheng, U. Bach, Perovskite Tandem Solar Cells, Adv. Energy Mater. (2017).

[75] J. Wang, J. Peng, Y. Sun, X. Liu, Y. Chen, Z. Liang, FAPbCl3 Perovskite as Alternative Interfacial Layer for Highly Efficient and Stable Polymer Solar Cells, Adv. Electron. Mater. 2 (2016) 1–6.

[76] Z. Xiao, Y. Yuan, Q. Wang, Y. Shao, Y. Bai, Y. Deng, Q. Dong, M. Hu, C. Bi, J. Huang, Thin-film semiconductor perspective of organometal trihalide perovskite materials for high-efficiency solar cells, Mater. Sci. Eng. R Reports. 101 (2016) 1–38.

[77] A. Walker, H. Snaith, F. De Angelis, E. Da Como, Unconventional Thin Film Photovoltaics: RSC Energy and Environment Series, (2016) 502. https://books.google.es/books?id=ucbRDAAAQBAJ.

[78] E.S. Parrott, R.L. Milot, T. Stergiopoulos, H.J. Snaith, M.B. Johnston, L.M. Herz, Effect of Structural Phase Transition on Charge-Carrier Lifetimes and Defects in CH3NH3SnI3 Perovskite, J. Phys. Chem. Lett. 7 (2016) 1321–1326.

[79] S. Yang, W. Fu, Z. Zhang, H. Chen, C.-Z. Li, Recent advances in perovskite solar cells: efficiency, stability and lead free perovskite, J. Mater. Chem. A. 5 (2017) 11462–11482.

[80] C. Zhang, L. Gao, S. Hayase, T. Ma, Current Advancements in Material Research and Techniques Focusing on Lead free Perovskite Solar Cells, Chem. Lett. 46 (2017) 1276–1284.

[81] S.H. Jo, Y. Tu, Z.P. Huang, D.L. Carnahan, D.Z. Wang, Z.F. Ren, Effect of length and spacing of vertically aligned carbon nanotubes on field emission properties, Appl. Phys. Lett. 82 (2003) 3520–3522.

[82] W. Travis, E.N.K. Glover, H. Bronstein, D.O. Scanlon, R.G. Palgrave, On the application of the tolerance factor to inorganic and hybrid halide perovskites: a revised system, Chem. Sci. 7 (2016) 4548–4556.

[83] L. Zhu, J. Shi, S. Lv, Y. Yang, X. Xu, Y. Xu, J. Xiao, H. Wu, Y. Luo, D. Li, Q. Meng, Temperature-assisted controlling morphology and charge transport property for highly efficient perovskite solar cells, Nano Energy. 15 (2015) 540 548.

[84] C.S. Ponseca, T.J. Savenije, M. a. Abdellah, K. Zheng, A.P. Yartsev, T.T. Pascher, T. Harlang, P. Chabera, T. Pullerits, A. Stepanov, J.-P. Wolf, V. Sundstrom, C.S. Ponseca Jr., T.J. Savenije, M. a. Abdellah, K. Zheng, A.P. Yartsev, T.T. Pascher, T. Harlang, P. Chabera, T. Pullerits, A. Stepanov, J.-P. Wolf, V. Sundstrom, Organometal halide perovskite solar cell

materials rationalized ultrafast charge generation, high and microsecond-long balanced mobilities and slow recombination, J. Am. Chem. Soc. 136 (2014) 5189–5192.

[85] M. Ouafi, B. Jaber, L. Atourki, R. Bekkari, L. Laânab, Improving UV stability of MAPbI3 perovskite thin films by bromide incorporation Mouad, J. Alloys Compd. (2018).

[86] K. Jemli, Synthèse et auto-assemblage de molécules de pérovskite pour la photonique et le marquage, L'UNIVERSITE PARIS-SACLAY. (2016).

[87] O.C.H.N.H. Pbi, G. Xing, Long-Range Balanced Electron- and Hole-Transport Lengths in Organic-Inorganic CH 3NH3PbI3, Sci. Www.Sciencemag.Org. 344 (2014).

[88] G.W. P, L.W. Veldhuizen, Y. Kuang, S. Brittman, R.E.I. Schropp, E.C. Garnett, Carrier Di ff usion Lengths in Hybrid Perovskites: Processing, Composition, Aging, and Surface Passivation E ff ects, Chem. Mater. 2016. (2016).

[89] M.A.G. Rui Sheng, Anita Ho-Baillie*, Shujuan Huang, Sheng Chen, Xiaoming Wen, Xiaojing Hao, Methylammonium Lead Bromide Perovskite- Based Solar Cells by Vapour-Assisted Deposition, J. Phys. Chem. C. (2015).

[90] N.K. Elumalai, M.A. Mahmud, D. Wang, A. Uddin, Perovskite solar cells: Progress and advancements, Energies. 9 (2016).

[91] Serea, E. S. A.; Mohamed, S. A.; Shalan, A. E.; Rashad, M. M. 14 - Hybrid Perovskite Photovoltaic Devices: Architecture and Fabrication Methods Based on Solution-Processed Metal Oxide Transport Layers. In Hybrid Perovskite Composite Materials; Khan, I., Khan, A., Khan, M. M. A., Khan, S., Verpoort, F., Umar, A., Eds.; Woodhead Publishing Series in Composites Science and Engineering; Woodhead Publishing, 2021; pp 291–313.

[92] Etgar, L.; Gao, P.; Xue, Z.; Peng, Q.; Chandiran, A. K.; Liu, B.; Nazeeruddin, Md. K.; Grätzel, M. Mesoscopic CH3NH3PbI3/TiO2 Heterojunction Solar Cells. J. Am. Chem. Soc. 2012, 134 (42), 17396–17399.

[93] Lee, M. M.; Teuscher, J.; Miyasaka, T.; Murakami, T. N.; Snaith, H. J. Efficient Hybrid Solar Cells Based on Meso-Superstructured Organometal Halide Perovskites. Science 2012, 338 (6107), 643–647.

[94] Motta, C.; El-Mellouhi, F.; Sanvito, S. Charge Carrier Mobility in Hybrid Halide Perovskites. Sci. Rep. 2015, 5 (1), 12746.

[95] Osman, B. A.; Abdolkader, T. M.; Ahmed, I. S. A Review of Perovskite Solar Cells. Int. J. Mater. Technol. Innov. 2021, 1 (2), 48–66.

[96] Kim, H.-S.; Lee, C.-R.; Im, J.-H.; Lee, K.-B.; Moehl, T.; Marchioro, A.; Moon, S.-J.; Humphry-Baker, R.; Yum, J.-H.; Moser, J. E.; Grätzel, M.; Park, N.-G. Lead Iodide Perovskite Sensitized All-Solid-State Submicron Thin Film Mesoscopic Solar Cell with Efficiency Exceeding 9%. Sci. Rep. 2012, 2 (1), 591.

[97] Cheif, I. editor in. IJCRT2002249 International Journal of Creative Research Thoughts (IJCRT) Www.Ijcrt.Org. IJCRT - Int. J. Creat. Res. Thoughts IJCRT.

[98] Tress, W.; Marinova, N.; Moehl, T.; Zakeeruddin, S. M.; Nazeeruddin, M. K.; Grätzel, M. Understanding the Rate-Dependent J–V Hysteresis, Slow Time Component, and Aging in CH3NH3PbI3 Perovskite Solar Cells: The Role of a Compensated Electric Field. Energy Environ. Sci. 2015, 8 (3), 995–1004.

[99] Heo, J. H.; Han, H. J.; Kim, D.; Ahn, T. K.; Im, S. H. Hysteresis-Less Inverted CH3NH3PbI3 Planar Perovskite Hybrid Solar Cells with 18.1% Power Conversion Efficiency. Energy Environ. Sci. 2015, 8 (5), 1602–1608.

[100] Hossain, A.; Bandyopadhyay, P.; Karmakar, A.; Ullah, A. K. M. A.; Manavalan, R. K.; Sakthipandi, K.; Alhokbany, N.; Alshehri, S. M.; Ahmed, J. The Hybrid Halide Perovskite: Synthesis Strategies, Fabrications, and Modern Applications. Ceram. Int. 2022, 48 (6), 7325–7343.

[101] Im, J.-H.; Kim, H.-S.; Park, N.-G. Morphology-Photovoltaic Property Correlation in Perovskite Solar Cells: One-Step versus Two-Step Deposition of CH3NH3PbI3. APL Mater. 2014, 2 (8), 081510.

[102] Saidaminov, M. I.; Abdelhady, A. L.; Murali, B.; Alarousu, E.; Burlakov, V. M.; Peng, W.; Dursun, I.; Wang, L.; He, Y.; Maculan, G.; Goriely, A.; Wu, T.; Mohammed, O. F.; Bakr, O. M. High-Quality Bulk Hybrid Perovskite Single Crystals within Minutes by Inverse Temperature Crystallization. Nat. Commun. 2015, 6 (1), 7586.

[103] Chiang, C.-H.; Tseng, Z.-L.; Wu, C.-G. Planar Heterojunction Perovskite/PC71BM Solar Cells with Enhanced Open-Circuit Voltage via a (2/1)-Step Spin-Coating Process. J. Mater. Chem. A 2014, 2 (38), 15897–15903.

[104] Raga, S. R.; Jiang, Y.; Ono, L. K.; Qi, Y. Application of Methylamine Gas in Fabricating Organic–Inorganic Hybrid Perovskite Solar Cells. Energy Technol. 2017, 5 (10), 1750 1761.

[105] Zhou, Z.; Wang, Z.; Zhou, Y.; Pang, S.; Wang, D.; Xu, H.; Liu, Z.; Padture, N. P.; Cui, G. Methylamine-Gas-Induced Defect-Healing Behavior of CH3NH3PbI3 Thin Films for Perovskite Solar Cells. Angew. Chem. Int. Ed. 2015, 54 (33), 9705–9709.

[106] Zhang, T.; Yang, M.; Benson, E. E.; Li, Z.; Lagemaat, J. van de; Luther, J. M.; Yan, Y.; Zhu, K.; Zhao, Y. A Facile Solvothermal Growth of Single Crystal Mixed Halide Perovskite CH3NH3Pb(Br1−xClx)3. Chem. Commun. 2015, 51 (37), 7820–7823.

[107] Cao, X.; Hao, L.; Liu, Z.; Su, G.; He, X.; Zeng, Q.; Wei, J. All Green Solvent Engineering of Organic–Inorganic Hybrid Perovskite Layer for High-Performance Solar Cells. Chem. Eng. J. 2022, 437, 135458.

[108] Zhou, H.; Chen, Q.; Yang, Y. Vapor-Assisted Solution Process for Perovskite Materials and Solar Cells. MRS Bull. 2015, 40 (8), 667–673.

[109] Li, M.-H.; Yeh, H.-H.; Chiang, Y.-H.; Jeng, U.-S.; Su, C.-J.; Shiu, H.-W.; Hsu, Y.-J.; Kosugi, N.; Ohigashi, T.; Chen, Y.-A.; Shen, P.-S.; Chen, P.; Guo, T.-F. Highly Efficient 2D/3D Hybrid Perovskite Solar Cells via Low-Pressure Vapor-Assisted Solution Process. Adv. Mater. 2018, 30 (30), 1801401.

[110] H. Diab, Propriétés optiques des pérovskites hybrides 3D pour le photovoltaique To cite this version : Propriétés optiques de pérovskites hybrides 3D pour le photovoltaïque, (2018).

[111] T.A. Berhe, W.-N. Su, C.-H. Chen, C.-J. Pan, J.-H. Cheng, H.-M. Chen, M.-C. Tsai, L.-Y. Chen, A.A. Dubale, B.-J. Hwang, Organometal halide perovskite solar cells: degradation and stability, Energy Environ. Sci. 9 (2016) Advance Article.

[112] L. Meng, J. You, T. Guo, Y. Yang, Recent Advances in the Inverted Planar Structure of Perovskite Solar Cells, Acc. Chem. Res. (2015).

[113] J.-H. Im, C.-R. Lee, J.-W. Lee, S.-W. Park, N.-G. Park, 6.5% Efficient Perovskite Quantum-Dot-Sensitized Solar Cell., Nanoscale. 3 (2011) 4088–93.

[114] H. Kim, C. Lee, J. Im, K. Lee, T. Moehl, A. Marchioro, S. Moon, R. Humphry-baker, J. Yum, J.E. Moser, M. Gra, Lead Iodide Perovskite Sensitized All-Solid-State Submicron Thin Film Mesoscopic Solar Cell with Efficiency Exceeding 9% Hui-Seon, Sci. Rep. (2012) 1–7.

[115] M. Lee, J. Teuscher, T. Miyasaka, T. Murakami, H. Snaith, Efficient hybrid solar cells based on meso-superstructured organometal halide perovskites, Science (80-.). 338 (2012) 643–647.

[116] H.-S. Kim, S.H. Im, N.-G. Park, Organolead Halide Perovskite: New Horizons in Solar Cell Research, J. Phys. Chem. C. (2014).

[117] J.S. Yun, J. Seidel, J. Kim, A.M. Soufiani, S. Huang, J. Lau, N.J. Jeon, S. Il Seok, M.A. Green, A. Ho-Baillie, Critical Role of Grain Boundaries for Ion Migration in Formamidinium and Methylammonium Lead Halide Perovskite Solar Cells, Adv. Energy Mater. 6 (2016) 1–8.

[118] J.A. Christians, J.S. Manser, P. V. Kamat, Best practices in perovskite solar cell efficiency measurements. Avoiding the error of Making Bad Cells Look Good, J. Phys. Chem. Lett. 6 (2015) 852–857.

[119] H.J. Snaith, Perovskites : The Emergence of a New Era for Low-Cost , High-, J. Phys. Chem. Lett. 4 (2013) 3623−3630.

[120] J. Padchasri, R. Yimnicycle, Effects of annealing temperature on stability of methylammonium lead iodide perovskite powders, J. Alloys Compd. 720 (2017) 63–69.

[121] F.U. Kosasih, C. Ducati, Characterising degradation of perovskite solar cells through in-situ and operando electron microscopy, Nano Energy. 47 (2018) 243–256.

[122] P. Darvishzadeh, M. Babanezhad, R. Ahmadi, N.E. Gorji, Modeling the degradation/recovery of open-circuit voltage in perovskite and thin film solar cells, Mater. Des. 114 (2017) 339–344.

[123] N. Aristidou, I. Sanchez-Molina, T. Chotchuangchutchaval, M. Brown, L. Martinez, T. Rath, S.A. Haque, The Role of Oxygen in the Degradation of Methylammonium Lead Trihalide Perovskite Photoactive Layers, Angew. Chemie - Int. Ed. 54 (2015) 8208–8212.

[124] D. Bryant, N. Aristidou, S. Pont, I. Sanchez-Molina, T. Chotchunangatchaval, S. Wheeler, J.R. Durrant, S.A. Haque, Light and oxygen induced degradation limits the operational stability of methylammonium lead triiodide perovskite solar cells, Energy Environ. Sci. 9 (2016) 1655–1660.

[125] A.J. Pearson, G.E. Eperon, P.E. Hopkinson, S.N. Habisreutinger, J.T.W. Wang, H.J. Snaith, N.C. Greenham, Oxygen Degradation in Mesoporous Al2O3/CH3NH3PbI3-xClx Perovskite Solar Cells: Kinetics and Mechanisms, Adv. Energy Mater. 6 (2016).

[126] Y. Han, S. Meyer, Y. Dkhissi, K. Weber, J.M. Pringle, U. Bach, L. Spiccia, Y.-B. Cheng, Degradation observations of encapsulated planar CH 3 NH 3 PbI 3 perovskite solar cells at high temperatures and humidity, J. Mater. Chem. A. 3 (2015) 8139–8147.

[127] T. Leijtens, G.E. Eperon, S. Pathak, A. Abate, M.M. Lee, H.J. Snaith, Overcoming ultraviolet light instability of sensitized TiO2 with meso-superstructured organometal tri-halide perovskite solar cells, Nat. Commun. 4 (2013) 28885.1-8.

[128] J. Zhao, B. Cai, Z. Luo, Y. Dong, Y. Zhang, H. Xu, B. Hong, Investigation of the Hydrolysis of Perovskite Organometallic Halide CH 3 NH 3 PbI 3 in Humidity Environment, Nat. Publ. Gr. (2016) 1–6.

[129] J.W. Lee, D.H. Kim, H.S. Kim, S.W. Seo, S.M. Cho, N.G. Park, Formamidinium and cesium hybridization for photo- and moisture-stable perovskite solar cell, Adv. Energy Mater. 5 (2015).

[130] J. Ciro, R. Betancur, S. Mesa, F. Jaramillo, High performance perovskite solar cells fabricated under high relative humidity conditions, Sol. Energy Mater. Sol. Cells. 163 (2017) 38–42.

[131] D.G. and W.H. Bobo Li, Yafang Li, Chaoyue Zheng, Advancements in stability of perovskite solar cells: degradation mechanisms and improvement approaches, RSC Adv. (2016).

[132] C. Bi, Understanding the Formation and Evolution of Interdiffusion Grown Organolead Halide Perovskite Thin Films by Thermal Annealing, J. Mater. Chem. A. 4 (2014) 1166–1169.

[133] S. Yang, Y. Wang, P. Liu, Y.B. Cheng, H.J. Zhao, H.G. Yang, Functionalization of perovskite thin films with moisture tolerant molecules, Nat. Energy. 1 (2016) 1–7.

[134] B. Salhi, Y.S. Wudil, M.K. Hossain, A. Al-Ahmed, F.A. Al-Sulaiman, Review of recent developments and persistent challenges in stability of perovskite solar cells, Renew. Sustain. Energy Rev. 90 (2018) 210–222.

[135] A. Dualeh, N. Tétreault, T. Moehl, P. Gao, Effect of Annealing Temperature on Film Morphology of Organic – Inorganic Hybrid Pervoskite Solid-State Solar Cells, (2014) 1–9.

[136] G. Divitini, S. Cacovich, F. Matteocci, L. Cinà, A. Di Carlo, C. Ducati, In situ observation of heat-induced degradation of perovskite solar cells, Nat. Energy. 1 (2016) 15012.

[137] B. Philippe, B.W. Park, R. Lindblad, J. Oscarsson, S. Ahmadi, E.M.J. Johansson, H. Rensmo, Chemical and electronic structure characterization of lead halide perovskites and stability behavior under different exposures-A photoelectron spectroscopy.

[138] Z. Yao, Z. Yang, Y. Liu, W. Zhao, X. Zhang, B. Liu, H. Wu, S. (Frank) Liu, Local temperature reduction induced crystallization of MASnI 3 and achieving a direct wafer production, RSC Adv. 7 (2017) 38155–38159.

[139] L. Dimesso, C. Fasel, K. Lakus-Wollny, T. Mayer, W. Jaegermann, Thermal stability of lead-free CH3NH3SnxI3systems ($0.9 \leq x \leq 1.1$) for photovoltaics, Mater. Sci. Semicond. Process. 68 (2017) 152–158.

[140] S. Aharon, A. Dymshits, A. Rotem, L. Etgar, Temperature dependence of hole conductor free formamidinium lead iodide perovskite based solar cells, J. Mater. Chem. A. 3 (2015) 9171–9178.

[141] W.G. Li, H.S. Rao, B.X. Chen, X.D. Wang, D. Bin Kuang, A formamidinium-methylammonium lead iodide perovskite single crystal exhibiting exceptional optoelectronic properties and long-term stability, J. Mater. Chem. A. 5 (2017) 19431–19438.

[142] D.P. McMeekin, G. Sadoughi, W. Rehman, G.E. Eperon, M. Saliba, M.T. Hörantner, A. Haghighirad, N. Sakai, L. Korte, B. Rech, M.B. Johnston, L.M. Herz, H.J. Snaith, A mixed-cation lead mixed-halide perovskite absorber for tandem solar cells, Science (80). 351 (2016) 151–155.

[143] W. Li, W. Zhang, S. Van Reenen, R.J. Sutton, J. Fan, A.A. Haghighirad, M.B. Johnston, L. Wang, H.J. Snaith, Enhanced UV-light stability of planar heterojunction perovskite solar cells with caesium bromide interface modification, Energy Environ. Sci. 9 (2016) 490–498.

[144] S. Ito, S. Tanaka, K. Manabe, H. Nishino, Effects of Surface Blocking Layer of Sb 2 S 3 on Nanocrystalline TiO 2 for CH 3 NH 3 PbI 3 Perovskite Solar Cells, J. Phys. Chem. C. (2014) 140501095518007.

[145] T. Leijtens, G.E. Eperon, S. Pathak, A. Abate, M.M. Lee, H.J. Snaith, Overcoming ultraviolet light instability of sensitized TiO2 with meso-superstructured organometal tri-halide perovskite solar cells, Nat. Commun. 4 (2013) 28885.1-8.

[146] Comin, R.; Walters, G.; Thibau, E. S.; Voznyy, O.; Lu, Z.-H.; Sargent, E. H. Structural, Optical, and Electronic Studies of Wide-Bandgap Lead Halide Perovskites. J. Mater. Chem. C, 3, 8839−8843 (2015)

[147] Tian, Y.; Ling, Y.; Shu, Y.; Zhou, C.; Besara, T.; Siegrist, T.; Gao, H.; Ma, B. A Solution-Processed Organometal Halide Perovskite Hole Transport Layer for Highly Efficient Organic Light-Emitting Diodes. Adv. Electron. Mater. 2016, 2, 1600165.

[148] Yu, H.; Wang, F.; Xie, F.; Li, W.; Chen, J.; Zhao, N. The Role of Chlorine in the Formation Process of "$CH_3NH_3PbI_3$−xClx" Perovskite. Adv. Funct. Mater. 24, 7102 −7108 (2014).

[149] Q. Chen, H. Zhou, Z. Hong, S. Luo, H.S. Duan, H.H. Wang, Y. Liu, G. Li, Y. Yang, Planar Hetero junction Perovskite Solar Cells via Vapor-Assisted Solution Process, J. Am. Chem. Soc. 136, 622-625 (2014).

[150] M. Liu, M.B. Johnston, H.J. Snaith, Efficient Planar Heterojunction Perovskite Solar Cells by Vapor Deposition, Nature, 501, 395-398 (2013).

[151] B.R. Sutherland, S. Hoogland, M.M. Adachi, P. Kanjanaboos, C.T.O. Wong, J.J. McDowell, J. Xu, O. Voznyy, Z. Ning, A.J. Houtepen, E. Sargent, Perovskite Thin Films via Atomic Layer Deposition, Adv. Mater. 27, 53-58 (2015).

[152] M. Ouafi, L. Atourki, L. Laanab, E. Vega, B. Mari, M. Mollar, B. Jaber, Hot airflow deposition: Toward high quality $MAPbI_3$ perovskite films journal of Alloys and Compounds 790, 1101-1107 (2019).

[153] Alexander R. Pascoe, Qinying Gu, Mathias U. Rothmann1, Wei Li, Yupeng Zhang, Andrew D. Scully, Xiongfeng Lin, Leone Spiccia, Udo Bach and Yi-Bing Cheng, Directing nucleation and growth kinetics in solution-processed hybrid perovskite thin-films.

[154] P. Scherrer, "Bestimmung der Grösse und der inneren Struktur von Kolloidteilchen mittels Röntgenstrahlen", Nachr. Ges. Wiss. Göttingen 26 98 (1918).

[155] J.I. Langford and A.J.C. Wilson, "Scherrer after Sixty Years: A Survey and Some New Results in the Determination of Crystallite Size", J. Appl. Cryst. 11 102 (1978).

[156] V. Uvarov and I. Popov, "Metrological characterization of X-ray diffraction methods for determination of crystallite size in nano-scale materials", Mater. Charac. 85 111 (2013).

[157] S. Sanchez, X. Hua, N. Phung, U. Steiner, A. Abate, Flash infrared annealing for antisolvent-free highly efficient perovskite solar cells, Adv. Energy Mater. 8, 1-7 (2018).

[158] H. El Masaoudi, I. Benabdallah, B. Jaber, M. Benaissa, Enhanced visible light photocatalytic activity of Cu^{2+}-doped Ag_3PO_4 nanoparticles, Chemical Physics 545, 111133 (2021).

[159] H. Yu, F. Wang, F. Xie, W. Li, J. Chen, N. Zhao, The role of chlorine in the formation process of "CH3NH3PbI3-xClx" perovskite, Adv. Funct. Mater. 24, 7102e7108 (2014).

[160] S. Sanchez, X. Hua, N. Phung, U. Steiner, A. Abate, Flash infrared annealing for antisolvent-free highly efficient perovskite solar cells, Adv. Energy Mater. 8, 1e7 (2018).

[161] N. Zayyoun, B. Jaber, L. Laânab, E. Ntsoenzok and R. Bekkari, Effect of solvent on the morphological and optical properties of CuO nanoparticles prepared by simple sol-gel process, J. Mater. Environ. Sci. 7, 1791-1797 (2016).

[162] Jena A. K., Kulkarni A., Miyasaka T., Halide Perovskite Photovoltaics: Background, Status, and Future Prospects. Chem. Rev. 2019, 119 (5), 3036–3103.

[163] Stranks S. D., Eperon G. E., Grancini G., Menelaou C., Alcocer M. J. P., Leijtens T., Herz L. M., Petrozza A., Snaith H. J., Electron-Hole Diffusion Lengths Exceeding 1 Micrometer in an Organometal Trihalide Perovskite Absorber. Science 2013, 342 (6156), 341–344.

[164] De Wolf S., Holovsky J., Moon S.-J., Löper P., Niesen B., Ledinsky M., Haug F.-J., Yum J.-H., Ballif C., Organometallic Halide Perovskites: Sharp Optical Absorption Edge and Its Relation to Photovoltaic Performance. J. Phys. Chem. Lett. 2014, 5 (6), 1035–1039.

[165] Eperon G. E., Stranks S. D., Menelaou C., Johnston M. B., Herz L. M., Snaith H. J., Formamidinium Lead Trihalide: A Broadly Tunable Perovskite for Efficient Planar Heterojunction Solar Cells. Energy Environ. Sci. 2014, 7 (3), 982–988.

[166] Kumavat S. R., Sonvane Y., Singh D., Gupta S. K., Two-Dimensional $CH_3NH_3PbI_3$ with High Efficiency and Superior Carrier Mobility: A Theoretical Study. J. Phys. Chem. C 2019, 123 (9), 5231–5239.

[167] Gu Y.-F., Du H.-J., Li N.-N., Yang L., Zhou C.-Y., Effect of Carrier Mobility on Performance of Perovskite Solar Cells. Chin. Phys. B 2019, 28 (4), 048802.

[168] Phillips L. J., Rashed A. M., Treharne R. E., Kay J., Yates P., Mitrovic I. Z., Weerakkody A., Hall S., Durose K., Maximizing the Optical Performance of Planar $CH_3NH_3PbI_3$ Hybrid Perovskite Heterojunction Stacks. Sol. Energy Mater. Sol. Cells 2016, 147, 327–333.

[169] Etienne T., Mosconi E., De Angelis F., Dynamical Origin of the Rashba Effect in Organohalide Lead Perovskites: A Key to Suppressed Carrier Recombination in Perovskite Solar Cells? J. Phys. Chem. Lett. 2016, 7 (9), 1638–1645.

[170] Y. Zhao, K. Zhu, Organic–inorganic hybrid lead halide perovskites for optoelectronic and electronic applications, Chem. Soc. Rev. 45 (2015) 655–689.

[171] M.D. McGehee, Perovskite solar cells: Continuing to soar, Nat. Mater. 13 (2014) 845–846.

[172] A. El-Yahyaoui, B. Jaber, L. Laanab, M. El Mahi, and E. M. Lotfi; The effect of temperature and distance of hot airflow on the quality of $MAPbCl_3$ thin films grown by sol–gel deposition; J Mater Sci: Mater Electron (2023) 34:252.

[173] Yunfei He, Shulin Xin, Yin Ren, Sisi Li, Jizhuang He, Jiahua Li, Chunlin Fu, Effects of anti-solvent temperature on microstructures and photovoltaic properties of TiO_2@$MAPbI_3$ core-shell nanowire arrays, Physica E: Low-dimensional Systems and Nanostructures, 147, (2023) 115610.

[174] Rabab Bekkari, Larbi Laânab, Boujemaâ Jaber, Effect of the bivalent dopant ionic radius, electronegativity and concentration on the physical properties of the sol–gel-derived ZnO thin films, Journal of Materials Science: Materials in Electronics, (2020).

[175] Zheng X., Chen B., Dai J., Fang Y., Bai Y., Lin Y., Wei H., Zeng X.C., Huang J., Defect Passivation in Hybrid Perovskite Solar Cells Using Quaternary Ammonium Halide Anions and Cations. Nat. Energy 2017, 2, 17102.

[176] Yerezhep D., Omarova Z., Aldiyarov A., Shinbayeva A., Tokmoldin N., IR Spectroscopic Degradation Study of Thin Organometal Halide Perovskite Films, Molecules 2023, 28, 1288.

Résumé

L'énergie joue un rôle majeur dans le monde moderne et contribue de manière significative au développement de l'humanité. Pour répondre à la croissante demande d'énergie et surmonter le problème du réchauffement climatique, de nombreux chercheurs se sont concentrés sur le développement des sources d'énergie renouvelables telles que l'énergie solaire. Dans cette optique plusieurs matériaux ont été étudiés pour être insérés dans les cellules photovoltaïques. Actuellement, les pérovskites hybrides d'halogénures de plomb utilisés comme absorbeurs de lumière dans les cellules photovoltaïques ont suscité un grand intérêt en raison de leurs propriétés optoélectroniques impressionnantes et de leur rendement élevé. Cependant, ils ont également montré certains inconvénients, tels que leur forte dégradation vis-à-vis des conditions climatiques (température, humidité, UV, …) qui influence leur performance.

L'objectif principal de ce travail de thèse est de synthétiser et d'étudier les propriétés physiques, la stabilité aux UV et la compacité des films minces à base de pérovskites hybrides $MAPbX_3$. Nous avons ensuite étudié l'intérêt d'associer un flux d'air chaud au procédé de spin-coating durant de la croissance du film $MAPbCl_3$. Les résultats obtenus dans ce contexte montrent que l'optimisation de la température et de la distance du flux permet de produire des structures cristallines de pérovskite $MAPbCl_3$ ayant un taux de couverture très élevée avec une nucléation homogène et significative. 100 °C et 5 cm sont donc la température et la distance optimales du flux d'air chaud pour une meilleure cristallinité et absorbance associée à une faible concentration de défauts non radiatifs. Dans la deuxième partie, nous avons aussi montré expérimentalement qu'il est possible d'améliorer significativement la stabilité contre les radiations UV de la pérovskite $MAPbI_3$ en modifiant sa composition chimique. Dans ce contexte, l'étude de l'effet de l'incorporation des atomes de chlorure dans la matrice pérovskite $MAPb(I_{1-x}Cl_x)_3$ sur les propriétés structurales, morphologiques et optiques a clairement montré qu'il est possible de rendre cette pérovskite plus stable par rapport à l'irradiation UV lorsqu'au moins 20% du chlorure sont incorporés dans la matrice. A partir de ce taux de chlorure, la structure pérovskite transite de la structure quadratique vers la structure cubique plus stable. Cette transition est à l'origine de la nette amélioration de la stabilité UV de la pérovskite $MAPbI_3$.

Mots-clefs (5): Perovskite; films minces $MAPbCl_3$; flux d'air chaud; revêtement par centrifugation; films minces $MAPb(I_{1-x}Cl_x)_3$.

Abstract

Nowadays it becomes more and more clear to the eye this Major role that Energy plays in the modern world.It contributes significantly to the development of humanity. Hence, to meet the increasing demand for energy and overcome the problem of global warming, The Majority of researchers have set their focus on the development of renewable energy sources such as solar energy. In this regard, several candidate materials have been studied to be implemented into photovoltaic cells. Currently, lead halide hybrid perovskites used as light absorbers in photovoltaic cells have attracted great interest due to their impressive optoelectronic properties and high efficiency. However, they have also shown some drawbacks, such as their strong degradation with respect to climatic conditions (temperature, humidity, UV, …) which influences their performance. This leads to the main objective of the current thesis, which is to synthesize and study the physical properties, UV stability and its improvement beside the compactness of thin films based on $MAPbX_3$ hybrid perovskites. We then studied the interesting effect of associating a hot air flow with the spin-coating process during the growth of the MAPbCl3 film. In this context, the obtained results show that the optimization of the temperature and the distance of the flow makes it possible to produce crystalline structures of $MAPbCl_3$ perovskite having a very high coverage rate with a homogeneous and significant nucleation. Also, it was shown that 100 °C and 5 cm are therefore the optimal temperature and distance of the hot air flow for a better crystallinity and absorbance associated with a low concentration of non-radiative defects. In the second part, we also experimentally proved that it is possible to significantly improve the stability against UV radiation of the MAPbI3 perovskite by modifying its chemical composition. In this regard, the study of the effect of the incorporation of chloride atoms in the $MAPb(I_{1-x}Cl_x)_3$ perovskite matrix on the structural, morphological and optical properties has clearly shown that it is possible to make this perovskite more stable with respect to UV irradiation when at least 20% of the chloride is incorporated into the matrix. Starting from this Chloride content, the perovskite structure transitions from the tetragonal structure to the more stable cubic structure. This transition is at the origin of the clear improvement in the UV stability of the MAPbI3 perovskite.

Keywords (5): Perovskite; $MAPbCl_3$ thin films; Hot airflow; Spin-coating; $MAPb(I_{1-x}Cl_x)_3$ thin films.